MICROSTRUCTURE – MECHANICAL PROPERTY RELATIONSHIPS IN

TRANSIENT LIQUID PHASE BONDED NICKEL-BASED

SUPERALLOYS AND IRON-BASED ODS ALLOYS

Except where reference is made to the work of others, the work described in this
dissertation is my own or was done in collaboration with my advisory
committee. This dissertation does not include proprietary, restricted
or classified information.

_____
Sreenivasa Charan Rajeev Aluru

Certificate of Approval:

_____   _____
Jeffery W. Fergus   William F. Gale, Chair
Associate Professor   Professor
Mechanical Engineering   Mechanical Engineering

_____   _____
Barton C. Prorok   Winfred Foster
Assistant Professor   Professor
Mechanical Engineering   Aerospace Engineering

_____   _____
Pradeep Lall   Stephen L. McFarland
Associate Professor   Dean
Aerospace Engineering   Graduate School

MICROSTRUCTURE – MECHANICAL PROPERTY RELATIONSHIPS IN

TRANSIENT LIQUID PHASE BONDED NICKEL-BASED

SUPERALLOYS AND IRON-BASED ODS ALLOYS

Sreenivasa Charan Rajeev Aluru

A Dissertation

Submitted to

the Graduate Faculty of

Auburn University

in Partial Fulfillment of the

Requirements for the

Degree of

Doctor of Philosophy

Auburn, Alabama
May 11, 2006

MICROSTRUCTURE – MECHANICAL PROPERTY RELATIONSHIPS IN

TRANSIENT LIQUID PHASE BONDED NICKEL-BASED

SUPERALLOYS AND IRON-BASED ODS ALLOYS

Sreenivasa Charan Rajeev Aluru

_____
Signature of Author

_____
Date of Graduation

iii

VITA

Sreenivasa Charan Rajeev Aluru, son of Venkata Ramana Rao and Jhansi Rani Aluru, was born on June 17th, 1980 in Nellore, India. He graduated from St. Xavier's High School, Ongole, India in March 1995 and Intermediate school from Adarsha Junior College, Ongole in March 1997. He joined Nagarjuna University, Guntur, India in August 1997 and graduated with a Bachelor of Technology in Mechanical Engineering in May 2001. He entered Auburn University in January 2002 as a graduate student in Mechanical Engineering and graduated with a Master of Mechanical Engineering degree in December 2004. He started working towards the Doctoral program in Materials Engineering at Auburn University in August 2002.

DISSERTATION ABSTRACT

MICROSTRUCTURE – MECHANICAL PROPERTY RELATIONSHIPS IN

TRANSIENT LIQUID PHASE BONDED NICKEL-BASED

SUPERALLOYS AND IRON-BASED ODS ALLOYS

Sreenivasa Charan Rajeev Aluru

Doctor of Philosophy, May 11th, 2006
(M.M.E, Auburn University, 2004)
(B.Tech, Nagarjuna University, 2001)

150 Typed Pages

Directed by Dr. William F. Gale

The research work presented here discusses the microstructure-mechanical

property relationships in wide gap transient liquid phase (TLP) bonds, between the single

crystal nickel-base superalloy CMSX-4 and two polycrystalline superalloys, IN 738 and

IN 939, using wide-gap style composite interlayers. Fabrication of complicated

geometries and successful repair development of gas turbine engine components made of

superalloys requires a high performance metallurgical joining technique and a complete

understanding of microstructure-mechanical property relationships. A number of joining

processes have been investigated, but all of them have significant disadvantages that limit their ability to produce sound joints. TLP bonding has proved to be a successful method and is the most preferred joining method for nickel-based superalloys, with microstructures and compositions of the joint similar to that of the bulk substrates resulting in mechanical properties close to that of the parent metal.

The current joining process used two proprietary wide-gap style composite interlayers, Niflex-110 and Niflex-115, consisting of a nickel-based core with boron-rich surfaces, and a conventional rapidly solidified metallic glass foil interlayer BNi-3 was chosen for comparison. When composite interlayers were employed, competition between wetting of the faying surfaces and formation of the eutectic along the grain boundaries was observed to lead to non-bonded regions at the faying surfaces, unless a boron-rich interlayer was employed. Composite interlayers resulted in the suppression of bondline boride formation. With the exception of this competition, adequate wetting of the substrates occurred for all interlayers.

Two factors dominated the room temperature mechanical properties of the wide-gap bonds. The first was the extent of gamma-prime formation at the bondline. Results from shear testing and fractography of the bonds indicated ductile shear failure at the bondline. This was due to the formation of insufficient gamma-prime within the joint, which left a relatively soft bondline region. The second factor was the presence of second phases in the diffusion zone of the polycrystalline substrate. This led to the formation of brittle secondary cracks. Overall, it is evident that the room temperature shear strength of the bonds was more dependent on the extent of formation of γ' on the bondline than on the secondary phases in the diffusion zone of the polycrystalline substrate.

ACKNOWLEDGEMENTS

Style manual or journal used   Metallurgical Transactions A

Computer software used   Microsoft Office XP

TABLE OF CONTENTS

LIST OF FIGURES

LIST OF TABLES

LIST OF ACRONYMS

APB - anti phase boundary
APBE – anti phase boundary energy
CBN - cubic boron nitride
CG - coarse grain
EBPVD - electron beam physical vapor deposition
EDM - electric discharge machining
EDS - energy dispersive spectroscopy
FCC - face centered cubic
FG - fine grain
GAR - grain aspect ratio
HAZ - heat affected zone
INEEL - Idaho national engineering and environmental laboratory
L-L - longitudinal - longitudinal
LM - light microscope
MA - mechanical alloying
MPD - melting point depressant
ODS - oxide dispersion strengthened
PBHT – post bond heat treatment
PBTE – post bond thermal exposure
PC - poly crystal
PWHT – post weld heat treatment
SC - single crystal
SEI - secondary electron imaging
SEM - scanning electron microscope
TCP - topologically close-packed phases
TEM - transmission electron microscope
TIG - tungsten inert gas
TLP - transient liquid phase
T-T - transverse- transverse
VIM - vacuum induction melting

1   INTRODUCTION

Superalloys are well known for their many high temperature applications, including their use in critical gas turbine components in aerospace and in land based power generation. They offer excellent high temperature tensile strength, stress rupture and creep properties, fatigue strength, oxidation and corrosion resistance, microstructural stability at elevated temperatures i.e., 600 ^{0}C or above [1-6]. A variety of strengthening mechanisms, such as precipitation hardening and solid solution strengthening, are employed for the manufacture of these materials [7]. There are three classes of superalloys: nickel-based superalloys, cobalt-based superalloys, and iron-based superalloys [3,5]. Nickel-based superalloys are the most complex and the most widely used in the high temperature applications. They currently comprise over 60% of the weight of advanced aircraft engines [8,9].

At high temperatures, superalloys are subjected to severe operating environments that include creep, thermo mechanical stresses, oxidation and corrosion. This results in the development of creep damage, thermal fatigue cracks and surface degradation. Repairing these service damaged components can result in substantial cost savings for the aerospace and power generation industry as compared with replacing them with new components. Thus joining of superalloys is a fundamental requirement for extensive post-service repair of gas turbine engine components [8-14]. Joining is also needed for primary fabrication, which includes high tolerance components such as jet fuel spray

nozzles [15], honeycombs [16] and solid walled structures [17]. Joining of dissimilar alloys (single crystal to polycrystalline) is also required owing to the difficulty in manufacturing large single crystal turbine blades. Conventional methods such as fusion welding [18-21], diffusion bonding [22-24], and brazing [23, 25] suffer from severe limitations when joining nickel-based superalloys. However, "transient liquid phase (TLP) Bonding" or "diffusion brazing" as the American Welding Society refers to this process has proven to be a successful joining technique for bonding nickel-based superalloys [25-28], although successful TLP bonding of superalloys still requires a better understanding of the microstructure-mechanical property relationships of the joint. Also, in many industrial applications, wide joint gaps (with a gap width of 100 μm or more) are not unusual. Thus, this research investigates the relationship between the microstructure, wettability, and mechanical properties of TLP bonded dissimilar nickel base superalloys using wide gap style composite interlayers.

This research investigates the relationship between microstructure and mechanical properties of TLP bonded dissimilar nickel-based superalloys. The microstructural bond development, long term microstructural stability of the bonds with time, mechanical properties of the joint using wide-gap style composite interlayer are examined and the results compared to those with a conventional interlayer (BNi-3 foil), chosen for comparison. Finally, a correlation between the microstructure-mechanical property relationships and wettabilty is drawn.

Precipitation hardened superalloys are very reliable at higher operating temperatures. However, as the precipitation hardened nickel base superalloys reach higher temperatures (0.6 times the melting temperature), the second phase precipitates

coarsen rapidly [29-31], losing some of their strengthening abilities. This is due to the transition in the strengthening mechanism from dislocation-particle shear to dislocation bypassing. At even higher temperatures (about 1100 ^{o}C), the second phase constituents dissolve into solution, losing their strengthening ability altogether [32]. On the other hand, the increasing demand for higher efficiencies drives the need for ever higher temperatures.

This demand has led to the development of a new class of materials, "oxide dispersion strengthened (ODS) superalloys" [16]. ODS alloys derive their superior high temperature strength from finely dispersed oxide particles (dispersoids) with high melting temperatures and low solubility in the primary phase, which are stable at extremely high temperatures and do not suffer from coarsening or dissolution effects [17]. There are two classes of ODS alloys - ferritic (iron - based) and austenitic (nickel - based) ODS alloys. In addition, ferritic ODS alloys are of interest as a fuel can material in the nuclear industry due to their better void swelling resistance and irradiation embrittlement properties compared to austenitic ODS alloys. These fuel can applications require the ability to metallurgically join end caps, which are also made of ferritic ODS alloys to the cans. Hence, the current research also focuses on the development of TLP bonds that retain their creep resistant microstructure for use in fuel can applications of ODS alloys.

Thus, the primary objective of the current research is to study the structure-property relationships of TLP bonded nickel-base superalloys and iron based ODS alloys.

2   LITERATURE REVIEW

2.1   Origin and Development of Superalloys

The origin and development of superalloys can be considered to be synonymous with the birth and advancement of gas turbines. Although the principles of gas turbines had been known for many years, industrial application was delayed for more than two decades due to the lack of adequate materials [34]. The availability of other suitable materials (chrome cast iron) for high temperature industrial and other strategic applications also restricted the rate of progress in this field. The development of superalloys has grown rapidly since World War II [35, 36]. Further contributions to this progress include many techniques such as vacuum induction melting (VIM) [35] to avoid oxidation of reactive elements and, advanced coatings to achieve superior environmental resistance [37, 38]. Other improvements include the use of directionally solidified (DS) and single crystal (SC) materials to achieve a combination of superior mechanical and environmental performance [37, 39].

Out of the three classes of superalloys (nickel-based, cobalt based and iron based), nickel-based superalloys are the principal high temperature material used for hot-zone components in an aircraft engine. The ongoing research and development of new superalloy designs and processes development has resulted in today's availability of many well-characterized nickel base superalloys with varying compositions, in-service temperatures, and a wide variety of applications as shown in Table 1.

4

SUPERALLOY	Alloy	Ni	Fe	Co	Cr	V	Ta	Mo	W	Re	Zr	Al	Ti	C	Other
Fe-Base	A-286	26	Bal	0	15	0.2	-	1.25	-	-	-	0.2	2.2	0.1	-
	N-155	20	Bal	-	21	-	-	3	2.5	-	-	-	-	0.2	1Nb
	IN 706	40	Bal	-	16	-	-	-	-	-	-	0.3	1.6	0.4	3Cb
	HK 40	20	Bal	-	24	-	-	-	-	-	-	-	-	0.5	-
	CG 27	38	Bal	-	13	-	-	5.5	-	-	-	1.5	2.5	0.1	0.06Nb
Ni-Base	IN 718	Bal	19	-	19	-	-	3	-	-	-	0.6	0.8	0.1	5.2Nb
	Mar-M247	Bal	-	10	8.2	-	3	0.6	10	-	0.1	5.5	1.4	0	1.5Hf
	Udimet-700	Bal	-	19	15	-	-	5.2	-	-	-	4.3	3.5	0.1	-
	CMSX-2	Bal	-	46	8	-	5.8	0.6	7.9	-	-	5.6	0.9	0	-
	IN 713 C	Bal	-	-	12	-	-	4.2	-	-	0.1	6.1	0.8	0.1	2Nb
	PWA 1480	Bal	-	5	10	-	12	-	4	-	-	5	1.5	-	-
	Waspalloy	Bal	-	13	19	-	-	4.3	-	-	0.1	1.3	3	0.1	-
	N-4	Bal	-	75	9.2	-	4	1.6	6	-	-	3.8	4.3	0	0.5Nb
	Rene-150	Bal	-	12	5	3	6	1	5	2.2	0	5.5	-	0.1	1.5Hf
	Alloy-D	Bal	-	-	-	15	2	2	4	-	0.2	4.5	2.5	0.1	-
	NTaC-13	Bal	-	3	4	5.4	8.1	-	3.1	6.3	-	5	-	0.5	-
Co-Base	HS 188	22	3	Bal	22	-	-	-	14	-	-	-	-	0.1	-
	X-40	10	-	Bal	25	-	-	-	7.5	-	-	-	-	0.5	-

Table 1: List of some commercially available iron, nickel and cobalt based superalloys and their typical compositions in wt% (Bal- Balance) [40, 41]

The first nickel-rich alloy developed for high temperature applications was "Nichrome" (Ni-20 wt% Cr) heater wire. The chromium provides oxidation and corrosion resistance at elevated temperatures; Chromium reacts with oxygen and results in the formation of a stable and continuous chromia (Cr_2O_3) layer. This serves as a barrier for the diffusion of oxygen into the bulk metal and provides excellent environmental resistance for these alloys. Likewise, different alloying elements may be added to improve the high temperature performance and environmental resistance. Table 2 shows the different types of alloying elements and their roles in improving nickel-base superalloy performance.

2.2 Microstructures and Mechanical properties

The microstructure of a typical nickel-based superalloy is shown in Figure 1, and consists of the following [1]:

1. Gamma matrix (γ): The gamma phase is an FCC nickel-based austenitic solid-solution phase and has a random distribution of different species of atoms. This comprises a high percentage of solid-solution elements such as cobalt, chromium, molybdenum, and tungsten.

2. Gamma Prime (γ'): Aluminum and/or titanium, the essential solutes, are added in amounts and mutual proportions with a total concentration of typically less than 10 wt % in order to precipitate high volume fractions of primitive cubic γ' [Ni_3(Al, Ti)] coherent with the γ matrix. The structures of the γ and γ' phases are shown in Figure 2.

6

3. Carbides: Carbon (0.05 - 0.2 wt %), combines with refractory and reactive elements such as titanium, and chromium, to form MC carbides, which after heat treatment and service generate lower carbides such as $M_{23}C_6$, and M_6C at grain boundaries.

4. Grain Boundary γ': Heat treatments and service exposures generate a film of γ' along the grain boundaries, which helps to improve creep rupture properties.

5. Borides: Carbon and boron are added as solid solutions for grain boundary strengthening (and thus are only used with polycrystalline alloys). When the solid solubility of boron is exceeded borides will be formed.

The high temperature strength of nickel-based superalloys arises from a combination of different strengthening mechanisms, including contributions from solid-solution elements, particles, and grain boundaries. The major strength provider, however is the coherent intermetallic compound γ' precipitated in a γ matrix [46].

At high temperatures, the thermal energy makes it easy for dislocations to move and for this reason the strength of most metals decreases. However, nickel-based superalloys are resistant to temperature and their strength increases with temperature up to a certain range. The normal burger's vector for an fcc γ lattice is (a/2) <110>. However, for γ', a primitive cubic structure, a <110> is the lattice vector, as shown in Figure 2. Thus, the motion of an (a/2) <110>$_γ$ dislocation into γ' disrupts the order of the γ', and an anti-phase boundary (APB) is formed. To minimize the energy increase associated with disordering, penetration of γ' has to occur by pairs of dislocations, known as super-dislocations. This requirement for pairing of dislocations makes it more difficult

for dislocations to penetrate through γ', thereby making the alloy stronger and giving it excellent creep resistance [47 - 49]. Neither single phase γ nor γ' are particularly creep resistant. In contrast, two phase γ/γ' is highly creep resistant. In both phases, there is elastic {square of burger's vector (b^2)} repulsion between like dislocations. In γ there is nothing to offset this repulsion. However, in γ' the antiphase boundary energy (APBE) of the antiphase boundary (APB) created by ½ <110> dislocations encourages these to move in pairs (the second dislocation removes the APB). Hence, the equilibrium spacing between the ½ <110> dislocations is governed by the balance of the elastic repulsion and the attraction due to the APB. Thus, dislocations are impeded in passing through two phase γ/γ', since the dislocations wish to be paired in γ' and separated in γ.

EFFECT	ALLOYING ELEMENTS
Solid-solution strengthening of γ	Ti, W, Mo, Cr, Co, Al
Solid-solution strengthening of γ'	Cr, Mo, W, Ti, Nb, Ta
Stability of γ'	W, Mo, Nb
Lattice mismatch increase	Nb, Ti, Ta
Lattice mismatch decrease	Cr, Mo, W
Antiphase boundary energy increase	Ti, Co, Mo
Antiphase boundary energy decrease	Al, Cr
Oxidation resistance improvement	Cr, Al
Precipitate formers	Ti, Ta, Al
Precipitation modification	Co
Grain boundary phases	B, C
Surface protection	Al, Cr
Grain boundary strengthening	Hf

Table 2: Role of some common alloying elements in nickel-base superalloys [42]
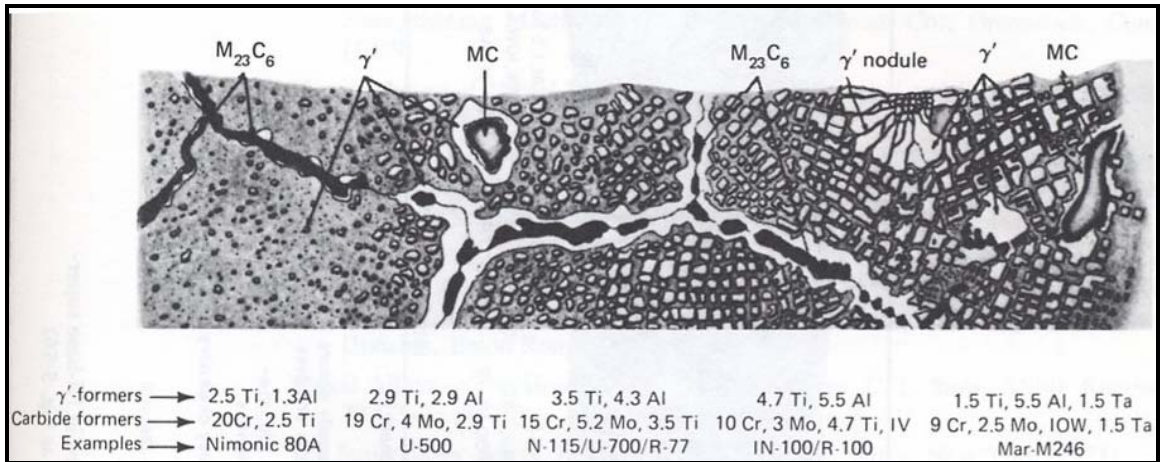
Figure 1: Schematic representation of the typical microstructure of nickel-base superalloys [43]
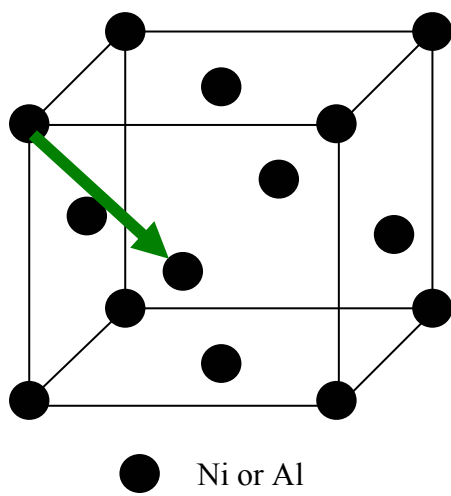
Crystal structure of γ
(cubic face centered)
Lattice vector a/2 <110>
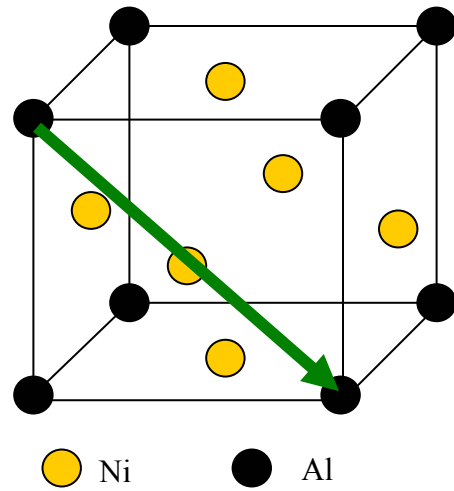
Crystal structure of γ'
(cubic primitive)
Lattice vector <110> shown

Figure 2-The crystal lattice structures of (a) NiAl and (b) Ni₃Al [44]

2.3 Joining of nickel-based superalloys

2.3.1 Need for Joining Superalloys

The need for joining superalloys can be classified into three categories:

- Repair joining (pre- and post service): The higher operating temperatures that improve the efficiency in gas turbines also result in rapid degradation of the components by enhancing levels of thermomechanical cycling, oxidation and creep. This damage necessitates the repair of these components in order to extend their service life and to produce cost savings for the industry. This often requires the damaged components to be repaired by joining new material to them [8-14].

- Primary fabrication: The complexity of gas turbine engine parts increases with the improved efficiencies. In addition, the increasing size of land-based turbines makes the large section components more prone to defects such as freckle formation. To minimize the problems and allow the manufacture of geometrically complex shapes, parts can be made in sections and then joined together. Therefore, a joining technique that bonds several small and relatively simple parts is often required for the primary fabrication of large complex components [15-17, 50].

- Joining of dissimilar (single crystal to polycrystalline) materials: Joining of dissimilar superalloys is also needed, for example as a result of the difficulty in manufacturing large single crystal turbine blades in land-based power generation applications.

The compositions and microstructures of superalloys, especially the latest generation alloys, have been designed and developed to meet the demanding requirements of

12

elevated temperature service. Likewise, the joining techniques used for these materials must also be carefully tailored in order to be compatible with these operating temperatures, stresses and environments. Fusion welding, diffusion bonding and brazing are the three main joining techniques used in the industry for joining high temperature materials [14]. As mentioned previously in the introduction, a number of joining processes, such as conventional fusion welding [18-21], diffusion bonding [22-24][23, 25, 27] and brazing [23, 25, 27], have been investigated, but all have limitations when used in joining superalloys. The disadvantages associated with these techniques are discussed below.

2.3.2 Fusion Welding

The use of conventional fusion welding, to join superalloys often results in hot cracking, post-weld heat treatment cracking, as well as the reduction in material properties of the joint [8, 26, 51, 52-60]. Weld metal and heat affected zone (HAZ) cracking, occurs during welding and during subsequent post weld heat treatments. The length of these cracks varies from microns to tens of mm and they propagate like brittle intergranular cracks exhibiting little plastic deformation. These cracks occur in the final stages of solidification and can be classified as solidification cracking (also known as liquation cracking [61].

As the solidification of the weld metal occurs, columnar grains grow from the fusion boundary towards the central region of the weld pool. This results in the rejection of impurities and alloying elements ahead of the weld pool and getting concentrated in the last liquid to solidify [56, 60]. This rejection results in the lowering the freezing point of the liquid, thereby allowing it to srvive for a period of time, even after the grains have

begun to meet the center of the weld pool. [54, 58, 60]. These liquid films formed reduce the surface contact of the grains forming regions of low ductility and thereby low strength in the weld. Also, the residual liquid is often insufficient to fill the voids present and the contraction stresses due to the cooling of weldment produces intergranular cracks along the weakened grain boundaries [54, 56, 58, 60]. In low γ' containing alloys, manipulation of weld parameters might minimize these effects, but in high γ' alloys, preheating the substrate to reduce the thermal gradients and strains in the weld zone might work. In addition, hot cracking is also dependant on other contributory factors such as solidification and microsegregation, viscous flow of liquid metal, crack initiation and propagation [52]. An extensive study of factors leading to solidification cracking and the analytical and finite element modelling methods used to simulate these phenomena has been discussed elsewhere [52].

Post weld heat treatment cracking (PWHT) or strain age cracking, generally, occurs in precipitation hardened superalloys during post-weld heat treatment or subsequent high temperature service. This is due to the presence of either residual stresses developed during welding, or applied stresses arising from service. These PWHT cracks are characterised by intergranular micro-cracking in either the HAZ or weld bead and form as a result of precipitation and hardening of the alloy during thermal exposure and transfer of solidification strains onto the grain boundaries [54, 55]. A common practice is to attempt to relieve residual stresses arising from the welding procedure by means of post weld heat treatment. However, often the stress-relieving temperature is greater than the aging temperature of the alloy and this leads to a transient precipitation period during post weld heating. This hardens the alloy resulting in excessive strain

14

localization on grain boundaries within the HAZ and weld bead during heating, leading to cracking. [54].

Other problems associated with fusion welding are the precipitation of brittle second phases in the weld joint and/or HAZ which might lead to reduction in mechanical properties such as tensile or yield strengths and ductility [53]. Also, the segregation of impurities and alloying elements at the joint may lead to a reduction in oxidation resistance. It has also been reported that fatigue strength of the weld joints was reduced relative to the base metal [65, 66].

2.3.3 Diffusion Bonding

Superalloys are designed to form a stable oxide layers to enhance their oxidation resistance. However, diffusion bonding suffers from the limitation of being unable to readily join systems with stable oxide layers [67]. Since diffusion bonding relies on the diffusion of interlayer species into the substrates, it thus requires longer bonding times to attain a perfect bond, with the elimination of non-bonded regions. This also requires high pressures, longer processing times, and if not conducted carefully may lead to some deformation in the components during bonding, making the process too expensive for many applications [25, 26]. When complex geometries are involved, it would be difficult to apply uniform bonding pressures normal to the mating surfaces and it might require expensive and sophisticated tooling.

2.3.4 Brazing

Brazing suffers from the limitations of the bond remelting temperature being less than the operating temperature of the superalloys and the formation of intermetallics

15

along the bondline [25, 26]. This results in bonds with poor mechanical and physical properties.

2.3.5   Transient Liquid Phase Bonding

In TLP bonding, a liquid forming interlayer (usually rich in the substrate material, with the addition of a melting point depressant (MPD)) is selected such that the melting point of the interlayer (initially) is significantly lower than the melting point of the substrates, and hence has the same initial condition as a braze joint [25, 26]. Once the bonding temperature is reached, which is greater than the melting point of the interlayer and below the melting point of the substrates, the interlayer melts forming an eutectic or alternatively can form a liquid by reaction between the interlayer and substrates. The further development of the bond can be described using three different, distinct stages. Figure 3 and Figure 4 show the different stages of TLP bonding.

- **Substrate dissolution** brings the compositions of the interlayer (usually starting from an eutectic) and the solid into local equilibrium i.e., the compositions of liquidus and solidus for the liquid and adjacent solid respectively, by diluting and widening the liquid interlayer. This stage is very rapid, since it does not rely on long-range diffusion in the solid phase.

- **Isothermal solidification:** In this stage**,** the solute (melting point depressant) diffuses from the interlayer into the substrates under local equilibrium concentrations and constant bonding temperatures, resulting in re-solidification of the joint at the bonding temperature. This stage is governed by long-range

16

diffusion in the solid phase. The time required for isothermal solidification to be completed depends on the system (substrates and interlayer) employed.

- **Solid-state homogenization** In this stage, diffusion of remaining MPD at the bondline into the substrates occurs and reduces the bondline concentration to below the room temperature solubility of MPD into the substrates. This produces a uniform solute concentration, homogenization of remaining solute and eliminates the formation of secondary phases at the bondline on cooling. Hence, the microstructure and mechanical properties of TLP bonds can approximate those of the substrate material, unlike brazing.[68, 69]

Transient liquid phase bonding is the preferred joining method for nickel-base superalloys because of its better joint properties compared to a brazed joint, the lower pressures required for bonding compared to a diffusion bond, its tolerance of stable oxide layers on the faying surfaces, the avoidance of both hot cracking in the joint and (as an isothermal process) the residual stresses that lead to post-weld heat treatment cracking, plus the elimination of brittle secondary phases along the joint.
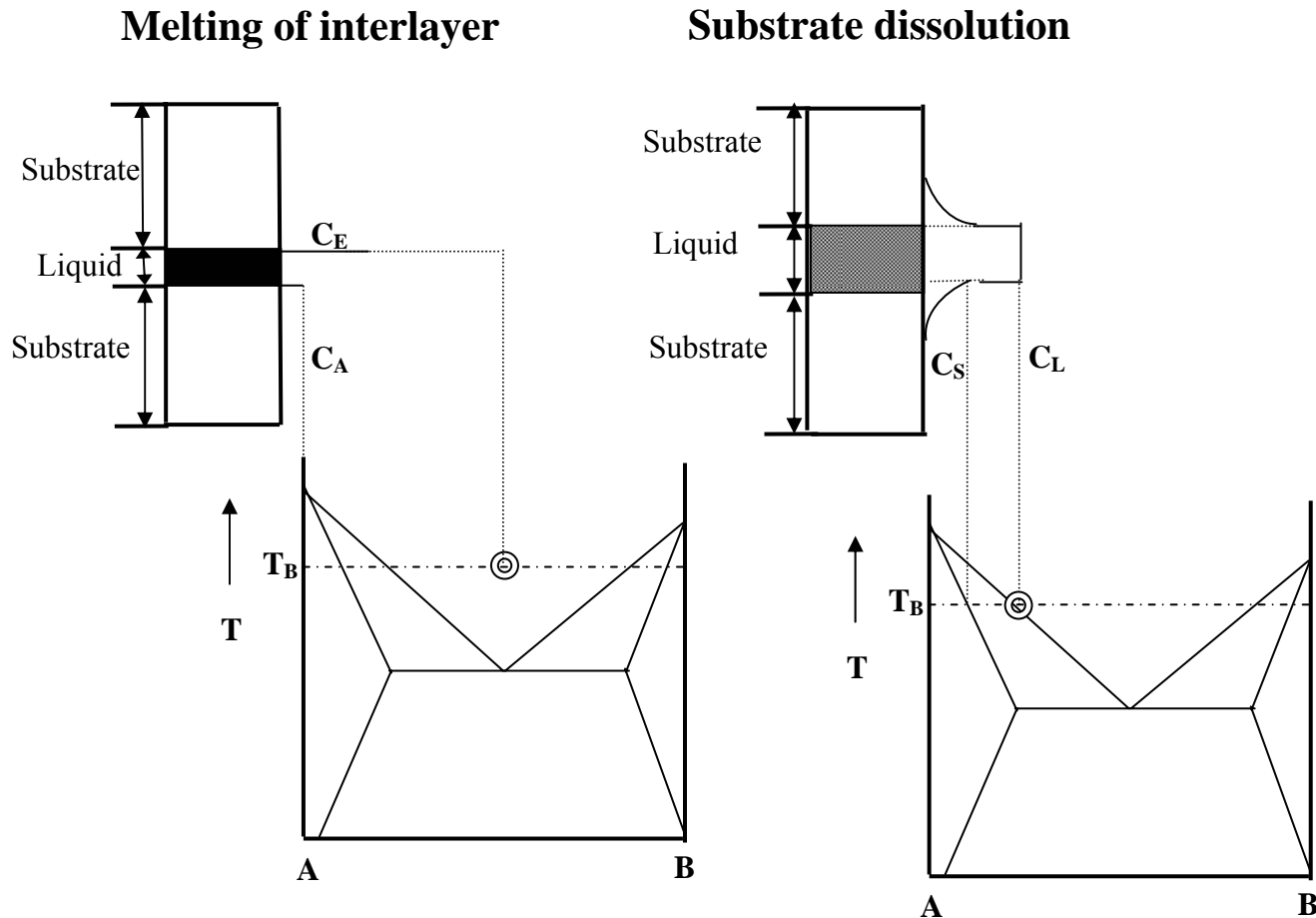
Figure 3 Stages of TLP bonding - Interlayer melting and substrate dissolution [**25, 27**]

Terminology:
A = substrate C_A = Composition of the substrate, C_E = Initial (eutectic)composition of the liquid T = Temperature
T_B = Bonding temperature C_s = Solidus composition C_L = Liquidus composition
MPD = Melting point depressant C_R = Room temperature solubility of MPD in A

Start of Isothermal solidification

End of Isothermal solidification
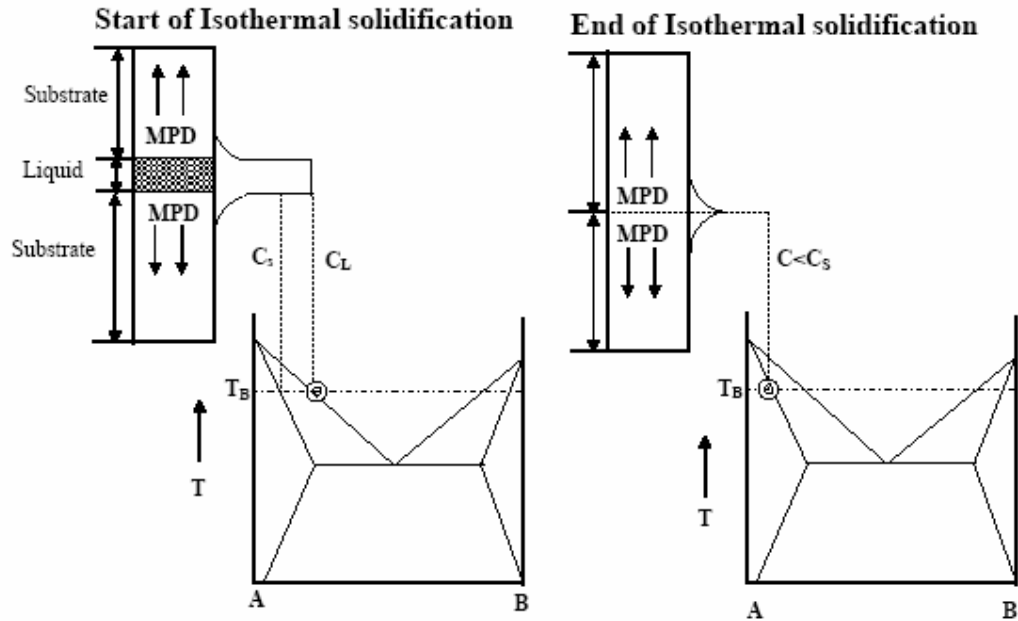
Solid-state homogenization
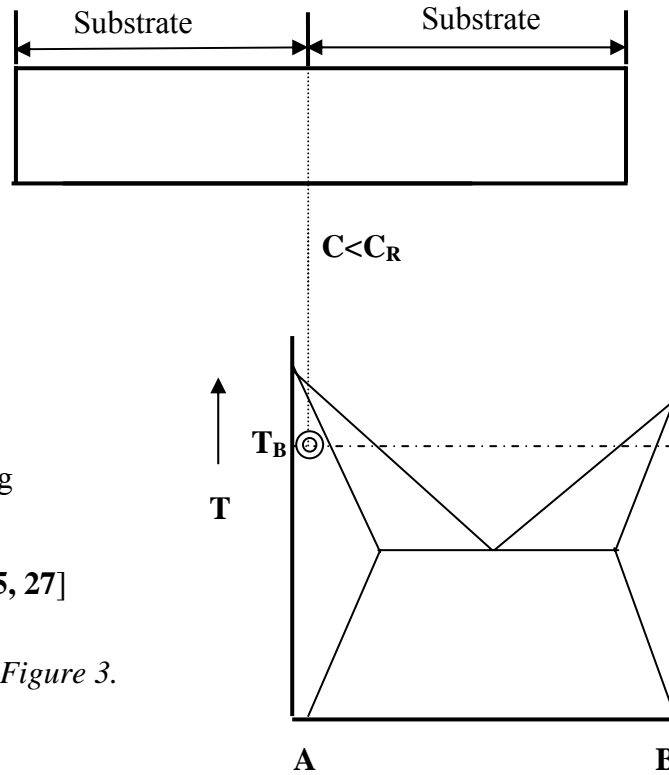
Figure 4 Stages of TLP bonding
Isothermal Solidification and
Solid-State Homogenization [**25, 27**]

The terminology is the same as Figure 3.

19

2.3.5.1 Advantages and Disadvantages of TLP bonding

While some of the advantages of TLP bonding have been mentioned already, the advantages and disadvantages can be summarized as follows [98]:

Advantages:

- TLP bonding, being an isothermal process unlike fusion welding, is ideal for joining materials susceptible to hot cracking or post-weld-heat treatment cracking [21].

- Large and intricate geometries such as honeycomb panels can be easily joined without expensive and complex tooling.

- The formation of undesirable brittle intermetallics in the bond- line can be avoided, resulting in a microstructure, and hence mechanical properties, of the joint that is similar to those of the bulk material.

- TLP bonding is tolerant to stable oxide layers on the faying surfaces and requires minimal fixturing pressures and surface preparation, unlike diffusion bonding [99]

These advantages have led to the use of TLP bonding for joining a wide range of materials, such as nickel-base superalloys [23, 26 ,100-103], oxide dispersion strengthened alloys [94, 95, 104, 105], metal matrix composites[106-108], and structural intermetallics [109-111]. TLP bonding also offers the advantage of joining dissimilar materials (for example, metals to ceramics) [112, 113], via derivatives of conventional TLP bonding.

Inspite of its wide variety of applications, it is also important to note some of the disadvantages associated with TLP bonding:

Disadvantages:

- Rapid heating rates must be employed in order to avoid the formation of brittle intermetallics during the heating process. This helps in minimizing the diffusion of interlayer and /or substrate constituents during heat-up.

- Long bonding and/or post bond heat treatment (PBHT) process times are often needed in order to attain complete microstructurally and chemically homogenized bond- line.

- Selection of interlayer composition and MPD becomes very difficult in some cases, and the bonding process is strongly dependent on this choice

2.3.6 Wide-gap Transient Liquid Phase Bonding

In TLP bonding, when thick interlayers are used to fill a wide joint gap (100 μm or more) extended bonding times are required in order to complete isothermal solidification and subsequent solid-state homogenization. Hence, conventional TLP bonds rarely employ a joint gap greater than 50 μm, and in some cases these may have an order of magnitude less than 50 μm [27]. However, wide joint gaps are often expected in industrial applications [70], so for TLP bonds using a wide joint gap, composite interlayers consisting of a liquid forming constituent coated on either side of a non-melting core can be employed. The liquid forming constituent is typically selected such that its melting point is slightly below the bonding temperature or to form a liquid by

reaction with the substrates and/or interlayer core, while the non-melting core is selected to have a composition and the solidus temperature similar to the base material [27, 71, 72]. The melting point depressant in the composite interlayers serves two functions. One is to increase the interfacial area between the liquid and solid phases, so that a more efficient path for the diffusion of the solute from liquid to solid will be created. These interlayers also reduce the amount of liquid necessary to fill the gap, so that less solute needs to be diffused in order to produce isothermal solidification and solid-state homogenization [27, 73, 74].

In the wide gap TLP process, the most important parameter is the choice of an appropriate amount of liquid former to be deposited on the non-melting core. If insufficient liquid former is deposited, premature isothermal solidification occurs and the liquid ceases to spread before it has had time to penetrate throughout the joint [75, 76]. This leads to excessive porosity at the joint. On the other hand, if a great deal of liquid is formed, then the amount of the solid-phase dissolved in order to produce a local equilibrium at the solid- liquid interface (i.e., solid-state dissolution) would be very high and the advantages of using the composite interlayer would be lost [27,77,78]. The use of excessive liquid former in a composite interlayer may also result in undesirable second phase precipitation in the bondline [54].

2.4   Development of Oxide Dispersion Strengthened Superalloys

Precipitation hardened superalloys are very consistent at higher operating temperatures in terms of their strength. However, as precipitation hardened nickel base superalloys reach higher temperatures (0.6 times the melting temperature), the second phase precipitates coarsen rapidly [29-31], losing some of their strengthening abilities.

This is due to a transition in the strengthening mechanism from dislocation-particle shear to dislocation bypassing. At even higher temperatures (around 1100 $^{\circ}$C), the second phase constituents dissolve into solution, losing their strengthening ability altogether [32]. Thus, the increasing demand for higher efficiencies has driven a need for ever more elevated temperatures, which has led to the development of a new class of materials, "oxide dispersion strengthened (ODS) superalloys" [80].

2.5   Mechanical Alloying

Although ODS alloys are manufactured using different techniques, such as mechanical mixing, internal oxidation, selective reduction and rapid solidification, these processes all suffer from drawbacks, namely too irregular interparticle spacing, non-uniform oxide size, difficulty in reduction of stable oxides, and limited solid-solubility, respectively [80, 81]. In contrast, mechanical alloying (MA) minimizes the above mentioned drawbacks and results in the optimum interparticle spacing and uniform oxide size that are required for high temperature operation. Mechanical alloying minimizes the interaction between the matrix and dispersoids and the oxide particles are included as an incoherent phase within the alloy matrix.

In mechanical alloying, the alloying powders are continuously cold welded, work hardened and fractured using a dry, high-energy ball milling technique. This process, which requires no liquids or surfactants, produces composite metallic powders with a controlled and fine microstructure. The mechanically alloyed powders are consolidated at 900 ^{0}C – 1100 ^{0}C by extrusion or by hot isostatic pressing in vacuum sealed cans [82-84]. No melting of the material takes place throughout the whole process. Final heat-

treatments are used to recrystallize the heavily deformed material, which will result in coarse columnar type grains [80,83,84,86].

The disadvantage of using the mechanical alloying process is the difficulty in controlling the final microstructure of the ODS alloys, which leads to inconsistent batch to batch properties and reproducibility. In addition, the operating temperatures of the ODS alloys are limited by the melting temperature of the matrix.

2.6   Properties and Applications

The dispersion of particles in a metal matrix produced by mechanical alloying markedly increases the strength and environmental resistance of these materials at high temperatures. The finely dispersed stable oxide particles (dispersoids), with high melting temperatures and low solubility in the primary phase, are stable at extremely high temperatures and do not suffer from either coarsening or dissolution effects[87].

The outstanding strength and corrosion resistance of ferritic ODS alloys is due to

- Nanosized yttria dispersoids, which are non-shearable and therefore act as obstacles to the dislocations by pinning them and help to achieve favorable high temperature creep and stress rupture strength.

- Coarse grain structure with a favorable texture and high grain aspect ratio (GAR), which improves the high temperature creep properties at intermediate and high temperatures (above 1000 ^{0}C). The coarse grain structure also helps in preventing grain boundary sliding and Nabarro-Herring creep at high temperatures [88].

- Adherent surface layer of protective alumina scale, which is formed during exposure at high temperatures, due to the high aluminium content in the matrix (5%), and provides excellent oxidation resistance. The presence of yttria (around

24

0.5%) is beneficial in improving the oxide scale adherence during thermal cycling [89].

There are two groups of ODS alloys.

- Austenitic (Ni-based) ODS alloys strengthened by oxide dispersions and γ' phase precipitates, which are used as blade materials for advanced gas turbines.

- Ferritic (Fe-based) alloys strengthened by oxide dispersions and have applications in aero engine and gas turbine chambers, and as cladding materials for fast breeder reactors and fuel cans in the nuclear industry [44].

The austenitic ODS alloys such as MA 6000 used in advanced gas turbine engines, combine the strengthening effects from the incoherent oxide particles and the coherent γ' precipitates in the γ matrix. Thus, even after the solutionizing temperature of γ' (at around 1000 ^{0}C), high temperature strength is provided by the dispersoids present in the alloy [85]. Ferritic ODS alloys find their potential applications in the nuclear industry as a fuel can material due to their better resistance to void swelling and irradiation embrittlement than austenitic superalloys.

2.7   Joining of ferritic based Superalloys

2.7.1   Conventional Techniques and Limitations

The need to be able to join ODS alloys arises from their applications in primary fabrication, pre and post service repair, and the difficulty in manufacturing large complex shaped parts. Conventional joining techniques such as fusion welding, friction welding and brazing have all been investigated by various researchers for use in joining ODS alloys, and these will be discussed in turn below.

As noted in section 2.3 for nickel-based superalloys, fusion welding is limited by melting of the base metal leading to the formation of dispersoid agglomerates in the joint, porosity in the joint, undesirable secondary fine recrystallized grains in the joint (boron present in the weld filler material diffuses into the substrates resulting in lattice strains and thereby providing additional energy for recrystallization), grain growth in the joint normal to that of the base metal [90] and formation of brittle second phases in the joint [91], all of which can lead to premature failure of the joint. In other experiments by Moilan et al. [92] using tungsten inert gas (TIG) welding, bondlines of lower hardness values were obtained due to oxide agglomeration and loss of grain orientation was observed. Yttria agglomeration resulted in a discontinuous chromia scale, as a result of which the sulphidation resistance of the TIG weld was low. The grain size in the welded joint was coarser than that of the substrate material. This resulted in bonds with poor room temperature mechanical properties.

Solid-state joining processes such as explosion welding and friction stir welding do not result in melting of the base material, so an effective undisturbed yttria dispersion can be retained in the joints using mechanically alloyed ODS alloys. However, adiabatic shear bands were observed at the bondline when two ODS alloy substrates were explosion welded and showed an impact on mechanical properties [91]. In conventional friction welding, the chemistry, dimensions and shape of the particles were all altered [93]. Reorientation of some of the grains has also been observed due to the final forging process in friction stir welding. Due to the high strain rates and oxidation involved, yttria agglomeration, large titanium-rich and aluminum-rich oxide particles were observed [93].

26

Brazing of ODS alloys also suffers from several disadvantages. The major drawback in brazed components is that the joint remains as a low-remelting region, hence restricting the joint to lower operating temperatures. In addition, a brazed joint assembly results in the formation of brittle secondary phases, leading to poor mechanical properties [26]. The formation of a protective oxide layer on ODS alloys also inhibits the flow of the braze filler metal.

2.7.2   Diffusion Bonding

Diffusion bonding is a solid-state joining technique in which the two surfaces to be joined are brought into contact and held together for extended periods of time under high pressures at elevated temperatures [115, 116]. The high temperatures allow the microscopic deformation of the points of contact between the two materials, thereby greatly increasing the true contact area. Diffusion bonding can be described in terms of three different stages [117].

Stage I: This stage corresponds to the initial state in which the two surfaces to be joined are brought into contact. When high pressures and temperatures are applied, the plastic deformation of asperities on the two faying surfaces results in the formation of a bond plane with a large number of pores.

Stage II: In this stage, further heating allows the migration of grain boundaries and the elimination of porosity through diffusion. Growth of metal crystals across the bond interface takes place, thereby causing the pores to shrink in size. This stage does not require the application of external pressure.

Stage III: This is the final stage of the bonding process, in which volume diffusion results in minimization of the final porosity. However, complete elimination of

27

the remaining final pores is extremely difficult at this stage and requires high pressures irrespective of heat treatments and longer bonding times. A careful selection of bonding pressures and temperatures in stage I and stage II yields better bonds with less porosity.

Diffusion bonding of ODS alloys using unrecrystallized and recrystallized ODS materials in the working direction results in fine grain layer formation at the bond-line [118-120]. This layer often produces deterioration in the properties of the joint. In addition, the need for a high bonding stress is a disadvantage for this process. For example, when recrystallized MA956 material was diffusion bonded by Zhang et al.[120], a thick layer of oxide was observed at the bondline at low bonding stresses. Higher bonding stresses (56 MPa and 72 MPa) resulted in bonds with tensile strengths comparable to that of the parent metal. However, the presence of circular voids at the bondline and a transverse grain boundary extending through out the length of the joint resulted in a reduction of the joint strength at high temperatures. An increase in bond time and bonding stress was suggested by the authors, which makes the process uneconomic for industrial applications. Diffusion bonding of MA6000, a nickel-base ODS alloy was studied by Moore and Glasgow [118]. Although, they obtained successful macroscopic joints, low stress rupture strength of the joints was observed.

Although, some success in diffusion bonding ODS alloys has been achieved for the bonding of unrecrystallized to recrystallized material and recrystallized material to itself, the very high stresses (200 – 300 MPa), high temperatures, longer processing times and extensive specimen preparation required make this process uneconomical.

2.7.3 Transient Liquid Phase bonding of ferritic based ODS Alloys

The advantages of TLP bonding, discussed earlier in section 2.3.5, indicate that it is a promising joining technique for oxide dispersion strengthened alloys when compared to conventional techniques. This is because it prevents base metal melting although localized dissolution of the substrates still does occur, eliminates brittle secondary phases in the joint and results in minimal or negligible microstructural disruption so that the bond will have the same properties as the bulk material. The vital issues in the TLP bonding of ODS alloys are the distribution of dispersoids after melting of the interlayer and the consequences of this for microstructural development and, hence, mechanical properties. Therefore, the study of microstructure-mechanical property relationships is crucial in TLP bonded ODS alloys.

Khan et al.[94, 95] successfully employed the TLP bonding technique to join ferritic ODS superalloys MA956 and PM2000 in the fine grained condition using an iron-based foil as an interlayer, with boron and silicon as the melting point depressants. The bonds obtained were free from precipitates, pores, and excessive agglomerations of dispersoids. However, the recrystallized grain size did not match that of the bulk material annealed under similar conditions. In addition, the joining process used is only suitable for narrow joint gaps (of a few μm), which are difficult to achieve consistently in many industrial applications.

3   RESEARCH OBJECTIVES

This research is aimed at the investigation of strategies for joining dissimilar superalloys, (single crystal to polycrystalline) for use in land-based gas turbines for electric power generation. As already mentioned in section 2.3.5 and 2.7.3, TLP bonding is much more suited for the joining of superalloys than conventional techniques. However, the successful application of TLP bonding to superalloys requires a complete understanding of microstructure-mechanical property relationships. In addition, this better understanding of TLP bonding process can be achieved only through a close correlation between real-world systems and analytical or numerical models. Also, the extended bonding times required for thicker (greater than 50 μm) interlayers and the wide joint gaps (a gap width of 100 μm) in real industrial applications requires an in depth study of wide gap TLP bonding.

Thus, the main objective of this research is to examine the details of microstructural bond development and their relationship with the mechanical properties in wide gap style TLP bonded superalloys. The objective also includes a study of the long-term microstructural stability of these bonds and the production of a joint free of brittle second phases, with a microstructure and, hence mechanical properties similar to the unbonded material. This work takes into account the effects of interfacial segregation and gravitational influences on the liquid phase and solid-state diffusion. Further, this study will address the wettability issues for wide-gap style composite interlayers on

the three substrates used in joining. A flow chart to aid in the understanding of the goals and investigations conducted is shown in Figure 5.

As mentioned already, the ever increasing demand for higher efficiencies drives the need for materials that retain their properties at elevated temperatures (higher than the solution temperature of γ'), have led to the development of mechanically alloyed ODS alloys. However, ODS alloys also need to be joined due to the various reasons mentioned in section 2.3.1. and as mentioned in section 2.7.3, TLP bonding has shown some promising results in joining ODS alloys.

Of the two classes of ODS alloys (ferritic and austenitic), ferritic ODS alloys are of particular interest as a potential fuel can material for use in the nuclear industry due to their better void swelling resistance and irradiation embrittlement compared to austenitic ODS alloys [96]. However, these fuel can applications require the ability to metallurgically join end caps, which are also made of ferritic ODS alloys. Hence, the current research also aims at developing TLP bonds that retain a creep resistant microstructure, for use in fuel can applications of ODS alloys.

Thus, the overall objective of the current research is to study the structure-property relationships of TLP bonded nickel-based and iron based superalloys. The specific objectives related to nickel-base superalloys and oxide dispersion strengthened superalloys are listed below.

Nickel-based superalloys:

- Investigate the bond development and long-term microstructural stability of wide gap style TLP bonded dissimilar nickel-based superalloys

31

- Produce a joint free of brittle second phases, with mechanical properties similar to that of the unbonded material

Oxide dispersion strengthened superalloys:

- Design and implement a TLP bonding process that provides reasonable dispersoid continuity across the bondline of ferritic ODS alloys

- Produce a continuous, recrystallized microstructure across the bondline, resulting in mechanical properties similar to that of the parent material.
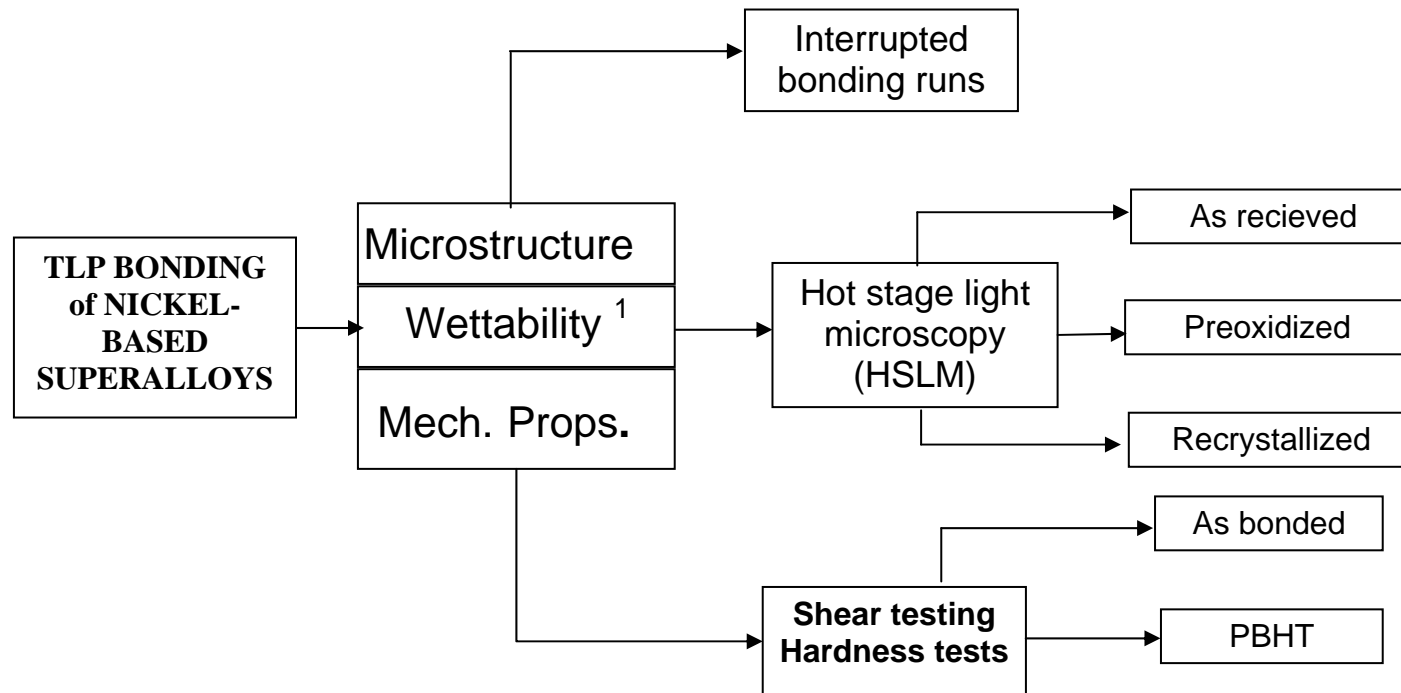
Figure 5: Flow chart of project objectives and investigations[1] for TLP bonding of dissimilar nickel-based superalloys

---

[1] Wettability studies are conducted by Subhadra Chitti and microscopy was done by Nofrijon Sofyan

4   MATERIALS AND EXPERIMENTAL PROCEDURE

4.1   Nickel-based superalloys

4.1.1   Materials

Single crystal CMSX-4, and polycrystalline IN 939 and IN 738 were the three nickel-based superalloys used in this research. CMSX-4 was joined to IN 738 and to IN 939. The joining process used proprietary wide-gap style composite interlayers Niflex-110 and Niflex-115 (the latter has a higher boron content than the former); a conventional foil interlayer BNi-3 (Ni-4.5 wt%, Si- 3.2 wt%, B) supplied by Metglas Inc. was chosen for comparison. The composite interlayers and substrate materials were provided by Siemens-Westinghouse, Orlando, Florida.

The as-received blocks were 52x48x23 mm. The microstructure of as-received CMSX-4 is shown in Figure 6. A high volume fraction of γ' with no rafting was observed in the as-received microstructure of the substrates. The substrates were ground to a 1000 grit finish using SiC paper.

The as-received interlayers were 50 μm in thickness. The composite interlayer consisted of a non-melting core with a melting point depressant (in this case, boron) coated on both sides of it. Thus, the liquid formed upon melting of the interlayer was in direct contact with the substrate surfaces, allowing the melting point depressant to diffuse readily into the substrate constituents. A schematic of a composite interlayer is shown in Figure 7. The advantages of using a wide-gap interlayer were discussed in section 2.3.6.
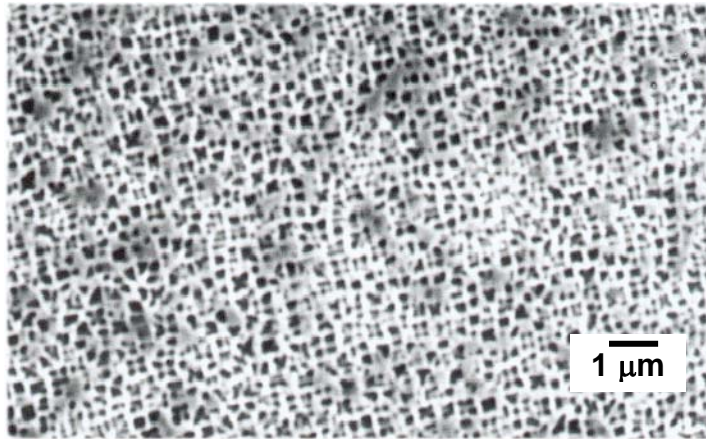
Figure 6 Microstructure of as-received single crystal CMSX-4 [97]
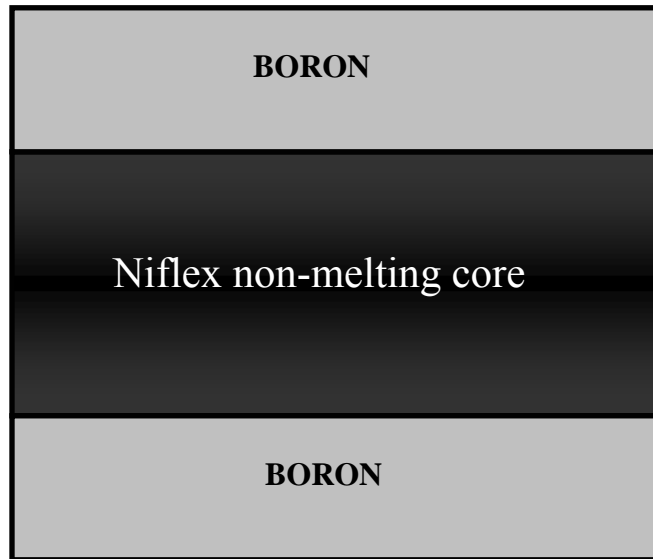
Figure 7: Schematic of wide gap composite interlayer

4.1.2   Joining Procedure

The substrates were ground to a 1000 grit finish using SiC paper and ultrasonically cleaned in an acetone bath. The interlayer was placed between the prepared CMSX-4 and IN 738/IN 939 substrates (Refer to

Table 3 for compositions); the whole assembly was wrapped with Ta wire for fixturing. The whole assembly was inserted in a tube furnace and joined in a vacuum (at least 13.3 mPa) using the bonding treatment conditions described below. The conditions of the as-bonded samples were:

- Bonding temperature: 1160°C

- Ramp time: ~140 min

- Bonding time: 4 hrs

- Cooling: Removed from the vacuum tube furnace and fan-cooled at room temperature after 4 hr of bonding

All the bonding trials were performed with the (001) plane of the CMSX-4 as the faying surface joined to the polycrystalline substrates IN 738 and IN 939.

To study the microstructural bond development, a series of interrupted bonding tests (with bonding times consisting of 0 min {i.e., heating to the bonding temperature and immediately cooling}, 1 min {i.e., heating to the bonding temperature, dwell for 1 min and then cooling} and so on) were conducted. Interrupted bonding studies at 2 min, 4 min, 10 min, 1 hr, 2 hrs, and 4 hrs (all at 1160 ^{0}C) were also performed.

4.1.3   Bond Heat Treatment (PBHT)

"Post-bond heat treatment" (PBHT) was performed on the as-bonded samples to allow the diffusion of aluminum from the substrates in order to form more γ' on the

37

bondline and to reform the γ' distribution in the bulk, which was dissolved during bonding. The assembly was heated (30 min ramp time) to 1093 °C and held for 1 hour. This is the temperature at which the γ' goes into the solution.

After 1 hour, the furnace was cooled to 1000 °C in vacuum and held for 4 hrs in vacuum. This heat treatment of 4 hrs at 1000 °C allowed the precipitation and growth of primary γ'.

The furnace was then cooled to 843 °C and held for 16 hours in a vacuum. This generated considerable quantities of secondary, fine γ', after which the sample was fan cooled to room temperature.

In summary, the PBHT consisted of:

- Heat to 1093°C and hold for 1 hour in vacuum;

- Cool to 1000°C and hold for 4 hrs in vacuum;

- Cool to 843°C and hold for 16 hrs in vacuum;

- Fan-cool to room temperature.

4.1.4 Post Bond Thermal Exposure (PBTE)

The "post bond thermal exposure" (PBTE) refers to studies designed to examine the microstructural stability of the bonds. In order to determine the microstructure-mechanical property relationships of the bond with time, post-bond thermal exposures of up to 1 week (168 hrs) at 1000 ^{0}C, were performed on the as-bonded samples.

Element	CMSX-4	IN 939	IN 738
Ni	60	48	61
Cr	6.5	22.4	16
Co	10	19	8.5
Mo	0.5	-	1.7
W	6.5	2	2.6
Ta	6.5	1.4	1.7
Nb	5.5	1.9	3.4
Al	5.5	1.9	3.4
Ti	1	3.7	3.4
Others	3	-	1

Table 3 Nominal compositions of nickel-based superalloys (given in wt %)

4.1.5 Metallographic Preparation

The as-bonded, PBHT and PBTE samples were sectioned using a wire EDM /
Struers Accutom-5 high speed wafering saw employing a cubic boron nitride (CBN)
blade. Once sectioned, the samples were mounted using a Struers Labpress-3. Samples
were ground to a 1200 FEPA grit finish and then polished using a 6 μm diamond spray,
followed by a 0.04 μm alumina suspension solution. The metallographic samples were
etched to show γ' using a mixture of 20 vol% conc. nitric acid and 80 vol% conc.
hydrochloric acid for 5-10 seconds at room temperature.

4.1.6 Microstructural Characterization

The samples, as-bonded, PBHT and PBTE, were primarily characterized using
light microscopy (LM) and scanning electron microscopy (SEM), supplemented with
SEM based energy dispersive X-ray spectroscopy (EDS). These studies[2] were conducted
on a JEOL JSM840 instrument operated at an accelerating voltage of 20 kV. Secondary
electron imaging (SEI) was used to collect all SEM micrographs. The SEM based EDS
analysis used ultra-thin window detectors and Oxford Instruments ISIS analyzers. EDS
analysis was used to determine the composition of phases observed in the bond- line and
compositional profiles across the joint.

4.1.7 Mechanical Testing

The study of bond mechanical properties was performed by means of shear and
hardness testing. All specimens for shear testing were extracted using an EDM and the
mechanical testing was supplemented by fractographic investigations using SEM and

---

2. As mentioned already, microscopy was conducted by Nofrijon Sofyan.

EDS analysis. The details of the mechanical testing procedures employed are discussed below.

Initial mechanical testing was done on specimens extracted from an as-bonded and PBHT samples via EDM, and then tested in four-point bending by Tao Zhou [97]. However, these samples deformed to the maximum displacement of the testing rig without failing, thus rendering the four-point bend test unusable. Double lap shear testing was conducted for this study, but problems were encountered due to the test grips slipping off the samples. Tensile testing was also unsatisfactory for these samples due to the limitation of testing the bulk in addition to the bond.

Thus, the shear testing method developed by Yan and Wallach [114], which is an easy, effective and inexpensive method of testing the bond was selected for use in this study as an acceptable alternative means of testing the bond strength.

4.1.7.1   Shear Testing

The shear tests were carried out with a specially designed grip developed by Yan and Wallach [114]. The schematic in Figure represents the assembled unit, with a loaded specimen in the geometry of Figure 8(a). The adjustable screw in the line drawing was adjusted in order to place the bond-line in the plane of shear. When the assembled unit was then placed in tension, the outer sheath maintained the shear along the bond-line until the specimen failed. The shear test samples were composed of a circular piece and a rectangular piece (see Figure 8). The disc shaped substrates were 12-13 mm in diameter and 3.5 mm thick and the rectangular substrates were 8 x 4 mm for faying surface dimension and 2 mm thick. All the tests were performed at room temperature. An MTS

Q-Test 100 screw-driven machine was employed to conduct these tests. Testing was

performed at a grip separation rate of 0.5 mm/min.
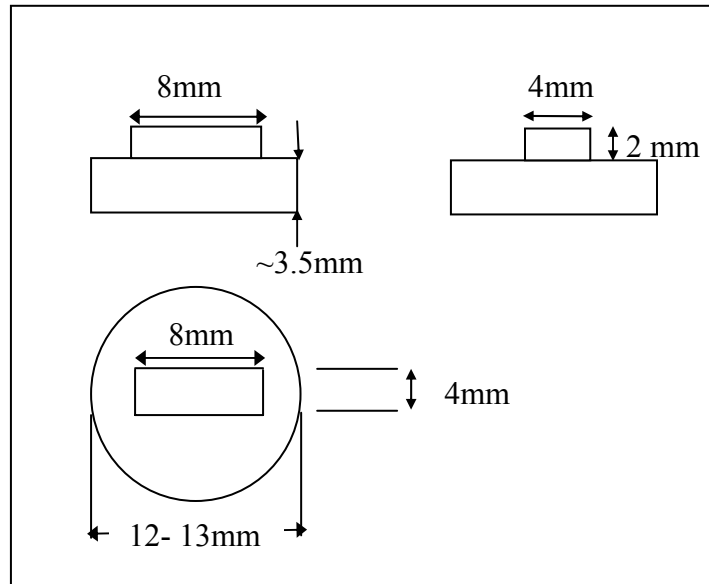
Figure 8(a): Schematic of sample used for shear testing [114]
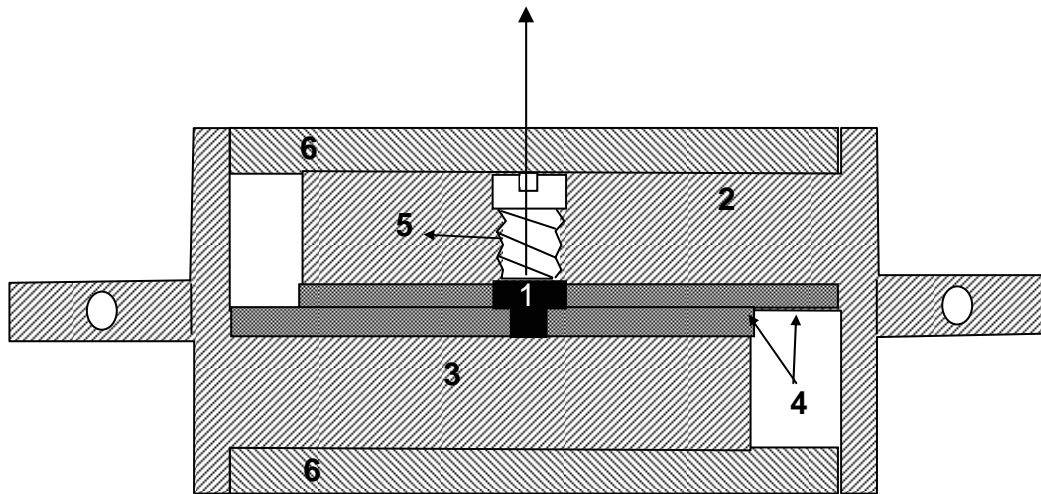
1. Sample   2. Down fixture   3. Up fixture

4. Hardened inserts   5. Screw   6. Shield

Figure 8(b): Schematic of grip used for shear testing [114]

4.1.7.2 Hardness Tests

Vickers microhardness testing was also employed in order to determine the hardness of the intermetallics present in the bond region and the hardness profile across the bond- line. Microhardness testing was conducted using a 300 g load for a duration of 10 s.

4.1.8 Wettability Studies

Wettability tests were conducted[3] using the sessile drop technique [121], in order to investigate the mechanisms involved and the ability of the Niflex interlayers to wet the superalloy substrates. Substrate samples with a geometry of 4mm X 4mm and 1mm thickness were cut using a Struers Accutom-5 and ground to 1200 FEPA grit. Disks with a diameter of 1 mm were mechanically punched from a 50 μm thick proprietary Niflex interlayer. The prepared substrates and the interlayer were then ultrasonically cleaned in an acetone bath before the experiments.

The sessile drop tests were dynamically observed on a real time dynamic hot stage light microscope, using a Leitz 1750 heating stage mounted on a Leitz DMR light microscope. The experiments were conducted in a 1.3 MPa vacuum atmosphere at the bonding temperature. These tests were video recorded, so that the displacement of the solid- liquid interface was measured[4] as a function of holding time. The wetted samples were cross-sectioned in order to study the wetting mechanisms and the microstructure. The displacement measurements were conducted by *Robert Love*.

---

3. As mentioned already, wettability tests were conducted by Subhadra Chitti
4. The displacement measurements were conducted by *Robert Love*

4.2   Oxide Dispersion Strengthened Iron Based Superalloys

4.2.1   Materials

The primary materials used were MA956, PM2000 and boron. MA956 and PM2000, the two ferritic based ODS alloys, were supplied by Idaho National Engineering and Environmental Laboratory (INEEL). MA956 was received in fine grain (11 mm x 11 mm square billets) and coarse grain (20 mm diameter rods) condition, and PM2000 (25 mm diameter rods) was received in fine grain condition. The compositions of the alloys are presented in Table 4. After the initial experiments on MA956, further more detailed investigations were done on PM2000 due to availability of the material.

Samples with dimensions of 11 mm x 10 mm and 2 mm in thickness were cut using an electric discharge machine (EDM) in longitudinal (along the direction of extrusion) orientation. The substrates were surface ground to maintain their flatness and to remove the copper layer formed during EDM cutting. A surface grinder from Gold International Machinery, Inc. was utilized for this. These substrates were then ultrasonically cleaned in an acetone bath and then stored in acetone to prevent any oxide formation prior to bonding.

Electron beam physical vapor deposited (EBPVD) boron on the substrates was used as the interlayer for TLP bonds. Boron was selected as the MPD due to its high diffusion coefficient in ferritic materials. Boron films with thicknesses of 250 nm, 500 nm and 1 μm were used as interlayers.

Alloy	Composition (wt %)						
	Fe	B	Cr	Al	Ti	Y_2O_3	C
MA956	bal	-	20	4.5	0.3	0.5	0.04
PM2000	bal	-	20	5.5	0.5	0.5	0.01

Table 4: Nominal compositions of Iron-based ODS superalloys (given in wt %)

4.2.2 Joining Procedure

Bonding was performed on the Gleeble 1500, a thermo-mechanical processing system that can provide high vacuum, thermomechanical cycling, and bonding force using compressed air or hydraulic loading system.

The two substrates (boron coated and uncoated) to be joined were brought into contact via carbon blocks on either side. Carbon blocks were used in order to provide effective thermal conduction between the water cooled copper blocks and the base metal. To prevent the formation of carbon-iron eutectic, niobium foil was inserted between the carbon blocks and the substrates. A K-type thermocouple, spot-welded to the substrate no more than 2 mm from the bondline, was used to monitor the bonding temperature.

Bonding was conducted at 1250 °C, above the binary Fe – B eutectic temperature of 1,174 °C in a 1.3 MPa vacuum atmosphere. Joining was performed using the base metal in both the unrecrystallized fine grain (FG) and recrystallized coarse grain (CG) forms. Compressive stresses of 1-5 MPa were used to extrude the excess liquid formed at the bondline.

4.2.3 Post Bond Heat Treatments

After the bonding process, post bond heat treatment (PBHT) was conducted in order to induce controlled recrystallization across the bondline. PBHT was performed in a radiantly heated Brew furnace, in a vacuum, under a pressure of 1.3 MPa, at 1300 °C and 1385 °C, the recrystallization temperatures of for MA956 and PM2000 respectively.

4.2.4 Metallographic Preparation

After PBHT, the samples were cut using a Struers Accutom-5 precision cutting machine and were mounted using a Labopress-3. The samples were ground to a 1200

FEPA grit finish and then polished using a 6 μm diamond spray, followed by a 0.04 μm alumina suspension solution. Polishing of the samples was done using a TegraSystem autopolisher. The samples were then water cleaned and air dried, followed by etching at room temperature in a solution of 40 vol.% hydrochloric acid and 60 vol.% methanol for 2 - 10 seconds and further cleaned with water.

4.2.5   Microstructural Characterization

The samples, both as-bonded and PBHT, were primarily characterized using light microscopy (LM) and scanning electron microscopy (SEM), supplemented with SEM based energy dispersive X-ray spectroscopy (EDS). These studies were conducted on a JEOL JSM840 instrument operated at an accelerating voltage of 20 kV. Secondary electron imaging (SEI) was used to collect all SEM micrographs. The SEM based EDS analysis used ultra-thin window detectors and Oxford Instruments ISIS analyzers. EDS analysis was used to determine the composition of phases observed in the bond-line and compositional profiles across the joint and detection of porosity or secondary phases.

4.2.6   Oxidation Studies

The excellent high temperature oxidation resistance of ferritic ODS alloys results from the formation of the stable, adherent alumina scale formed during the high temperature exposure. The yttria present in the matrix plays a significant role in the adhesion of the alumina scale [42-46]. In order to study the effect of TLP bonding on the oxidation resistance of the ODS alloy (PM 2000), oxidation tests were conducted on the bulk material to provide a baseline for comparison.

Samples with dimensions of 10 mmx9 mm and 2 mm in thickness were cut using EDM and the Accutom-5. The samples were surface ground to remove the oxide layer.

The samples were exposed to air at 1200 ^{0}C for 6, 12, 24, 48, 96 hours. The weight of the samples was measured before and after oxidation. The samples were then cut using the Accutom-5 apparatus mounted using Labopress-3, and polished as explained in section 4.2.4. The bonds were then characterized using SEM, EDS, and LM.

4.2.7 Mechanical Testing

Shear testing was perfomed using the rig designed by Yan and Wallach, as explained previously in section 4.1.7.1.

.

5 RESULTS AND DISCUSSION

5.1 Nickel-based superalloys

5.1.1 Microstructural Characterization

5.1.1.1 Porosity at the bondline

The results of bondline porosity for joints incorporating the two different composite interlayers Niflex-110 and Niflex-115, were compared to those joints obtained using a conventional BNi-3 interlayer.

5.1.1.1.1 Niflex-110 interlayer:

Microstructural studies showed that all of the TLP bonds between CMSX-4 - IN 738 and CMSX-4 – IN 939 with a Niflex-110 wide-gap style interlayer formed an eutectic along the grain boundaries of the Niflex core, as shown in Figures 9(a) and 10(a). After allowing time for isothermal solidification and solid-state homogenization, non-bonded regions were seen at the substrate-interlayer interface.

This grain boundary eutectic formation infers that a competition existed between wetting of the faying surfaces and eutectic formation in the grain boundaries of the Niflex core, thus leaving non-bonded regions at the interface. Note that, once formed, these pores did not change with time at the bonding or post-bond heat treatment temperature

and so probably are not Kirkendall pores. The pores were visible before etching and so are not etching artifacts, although etching did change the shape of the pores somewhat by removing adjacent γ' and hence leaving a facetted appearance. Additionally, the grain boundary dissolution of the composite interlayer leads to an increase in the solid-liquid interfacial area, permitting the interlayer elements to readily diffuse from the liquid phase into the interlayer's matrix, ultimately reducing the amount of liquid available for spreading, resulting in porosity at the substrate-interlayer interface.

As mentioned in the literature review, a key parameter in the wide gap bonding process is the selection of the ratio of liquid former to non-melting phase for the substrates to be joined. Thus, if insufficient liquid former is employed, the liquid will begin to isothermally solidify, and hence cease to spread, before it has been able to penetrate throughout the joint. This would result in a joint with porosity, as shown in Figures 9(b) and 10(b).
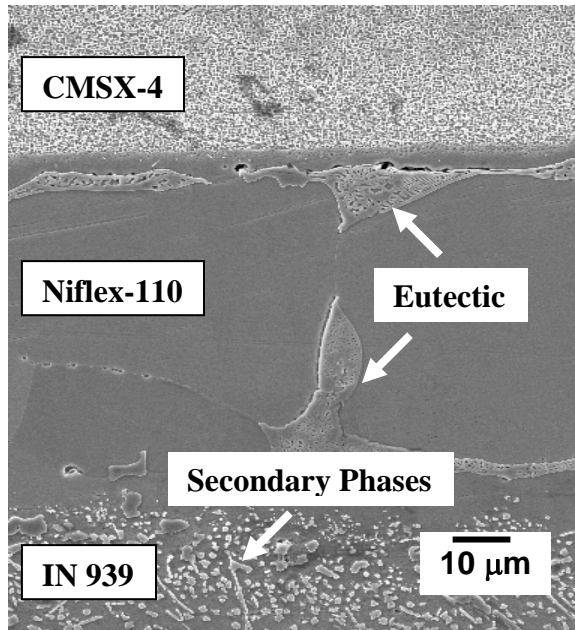
(a)
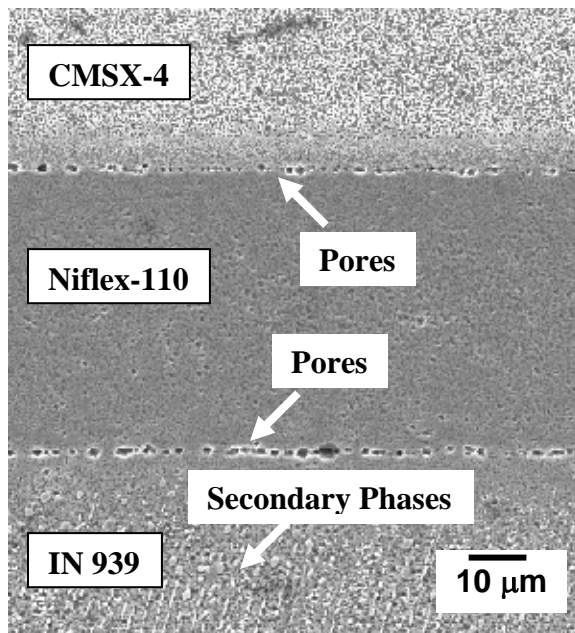
(b)

Figure 9 - SEM micrographs in SEI mode, of CMSX-4 -Niflex-110 – IN 939 joint showing (a) grain boundary eutectic formation after 0 minutes at 1160 ^{0}C and (b) porosity on the substrate- interlayer interface in the initial stages after 4 minutes at 1160 ^{0}C. The secondary phases in the diffusion zone of the polycrystalline substrate are also shown
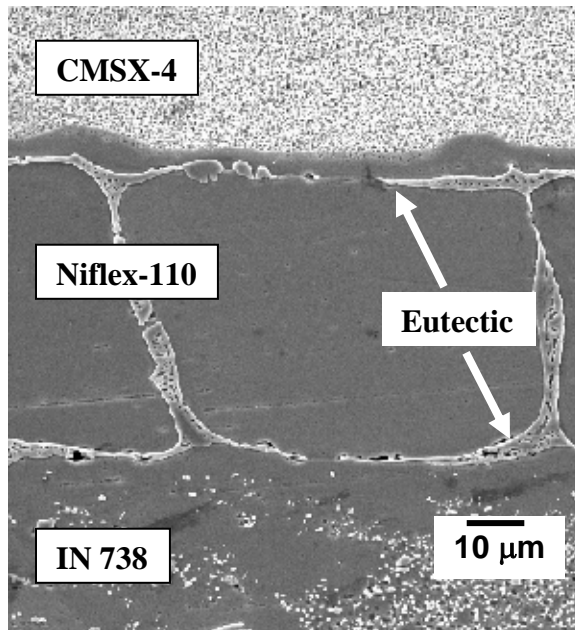
Figure 10(a)
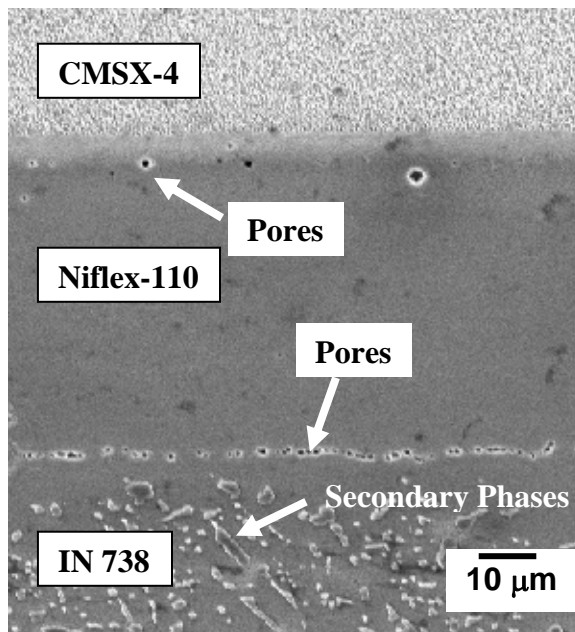
Figure 10(b)

Figure 10 -SEM micrographs in SEI mode, of CMSX-4 -Niflex-110 – IN 738 joint showing (a) grain boundary eutectic formation after 0 minutes at 1160 ^{0}C and (b) porosity on the substrate- interlayer interface after 4 minutes at 1160 ^{0}C. The secondary phases in the diffusion zone of the polycrystalline substrate were also shown.

5.1.1.1.2 Niflex-115 interlayer:

The microstructural studies of the bonds made using Niflex-115 interlayer also showed the formation of eutectic along the grain boundaries of Niflex core, as illustrated in Figure 11(a). However, no porosity was seen in the bonds made using a Niflex-115 interlayer. This can be attributed to the higher boron content in the Niflex-115 interlayer available for wetting of the faying surfaces as compared to Niflex-110. Although, eutectic formation was seen at the grain boundaries of Niflex-115, the greater amounts of liquid present at the interface eliminated the problem of non-bonded regions. The same behavior was observed both in CMSX-4 – IN 738 and CMSX-4 – IN 939 joints.

5.1.1.1.3 BNi-3 interlayer:

Microstructural studies of bonds employing a conventional BNi-3 interlayer showed that the bonds were free of non-bonded regions as shown in Figure 12(a). This can be attributed to the nature of the interlayer. BNi-3 is an interlayer with a completely melting core and boron distributed throughout the foil, unlike the two composite interlayers which had boron only at the outer surfaces. Thus, the amount of liquid formed at the bondline is higher than that obtained for a composite interlayer and this helps in better wetting of the faying surfaces, thereby resulting in the elimination of non-bonded regions. Although BNi-3 foil, as expected, did not show any porosity or premature isothermal solidification, formation of borides at the bondline was observed with the BNi-3 foil interlayer. This will be discussed in detail in Section 5.1.1.2.

Although it is desirable from the standpoint of reducing the amount of MPD that must be diffused, reducing the boron content of the interlayer results in an insufficient

boron content, which leads to insufficient liquid for wetting and to premature isothermal solidification. On the other hand, a high boron content might result in the formation of borides at the bondline and in the diffusion zone of the substrates. Therefore, it is necessary to optimize the amount of boron in the interlayer. BNi-3 contains boron throughout its thickness, whereas Niflex-115 and Niflex-110 contain boron-rich surfaces and a boron free core; the net effect is a reduction of the amount of boron that must be diffused per unit gap width. In summary, higher boron content foil (BNi-3) produced good joint after wetting, but the comparatively low boron content foil Ni-Flex 110, showed a significant amount of porosity at the substrate-interlayer interface. This problem was overcome by using a relatively boron-rich Niflex-115 wide gap style composite interlayer.
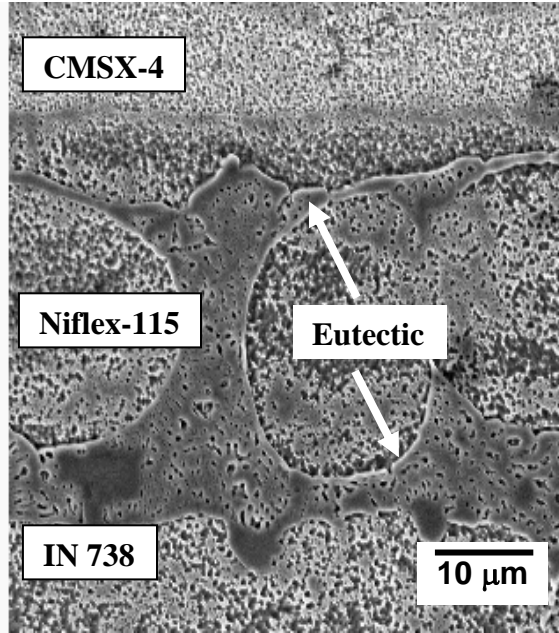
(a)
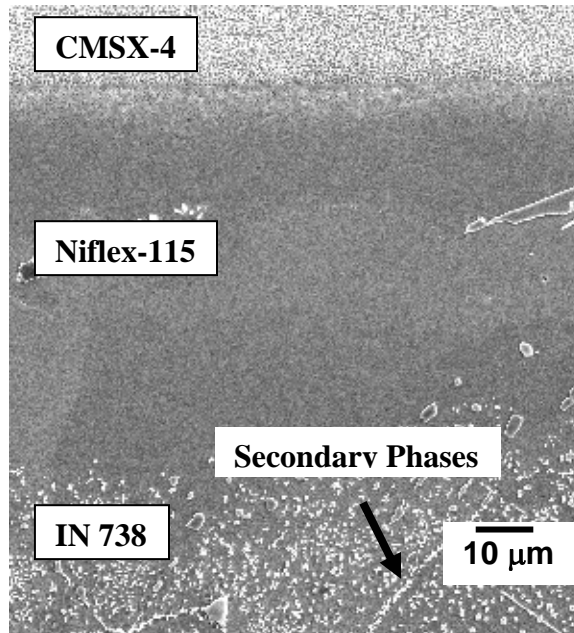
(b)

Figure 11- SEM micrographs in SEI mode, of CMSX-4 -Niflex-115 – IN 738 joint showing (a) grain boundary eutectic formation after 0 minutes at 1160 ^{0}C and (b) substrate- interlayer interface with no porosity after 60 minutes at 1160 ^{0}C. The secondary phases in the diffusion zone of the polycrystalline substrate are also shown.
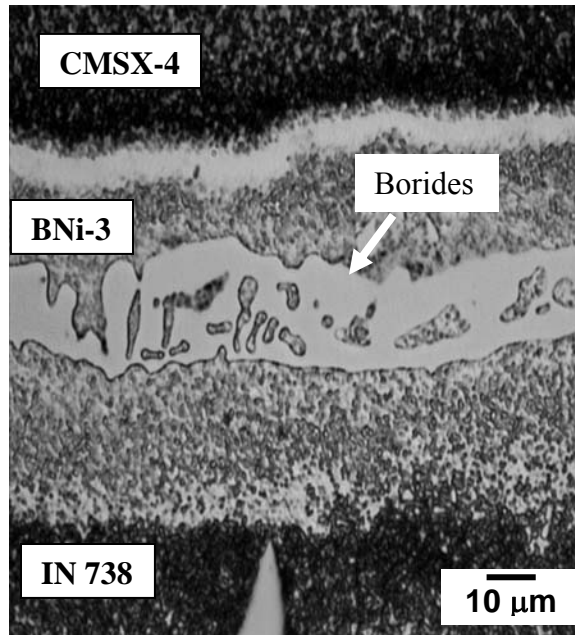
(a)
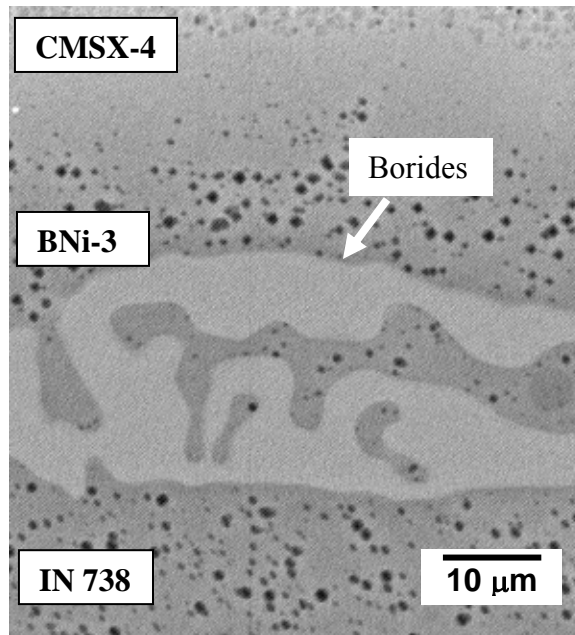
(b)

Figure 12 – (a)LM micrograph of CMSX-4 – BNi-3 – IN 738 after 0 minutes at 1160 ^{0}C, showing borides at the bondline. No grain boundary eutectic formation was observed. (b) SEM micrograph in BEI mode after 0 minutes at 1160 ^{0}C, showing borides at the bondline. The substrate- interlayer interface here is free of non-bonded regions.

5.1.1.2   Bondline Boride Formation

Borides are hard, brittle intermetallics formed during the heat ramp up stage of the bonding process and/or during cooling of the joint. These secondary phases formed in the joint may have undesirable effects on bond properties, for example decrease in bond strength.

Microstructural investigations of bonds made using BNi-3 foil as an interlayer confirmed the formation of borides at the bondline during the initial stages of bond formation as shown in Figure 12(a) and (b). Even after holding for sufficient time for isothermal solidification and solid-state homogenization to occur, residual borides were still visible at the bondline. In contrast, bondline boride formation was suppressed by using wide-gap style interlayers, as shown in Figures 9, 10, and 11.

The suppression of borides in composite interlayers can be attributed to their structure, with boron present on either side of the non-melting core, unlike the conventional BNi-3 foil interlayer, where boron is distributed uniformly throughout the interlayer with a fully melting core. Also, the amount of boron present in the composite interlayers is relatively low compared to a BNi-3 foil interlayer. Hardness tests on the bondline of the joints made using a BNi-3 foil interlayer resulted in high hardness values, as shown in Figure 13. Microstructural investigations using SEM on the tested samples revealed that borides were present at the joint.

5.1.1.3   Microstructural Bond Development

As mentioned in section 4.2.2, interrupted bonding runs were conducted in order to study the bond microstructural development. Bond development in the initial stages (0 minutes to 10 minutes), intermediate stages (60 min to 120 min), and final

stages (120-240 min) at bonding temperature (1160 ^{0}C), are discussed in turn below. The initial stage represents the eutectic formation and substrate dissolution. The intermediate stage represents isothermal solidification, where the MPD elements start diffusing into the substrates. The final stage represents solid stage homogenization that produces a uniform solute concentration at the bondline. Table 5 presents a summary of the microstructures observed in these three stages.

In the initial stages, when the wide gap style composite interlayer Niflex-110 was used to join CMSX-4 to IN 738 and IN 939, a eutectic was formed in the grain boundaries of the Niflex core as mentioned earlier in Section 5.1.1.1. [Figure 9(a) and Figure 10(a)]. As a result, a competition existed between liquid wetting the faying surfaces and the grain boundary eutectic formation which resulted in porosity in the bonds, that was overcome by using Niflex-115, which has boron content relatively higher than that of Niflex-110. When a BNi-3 interlayer was used to join CMSX-4 to IN 738 and IN 939, no porosity was visible at the substrate-interlayer interface due to the uniform distribution of boron and better wetting [Figure 12].

The wide-gap style interlayers Niflex-110 and Niflex-115 also resulted in the suppression of bondline boride formation. In comparison, the conventional BNi-3 interlayer resulted in substantial boride formation at the bondline in the initial stages (Figure 12), which was confirmed by a back scattered image of a CMSX-4 – IN 738 joint obtained using BNi-3 interlayer. In addition, a variety of second phases which are assumed to be borides/carbides/TCP phases were formed in the substrate diffusion zone in the joints made using both composite interlayers and the conventional BNi-3

interlayer. This formation of secondary phases was observed in all of the interlayer and substrate combinations in the initial stages, and is shown in Figures 9 through 11.

In the intermediate stages (60 min-120 min), once time has been allowed for isothermal solidification to occur, the porosity at the bondline in Niflex-110 interlayer bonds was not eliminated, unlike that in bonds with the other two interlayers (Niflex-115 and BNi-3). This can be attributed to the competition mentioned earlier and the lower boron content present in the Niflex-110 interlayer compared to Niflex-115. On the other hand, in bonds using a BNi-3 interlayer, although some of the boron diffused due to isothermal solidification, borides were still present in the intermediate stages. In addition, secondary phases in the diffusion zone were present in the case of the CMSX-4 – IN 738 joint with BNi-3 foil, unlike the other two interlayers. However, for CMSX-4 – IN 939 joints, secondary phases in the diffusion zone were present for all of the interlayer combinations.

In the final stages of the bond formation, use of the Niflex-110 interlayer resulted in a joint with significant porosity at the substrate-interlayer interface as shown in Figure 14, secondary phases in the diffusion zone of the polycrystalline substrate in the case of the IN 939 joint, and with no borides at the bondline as shown in Figure 15. The other composite interlayer, Niflex-115, resulted in a joint with no porosity and no bondline borides although secondary phase formation was seen in the polycrystalline substrate diffusion zone when IN 939 was used as the polycrystalline substrate. (Figure 16(a) and the points of interest highlighted in Table 5). In contrast, BNi-3 foil interlayer bonds had numerous borides present at the bondline, and secondary phases present in the diffusion zone, although there was no porosity [Figure 16(b)]. A compositional analysis of the

composite interlayer bonds revealed a fairly uniform composition across the CMSX-4 –

Niflex-110 - IN 738 andCMSX-4 – Niflex-110 - IN 939 bondline after 240 minutes of

bondtime at 1160 ^{0}C, as shown in Figure 18 and Figure 19.

5.1.1.4 Secondary Phases in the diffusion zone

As mentioned in previous sections, a variety of second phases, which appear to

include borides/carbides and/or topologically close-packed (TCP) phases, were observed

to form in the substrate diffusion zone on the polycrystalline side of both the CMSX-4 –

IN738 and CMSX-4 – IN939 bonds, as shown in Figure 15 and Figure 16 respectively. In

the case of bonds involving IN738, the formation of these second phases could be

suppressed by increasing the bonding time to 4 h at 1160 ^{o}C when using either of the two

composite interlayers although these phases could not be avoided in the bonds using BNi-

3 foil as an interlayer, as shown in Figure 15. The compositional analysis done on a

CMSX-4 – Niflex-110 - IN 738 joint after 4 minutes of bonding time can be seen in

Figure 17. Chromium and cobalt peaks were observed in EDS spectra from the diffusion

zone of the polycrystalline substrate, which can be directly related to the secondary

phases seen in the microstructural studies.

In contrast, when bonding IN939, the second phases remained stable for all

times examined and for all the interlayers, including post-bond thermal exposures of up

to 1 week at 1,000 ^{o}C, which will be discussed in Section 5.1.5.2. These secondary

phases also had an impact on the mechanical properties of the bonds which will be

discussed in section 5.1.4. This is perhaps due to the high chromium content present in IN

939, since chromium can be involved in the formation of both borides and TCP phases.

Initial stages (0-10 minutes)					
Substrate	Interlayer	Eutectic formation in grain boundaries (gbs) of Niflex core	Porosity	Bondline boride formation	Secondary phases in diffusion zone of PC
CMSX-4 - IN 738	Niflex-110	Yes	Yes	No	Yes
CMSX-4 - IN 939	Niflex-110	Yes	Yes	No	Yes
CMSX-4 - IN 738	Niflex-115	Yes	No	No	Yes
CMSX-4 - IN 939	Niflex-115	Yes	No	No	Yes
CMSX-4 - IN 738	BNi-3	No	No	Yes	Yes
CMSX-4 - IN 939	BNi-3	No	No	Yes	Yes

Intermediate stages (60-120 minutes)					
Substrate	Interlayer	Eutectic formation in gbs of Niflex core	Porosity	Bondline boride formation	Secondary phases in diffusion zone of PC
CMSX-4 - IN 738	Niflex-110	No	Yes	No	No
CMSX-4 - IN 939	Niflex-110	No	Yes	No	Yes
CMSX-4 - IN 738	Niflex-115	No	No	No	No
CMSX-4 - IN 939	Niflex-115	No	No	No	Yes
CMSX-4 - IN 738	BNi-3	No	No	Yes	Yes
CMSX-4 - IN 939	BNi-3	No	No	Yes	Yes

Final stages (240 minutes)					
Substrate	Interlayer	Eutectic formation in gbs of Niflex core	Porosity	Bondline boride formation	Secondary phases in diffusion zone of PC
CMSX-4 - IN 738	Niflex-110	No	*Yes*	No	*No*
CMSX-4 - IN 939	Niflex-110	No	*Yes*	No	Yes
CMSX-4 - IN 738	Niflex-115	No	No	No	*No*
CMSX-4 - IN 939	Niflex-115	No	No	No	Yes
CMSX-4 - IN 738	BNi-3	No	No	*Yes*	*No*
CMSX-4 - IN 939	BNi-3	No	No	*Yes*	Yes

Table 5: Microstructural bond development, for all substrate-interlayer combinations (CMSX-4 – IN 738 and CMSX-4 – IN 939 with Niflex-110, Niflex-115, BNi-3) {Italics signify the microstructural features that influenced mechanical properties}
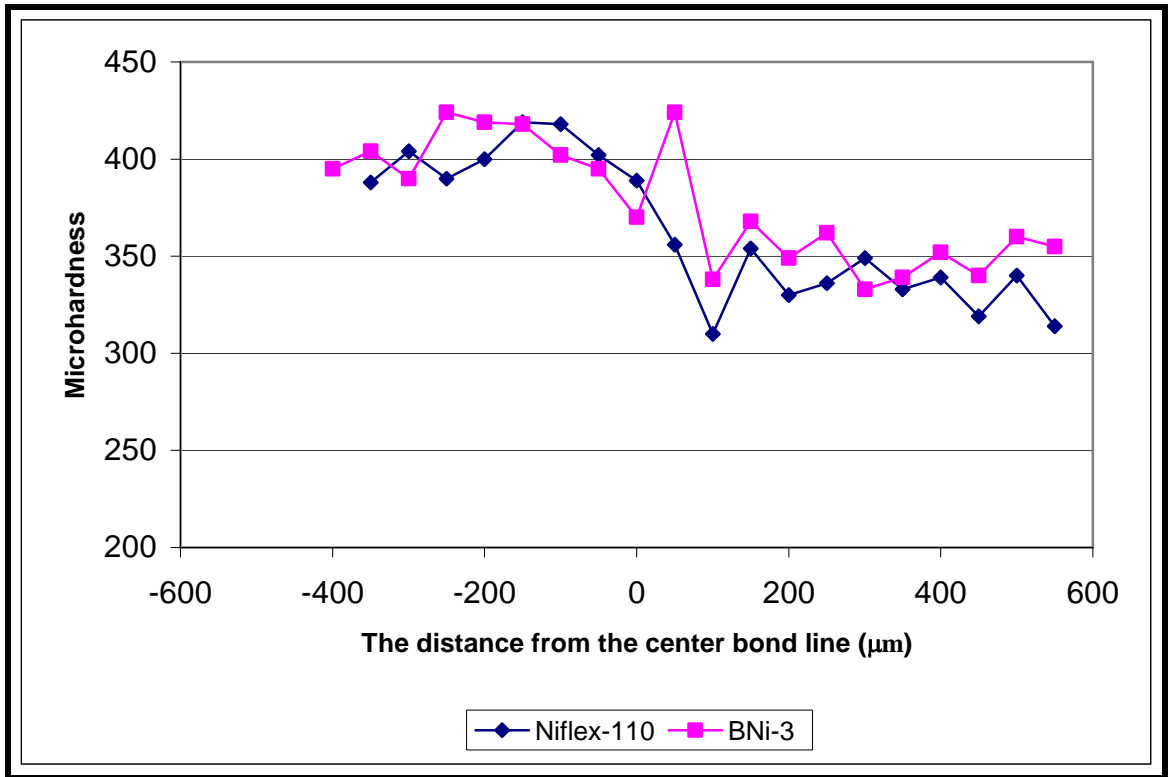
Figure 13: Comparison of Vickers microhardness across bondline of CMSX-4 – IN 939 bond after 240 minutes at 1160 ^{0}C using Niflex-110 and BNi-3 foil interlayers. Note the high hardness values for the BNi-3 joint, that might be due to the borides present.
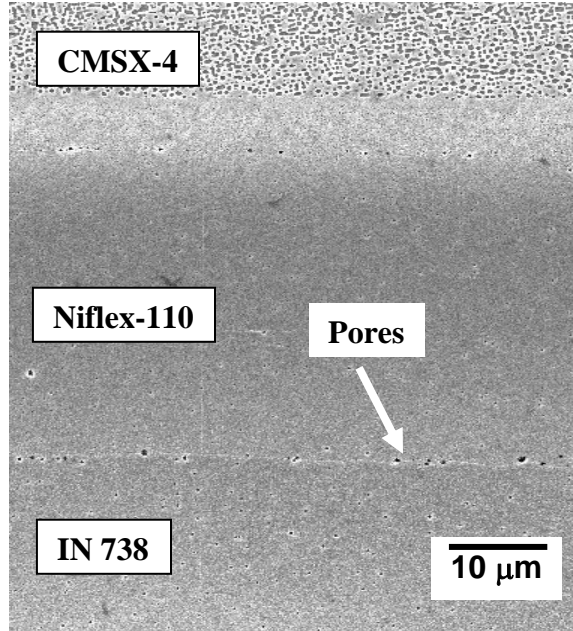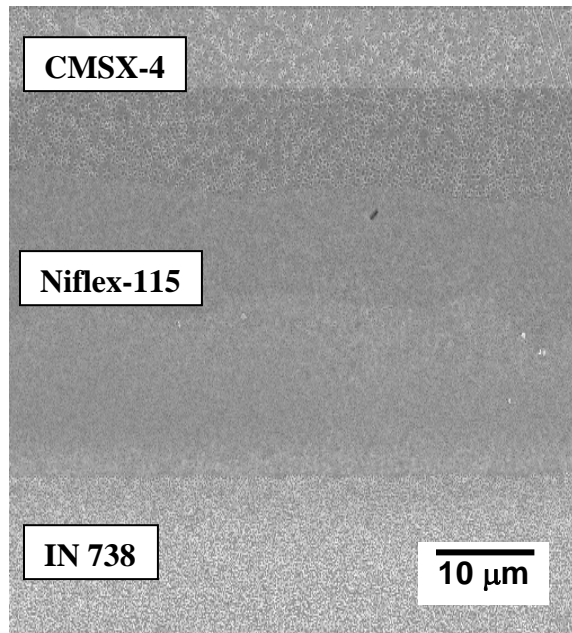
Figure 14: SEM micrographs in SEI mode, of CMSX-4 – IN 738 bonds after 240 minutes at 1160 ^{0}C showing (a) porosity at the bondline in Niflex-110 and (b) bond free from porosity and free from secondary phases in the diffusion zone, using Niflex-115 interlayer.
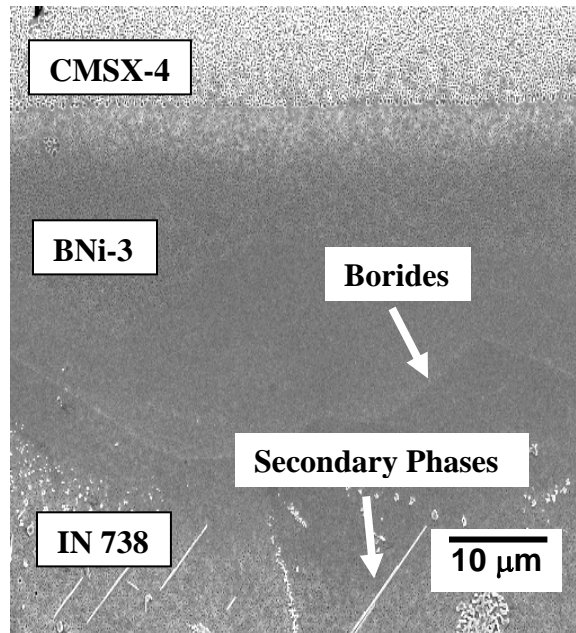
Figure 15: SEM micrographs in SEI mode, of CMSX-4 – BNi-3 - IN 738 bond after 240 minutes at 1160 ^{0}C, showing borides at the joint and secondary phases in the diffusion zone of IN 738.
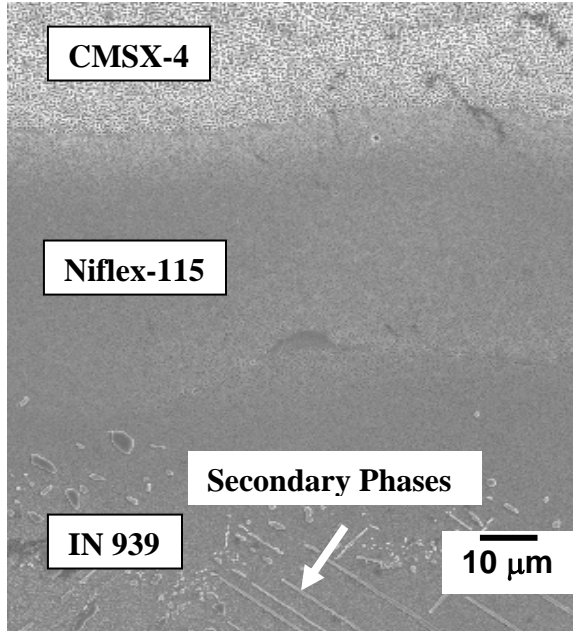
(a)
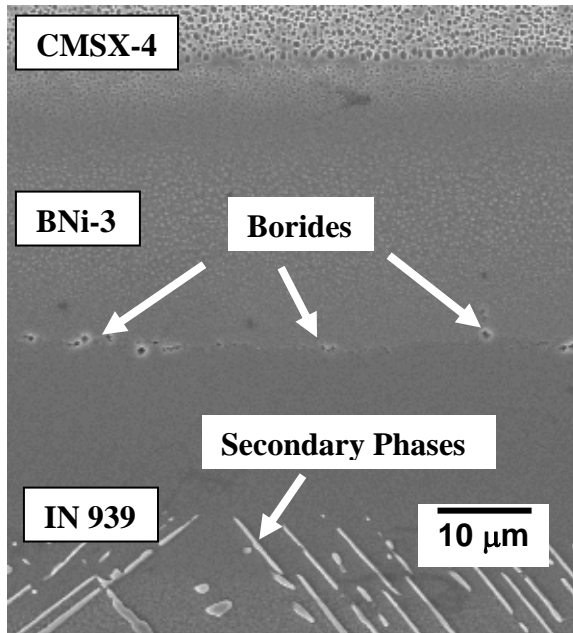
(b)

Figure 16: SEM micrographs in SEI mode, of CMSX-4 – IN 939 bond after 240 minutes at 1160 ^{0}C showing (a) secondary phases in diffusion zone of polycrystalline substrate in Niflex-115 interlayer bond, and (b) borides at the joint and secondary phases in the diffusion zone of IN 939, for bonds using BNi-3 interlayer.
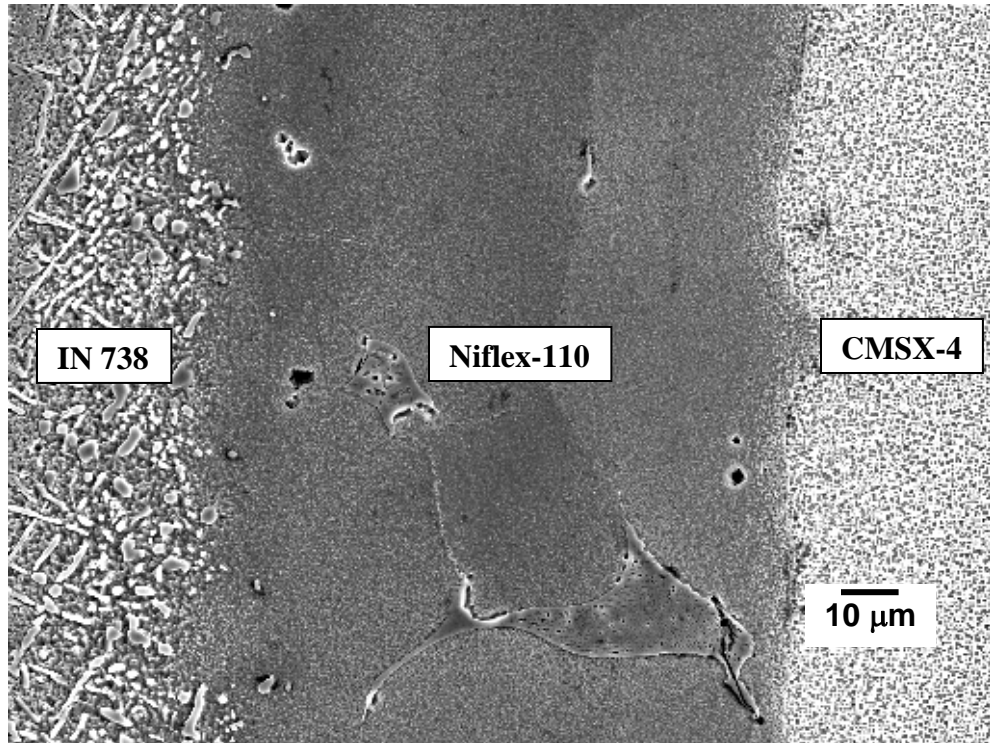
(a)
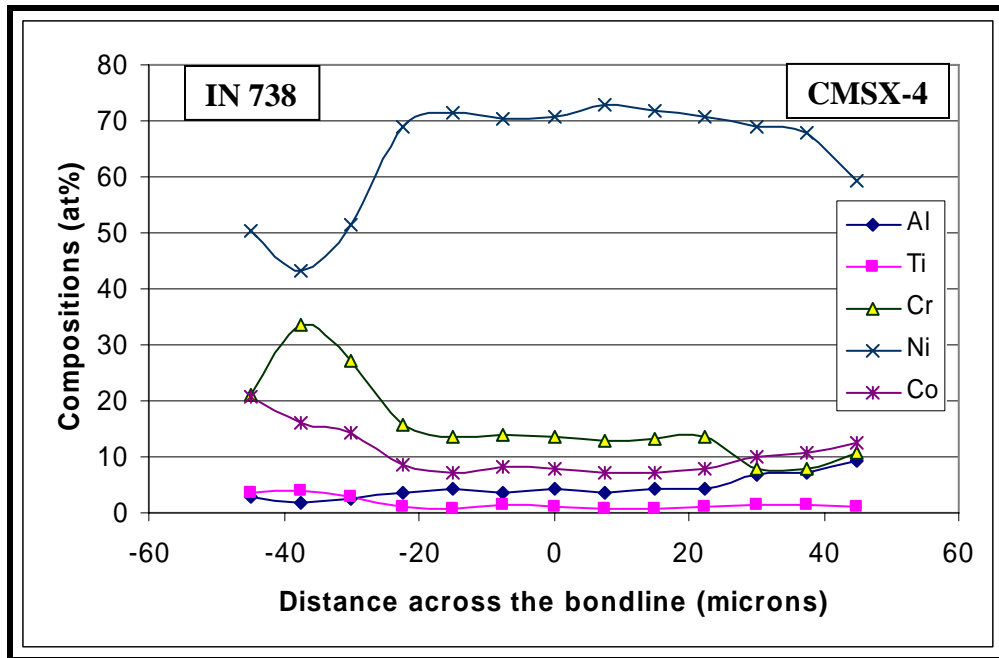
(b)

Figure 17: Composition profile, obtained using SEM-based EDS analysis, across bondline of CMSX-4 – Niflex-110 – IN 738 joint after 4 minutes of bonding time at 1160 ^{0}C Note the chromium and cobalt peak observed at the diffusion zone of the polycrystalline substrate that might be carbides, borides, TCP phases formed.
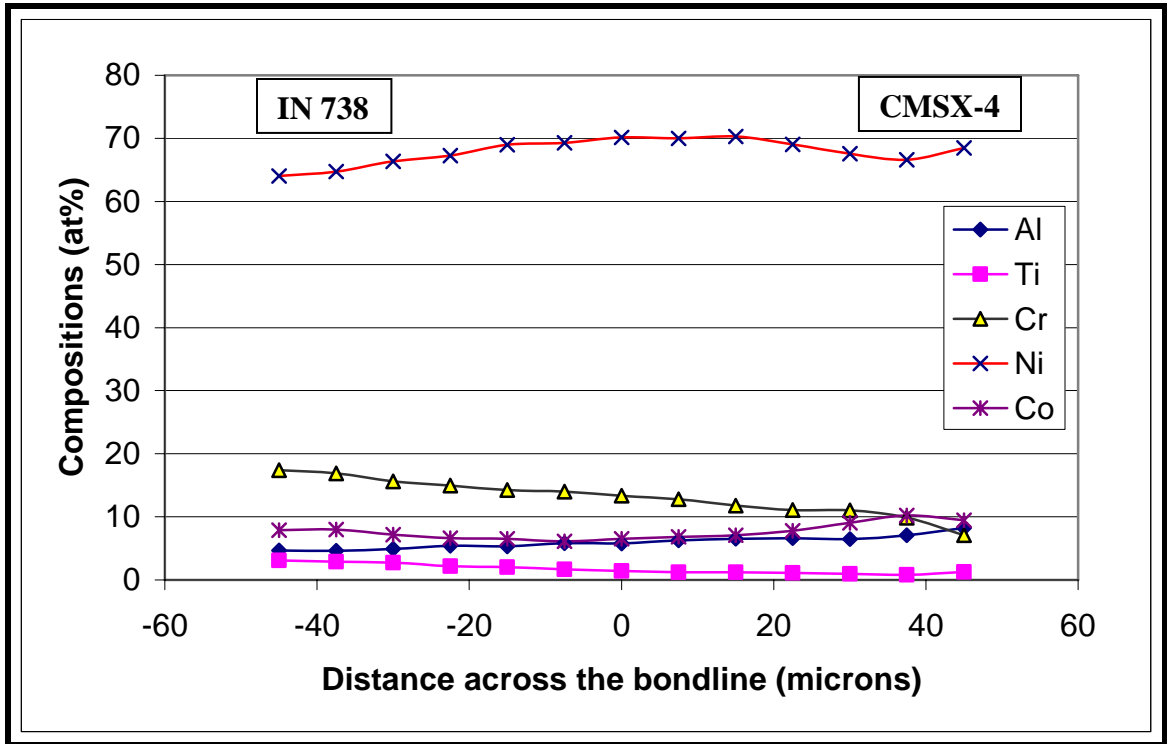
Figure 18: Composition profile obtained using SEM-based EDS analysis, across bondline of CMSX-4 – Niflex-110 – IN 738 joint after 240 minutes of bonding time at 1160 ^{0}C. Notice that the composition of the joint is fairly uniform after allowing time for isothermal solidification.
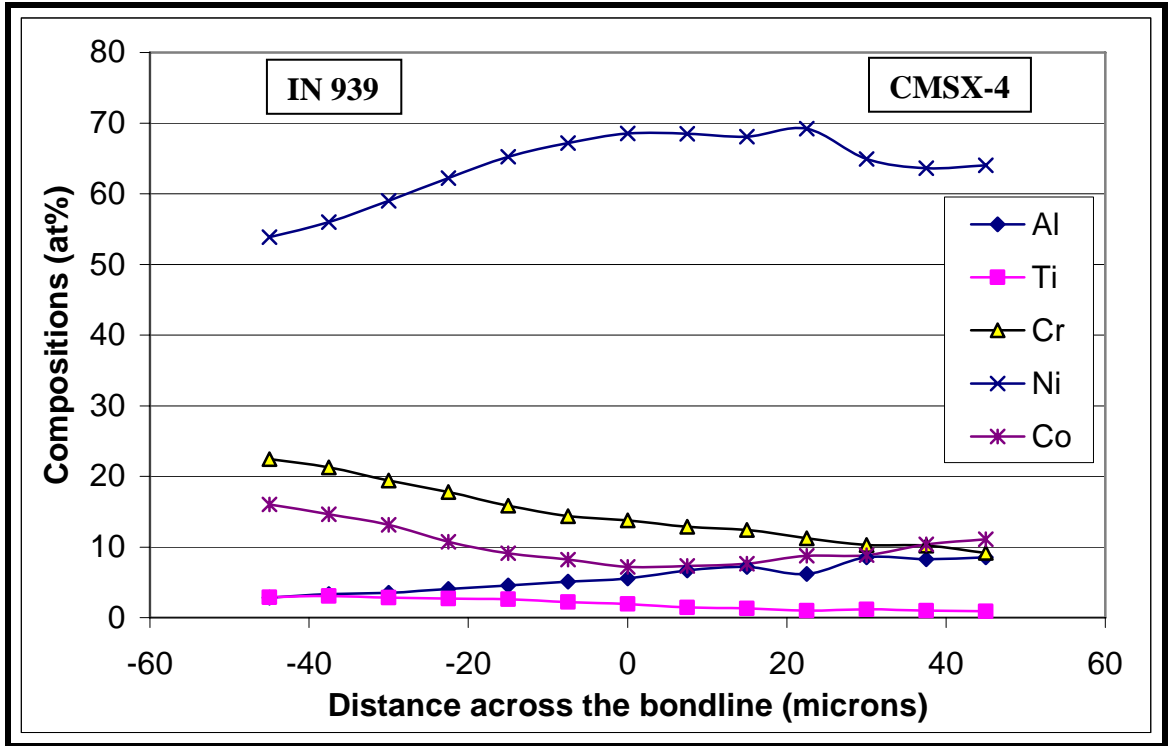
Figure 19: Composition profile obtained using SEM-based EDS analysis, across bondline of CMSX-4 – Niflex-110 – IN 939 joint after 240 minutes of bonding time at 1160 ^{0}C. Notice that the composition of the joint is fairly uniform after allowing time for isothermal solidification.

5.1.2   Comparison with the wettability studies

The results of the microstructural investigations performed for this study were correlated with the results of wettability studies conducted by Chitti et al. [131]. The eutectic formation in the grain boundaries of the Niflex core, which was in competition with the wetting of the faying surfaces of the composite interlayers, was also evident in the cross sections of the wetted samples, as shown in Figure 20 and Figure 21. As mentioned in Section 5.1.1.1.1, the non-melting core acts as a sink for boron diffusion. With a Niflex-110 interlayer, due to the competition between the wetting of the faying surfaces and the grain boundary liquid formation, the available boron content was insufficient to wet the faying surfaces, leading to premature isothermal solidification. In addition, the grain boundary dissolution of the composite interlayer led to an increase in the solid-liquid interfacial area. This resulted in an increase in the rate of boron loss from the liquid and consequent diffusion into the substrate matrix, ultimately reducing the amount of liquid available for spreading and resulting in porosity at the substrate-interlayer interface.

Wettability studies also confirmed the formation of secondary phases in the diffusion zone of the polycrystalline substrate. This can be seen in Figure 20(b) and Figure 21(b). Due to the high heating rates employed in the wettability studies, the formation of borides/carbides during heating ramp up would be minimal, so the secondary phases such as borides and carbides are likely to have been formed during cooling of the joint to room temperature.

Wettability studies also confirmed the formation of bondline borides. In general, high heating rates [high temperature increments per unit time] are employed to avoid the

formation of borides during the heating stage. The hot stage light microscope with the high heating rates employed in the wettability studies, minimized boride formation during heating to the bonding temperature and thus any borides formed during cooling could be identified.

5.1.2.1 Effect of substrate on wettability

Wettability studies were conducted on single crystal CMSX-4 in unrecrystallized and recrystallized condition and on polycrystalline IN 738 and IN 939. All the three interlayers exhibited a greater extent of spreading on the single crystal alloy CMSX–4 when compared to the polycrystalline alloys IN 738 , IN 939 and recrystallized CMSX-4 [referred to here as CMSX-4 (R)] [Figure 23, Figure 24 and Figure 25]. The reduction in the extent of spreading of the liquid in CMSX-4 (R) compared to CMSX-4 can be attributed to two factors. The polycrystalline/recrystallized alloy contains grain boundaries, which are potential paths for the diffusion of interlayer species (boron), allowing it to easily diffuse into the substrate. In addition, substrate dissolution also occurs at the substrate grain boundaries which increases the solid-liquid interfacial area and hence hastens isothermal solidification. Note that as the homologous temperature increases, the relative role of preferential grain boundary diffusion as compared to bulk diffusion decreases. Given that bonding was conducted at approximately 85-90 % of the absolute melting point of the substrates, preferential grain boundary diffusion is unlikely to have made a very significant contribution to microstructural development. In contrast, grain boundary dissolution can have a marked effect.

In addition, the time taken for significant premature isothermal solidification and hence the termination of spreading was much lower for composite interlayers (Niflex-110

and Niflex-115 foils), when compared to the BNi-3 foil. [Refer to the difference in termination of spreading time in Figure 23, Figure 24 and Figure 25]. For instance, the termination of spreading for BNi-3 interlayer on CMSX-4 occurred approximately at 190 seconds, in contrast to 50 seconds and 115 seconds approximately for Niflex-110 and Niflex-115 interlayers respectively. This was because of the smaller amount of liquid available for wetting, as well as the preferential flow of the eutectic liquid into the interlayer grain boundaries in the composite interlayers, creating a competition in wetting between the interlayer non-melting core and the substrate itself. Figure 26 shows the spreading measurements of BNi-3 foil on CMSX-4 in two different runs under identical conditions, showing repeatability of spreading measurements.
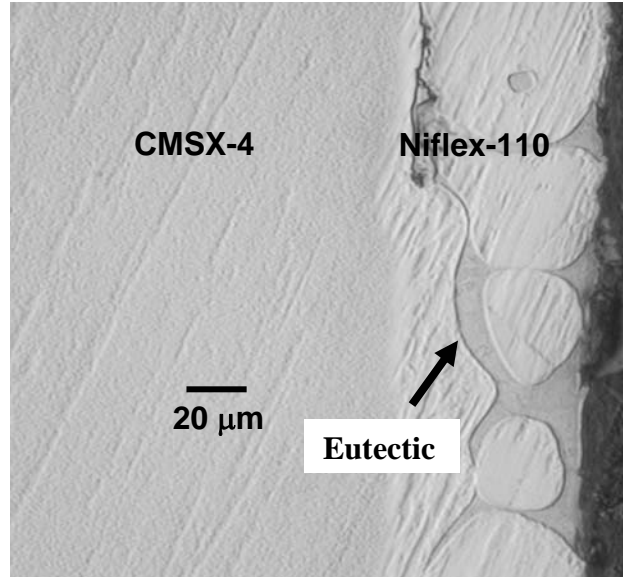
(a)
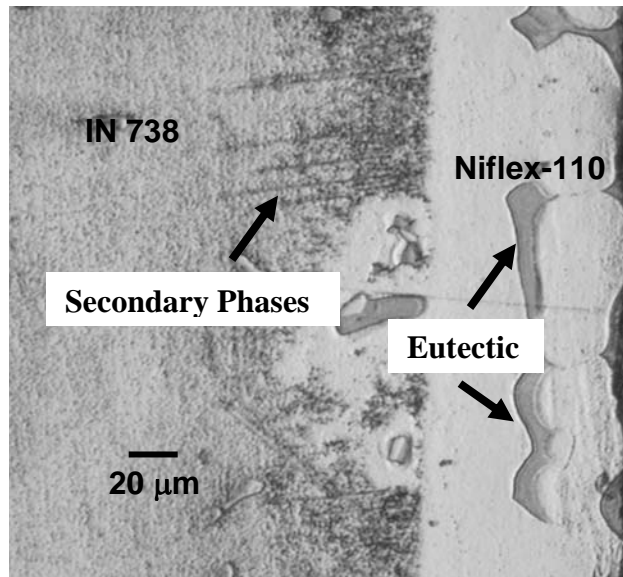
(b)

Figure 20: LM micrograph, showing eutectic formation in the grain boundaries of inner Niflex core for a Niflex-110 interlayer wetted on (a) CMSX-4 and (b) IN 738. The secondary phases formed in the diffusion zone of the polycrystalline substrate IN 738 are also visible [121].
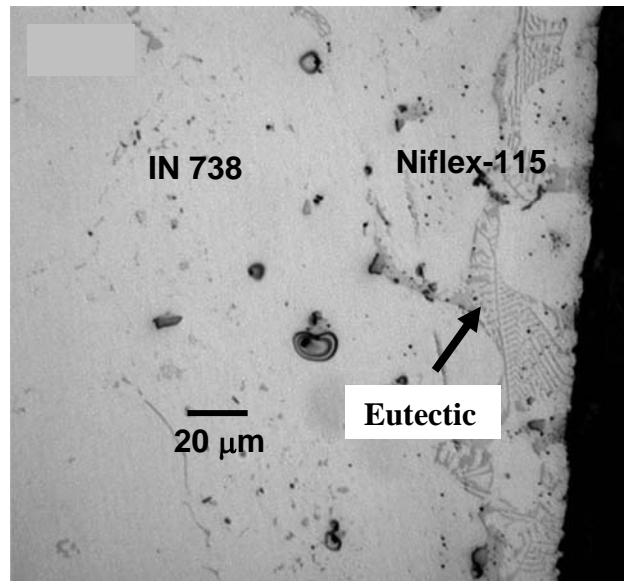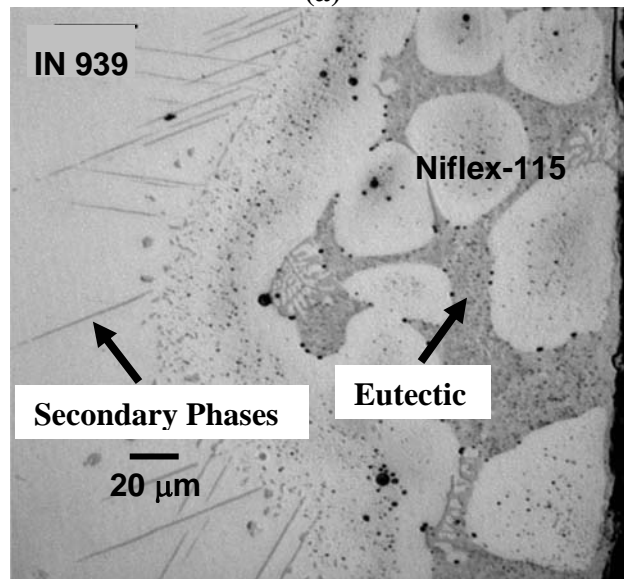
Figure 21: LM micrograph, showing eutectic formation in grain boundaries of inner Niflex core for Niflex-110 interlayer wetted on (a) CMSX-4 and (b) IN 939. The secondary phases formed in the diffusion zone of the polycrystalline substrate IN 939 are visible [121].
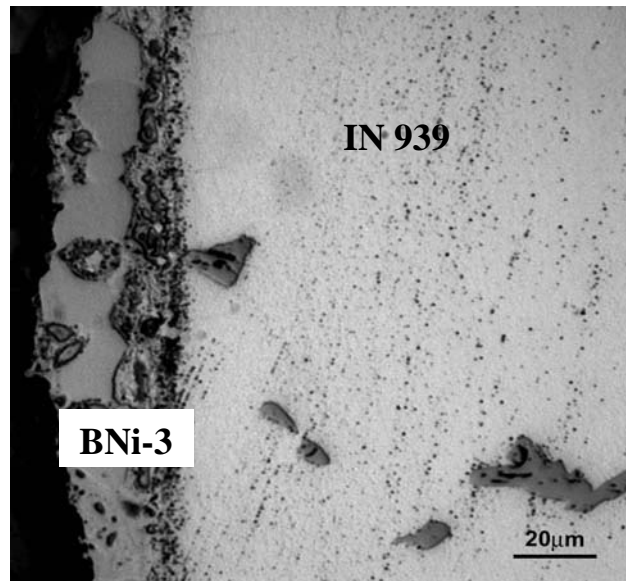
Figure 22: LM micrograph, of the cross-section of IN 939 wetted with BNi-3 foil showing the formation of borides at the joint interface [121].
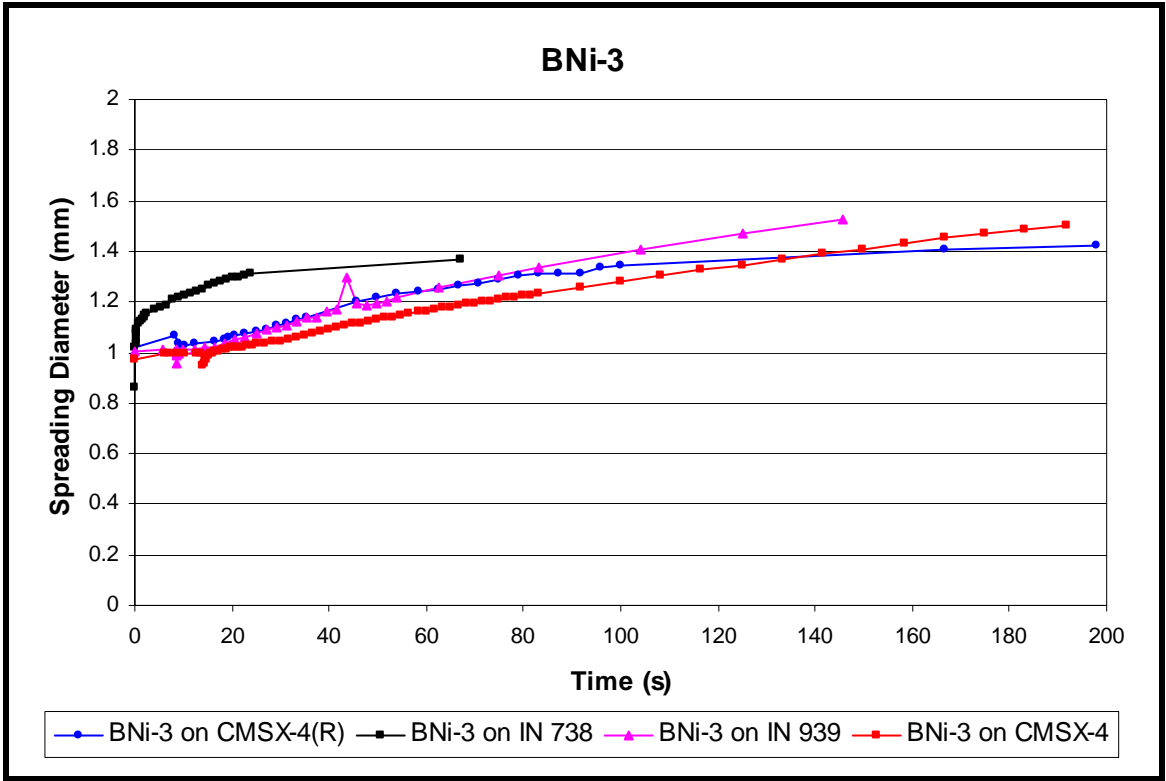
Figure 23: Wettability of BNi-3 on CMSX-4, IN 738 and IN 939 CMSX-4(R). [121]
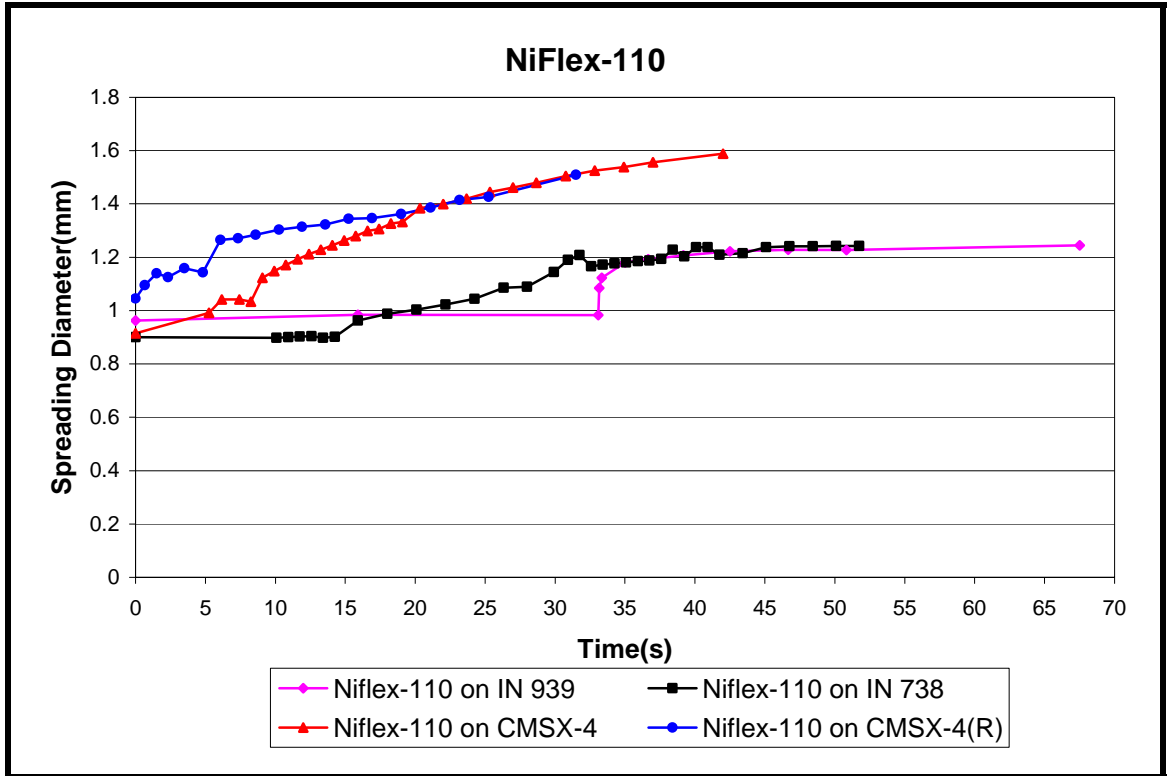
Figure 24: Wettability of Niflex-110 on CMSX-4, IN 738, IN 939 and CMSX-4(R). Compare this to previous Figure and notice the reduction in time required for termination of spreading compared to BNi-3 [121].
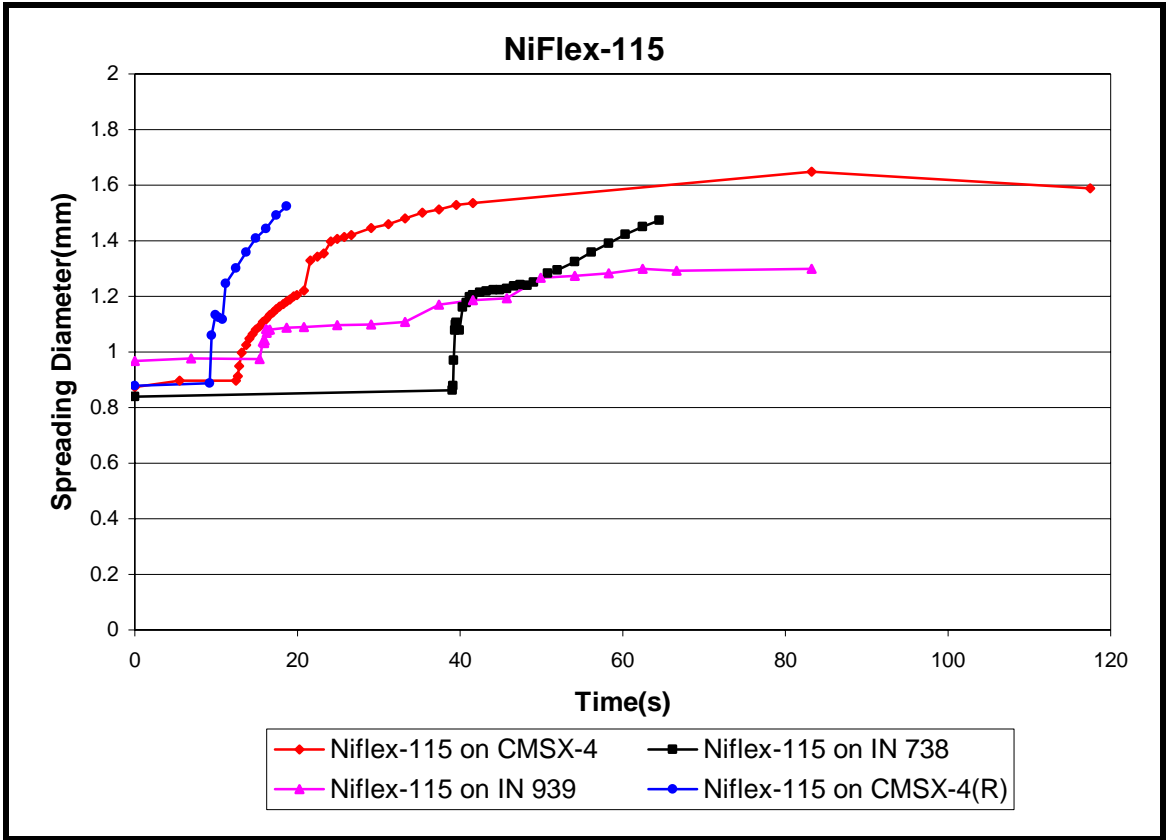
Figure 25: Wettability of Niflex-115 on CMSX-4, IN 738, IN 939 and CMSX-4(R). Compare this to previous two Figures and notice the reduction in time required for termination of spreading compared to BNi-3 [121].
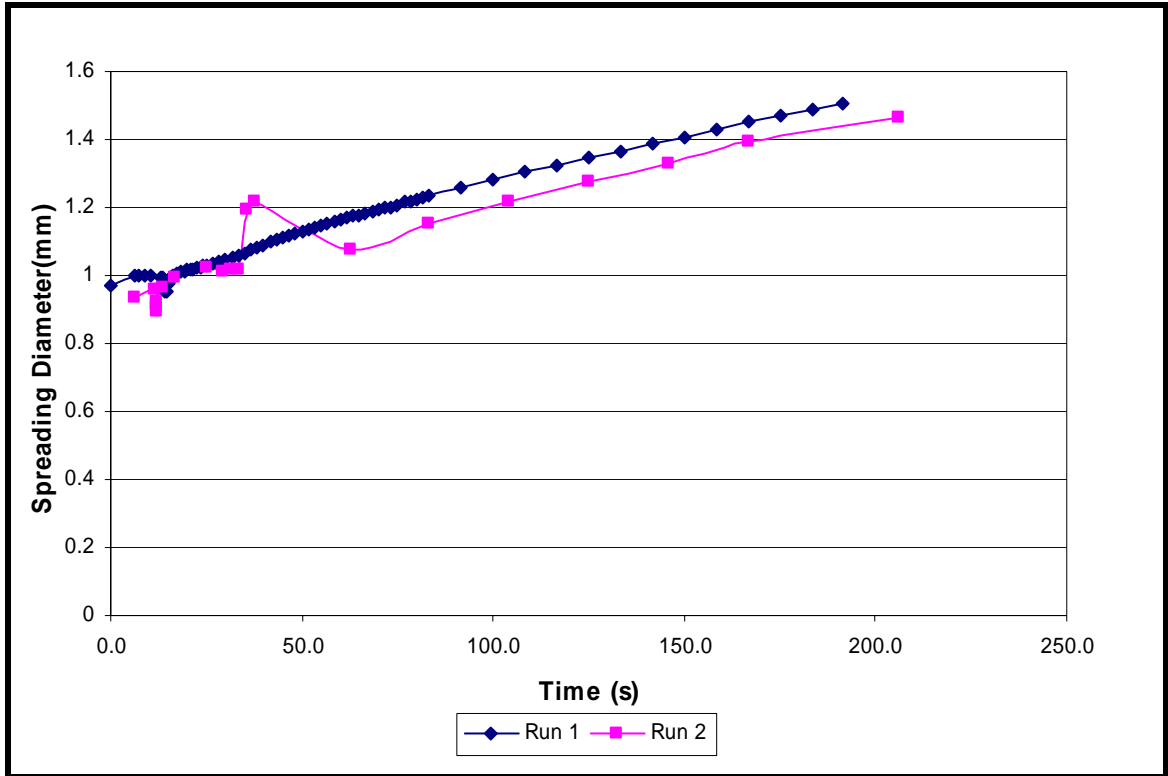
Figure 26: Wettability of BNi-3 on CMSX-4 on two different runs in identical conditions showing repeatability of data. [121].

5.1.2.2 Effect of Boron Content

Boron was used as the MPD in all three of the interlayer materials chosen. Although reducing the boron content of the interlayers is desirable from the standpoint of reducing the amount of MPD that must be diffused, an insufficient boron content also creates insufficient liquid for wetting, leading to premature isothermal solidification. On the other hand, a higher boron content is likely to result in increased isothermal solidification times leading to higher bonding process times, and also the formation of borides at the bondline and in the substrates. Therefore, it is important to carefully select the amount of boron in the interlayer. BNi-3 contains boron throughout its thickness, whereas Ni-Flex 115 and Ni-Flex 110 are composed of boron-rich surfaces on a boron free core; the net effect reduces the amount of boron that must be diffused per unit gap width. Spreading diameter vs. time plots revealed that the extent of spreading of the BNi-3 foil was greater compared to the other two foils. Post wetting SEM/EDS work on cross-sectioned samples of higher boron content foil (BNi-3) showed good joint with no porosity, but the comparatively low boron content foil, Ni-Flex 110 showed substantial porosity at the substrate-interlayer interface [Figure 9]. However, the problem was overcome by using a relatively boron-rich Niflex-115 interlayer.

5.1.2.3 Effect of Boride Formers

The primary boride formers in superalloys are molybdenum, titanium, chromium and nickel with molybdenum and titanium forming the most stable borides, followed by chromium and then nickel. Boride formation tends to cause premature isothermal solidification during bonding leading to porosity at the faying surfaces. Post wettability analysis showed the presence of significant amounts of titanium and chromium at the

outer rings of the solidified liquid on the IN 939 substrates which corresponded to borides, visible in cross-sections. This showed that some interdiffusion of the substrate and interlayer species did occur.

5.1.3 Gamma-prime at the bondline

In all the bonds examined, there was relatively little gamma-prime at the bondline when compared with the bulk substrates. This might be due to the lack of heat treatments to reform the γ', in the bonding cycle. For a given wide-gap interlayer, more gamma-prime was formed at the bondline of CMSX-4 – IN939 when compared to that of CMSX-4 – IN738, as shown in Figure 27 and Figure 28. This can be attributed to the difference in solution temperatures of the alloys (IN 939 and IN 738) and the cooling rates which might have affected the formation of γ'. The amount of gamma-prime formed at the bondline, did however have an impact on the mechanical properties of the bond, which will be discussed in the next section. This is suprising, given that IN 939 is lower in Al (1.9 wt% versus 3.4 wt%) and higher in chromium (22.4 versus 16 wt%) than IN 738, and it can only be assumed that the presence of γ' formers other than Al and γ stabilizers other than Cr must have influenced the overall behavior of the bonds.
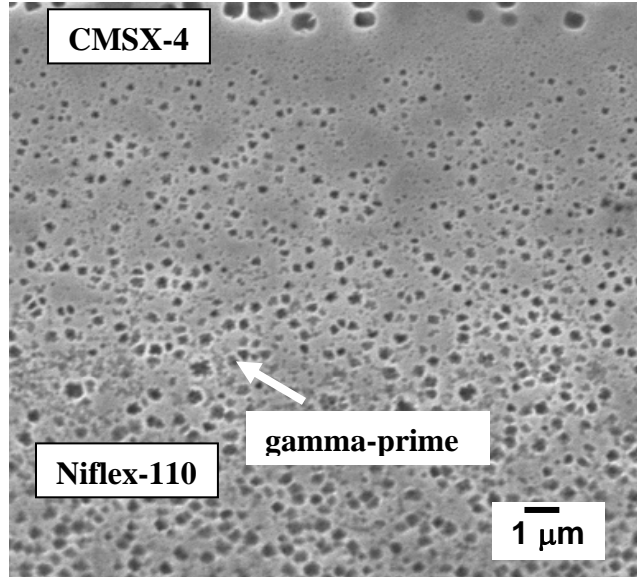
(a)
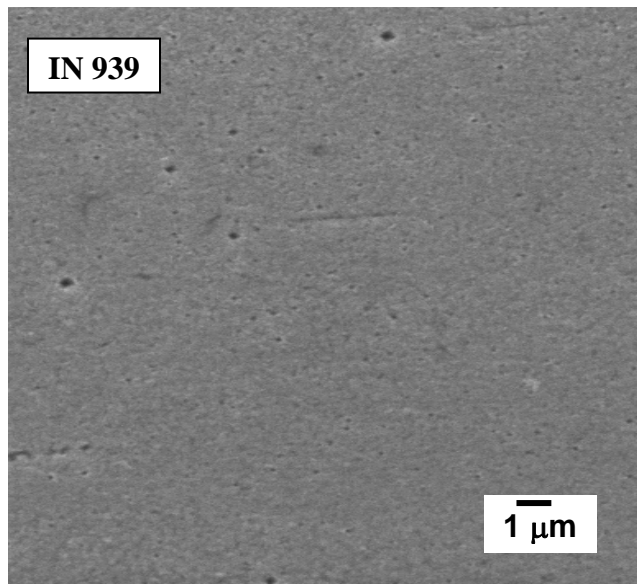
(b)

Figure 27: SEM micrographs in SEI mode, of CMSX-4 – Niflex-110 – IN 939 bond showing (a) gamma-prime (γ') at the bondline (b) Polycrystalline substrate IN 939 of the bond with no resolvable (γ').
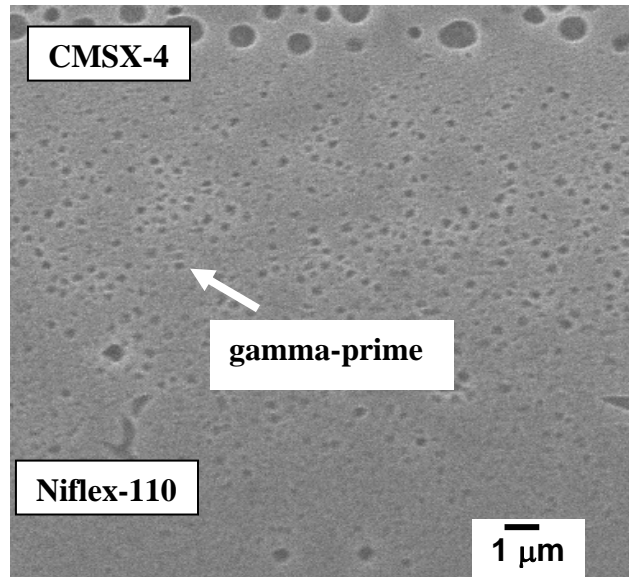
(a)
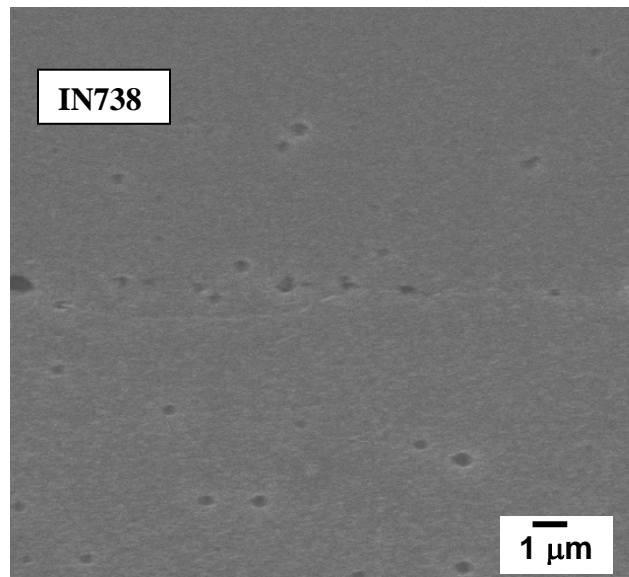
(b)

Figure 28: SEM micrographs in SEI mode, of CMSX-4 – Niflex-110 – IN 738 bond showing (a) gamma-prime (γ') at the bondline (b) Polycrystalline substrate IN 738 of the bond with no resolvable (γ').

Notice the smaller amount of γ' on IN 738 bondline when compared to IN 939 bondline [Figure 27]

5.1.4 Structure-Property Relationships of As-bonded TLP bonds

5.1.4.1 Shear tests

Before conducting shear tests on as-bonded samples, bulk samples were machined from as-received substrates and tested using a shear rig. For this study, IN 939 and IN 738 substrates were machined and shear tested, to serve as a baseline for a comparison of the bond strengths for CMSX-4 – IN 939 and CMSX-4 – IN 738 bonds respectively. Figure 29 shows fractographic images of a shear tested bulk IN 939 and IN 738 samples. The fracture path was macroscopically flat and was dominated by a ductile shear fracture with dimpling.

Shear testing conducted on as-bonded CMSX-4 – IN 939 resulted, on an average of 92% of the bulk shear strength and 69% of the UTS of the weakest bulk material in the bond (in this case IN 939) [Table 6]. Shear testing of CMSX-4 – IN 738 resulted, on an average of 73 % of the bulk shear strength and 55% of the UTS of the weakest bulk material in the bond [Table 7].

A schematic showing the crack path upon application of shear force is given in Figure 30. Figure 32 shows fractographic images of shear tested CMSX-4 – Niflex-110 – IN 939 and CMSX-4 – Niflex-110 – IN 738 bonds. A ductile shear fracture was seen on the bondline in all of the bonds. In the CMSX-4 – IN 939 bonds, secondary cracking was seen on the fracture surfaces in addition to the ductile shear, which is also shown in Figure 31. In addition, no secondary cracking, but rather dimpling, was seen on the fracture surfaces of the CMSX-4 – IN 738 bonds as shown in Figure 32.

The shear testing of the as-bonded specimens correlated well with the microstructural investigations. The ductile shear fracture observed in all of the bonds can

be attributed to the insufficient γ' formation at the bondline. As mentioned earlier, the shear strengths of bonds between CMSX-4 – IN939 are higher than those of CMSX-4 – IN738 bonds. The higher shear strength of CMSX-4 – IN 939 relative to CMSX-4 - IN 738 using a Niflex-110 interlayer might be due to the greater amount of γ' formed at the bondline in the former. In addition, the secondary phases in the diffusion zone of the polycrystalline substrate of the bondline might have resulted in secondary brittle cracking in addition to the main ductile shear fracture for all the CMSX-4 – IN 939 bonds. In contrast, CMSX-4 – IN 738 bonds free of secondary phases in the diffusion zone showed no secondary cracking but rather dimpling on the fracture surfaces, as shown in Figure 32. No evidence was found for a role of the porosity observed at the faying surfaces in the shear strength of the bonds. However, it should be cautioned that this porosity could have a large effect on fatigue resistance, although this was not investigated here.

From the above observations, on CMSX-4 – IN 939 and CMSX-4 – IN 738, the extent of bondline gamma-prime formation (relatively high in bonds with IN 939, low in bonds with IN 738) would appear to be more important for the room-temperature properties than the presence of brittle second phases in the polycrystalline substrate (which are invariably present in IN 939, but avoidable with a suitable bonding treatment in IN 738). Also, fatigue tests conducted on aluminide coated superalloys by Veys et al., and Grunlig et al., [122, 123] revealed that, brittle secondary phases present in the transition zone (similar to the secondary phases present in the diffusion zone in the current observations) were expected to change the final crack path and behavior of fatigue crack originated at a surface [124].

5.1.4.2 Hardness testing

The hardness profile of the bonds is presented in Figure 33, which shows that the Vickers microhardness of the bond line is similar to that of the IN 939, while the CMSX-4 alloy has a higher microhardness than the bond line and the IN 939. This infers that the formation of insufficient gamma-prime within the joint left a relatively soft bondline region, as is evident from the hardness data for the bond. Bonds made using a BNi-3 foil interlayer resulted in higher hardness values at the bondline compared to the bonds made using Niflex-110 and Niflex-115 interlayers. This can be attributed to the formation of borides at the bondline when the BNi-3 interlayer was used.
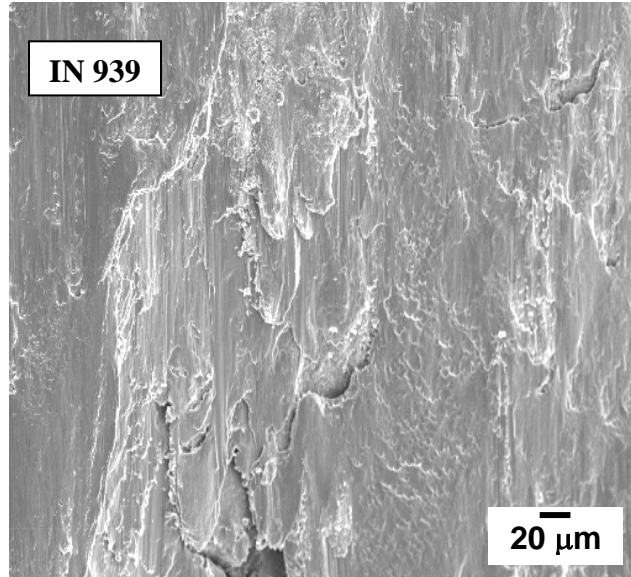
(a)
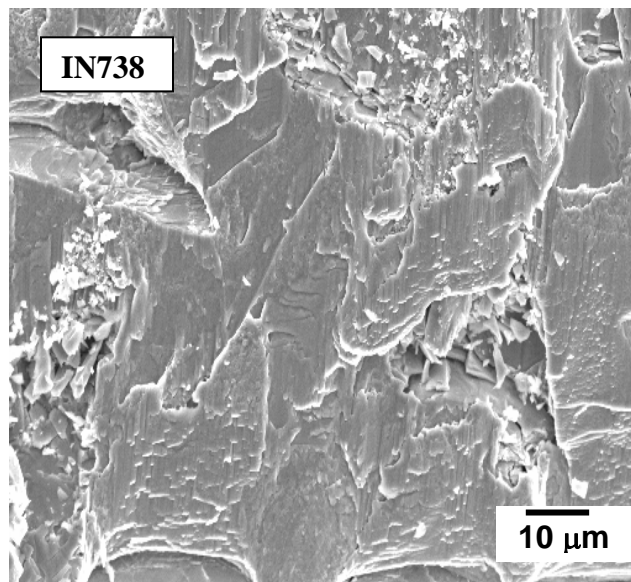
(b)

Figure 29: SEM micrograph in SEI mode, showing fracture surface of as-received (a) IN 939 bulk material and (b) IN 738 bulk material. The fracture path was macroscopically flat and dominated by ductile shear fracture with dimpling.

Asbonded CMSX-4 - IN 939				
CMSX-4/IN 939 **Sample ID**	Dimensions (mm)	Peak stress (MPa)	%Bulk Shear strength (IN939) Bulk Shear strength=783.25	% of UTS of Bulk IN 939 UTS Bulk =1050 MPa [2]
1	8.00x3.7	741.82	0.95	0.71
2	8.00x3.7	778.9	0.99	0.74
3	8.12x3.88	743.4	0.95	0.71
4	8.12x4.100	695.1	0.89	0.66
5	8.12x4.100	672.1	0.86	0.64
Mean	--------	726.3	0.93	0.69
Std.Dev.	--------	42.5	0.05	0.04
6(low load fail)	8.00x3.750	189.8	0.24	0.18
Asbonded +PBHT [CMSX-4 - IN 939]				
CMSX-4/IN 939				
1	7.81x3.96	709	0.91	0.68
2	7.79x3.98	673.9	0.86	0.64
3	7.85x3.94	741.5	0.95	0.71
4	7.83x3.87	664.8	0.85	0.63
5	7.85x3.94	806.4	1.03	0.77
6	8.06x3.89	681.1	0.87	0.65
Mean		712.8	0.91	0.68
Std.Dev.		53.7	0.07	0.05
Asbonded + PBTE [CMSX-4 - IN 939]				
CMSX-4/IN 939				
1	8.12x4.00	605.9	0.77	0.58
2	8.22x4.00	571	0.73	0.54
3	7.91x3.88	604.6	0.77	0.58
4	8.33x3.98	582.9	0.74	0.56
5	8.06x3.86	591.7	0.76	0.56
6	7.96x4.00	544.5	0.70	0.52
Mean		583.43	**0.74**	0.56
Std.Dev		23.20	0.03	0.02

Table 6: Shear testing data of CMSX-4 – IN 939 bonds using Niflex-110 interlayer at different conditions. PBHT- Post bond heat treatments as mentioned in section 4.1.3 and PBTE- post bond thermal exposure as explained in section 4.1.4.

Asbonded CMSX-4 - IN 738				
CMSX-4/IN 738			%Bulk Shear strength IN 738=785.6	%UTS Bulk IN 738=1035MPa
1	8.24x4.020	617.6	0.79	0.60
2	8.24x3.88	509.8	0.65	0.49
3	8.00x3.870	589.3	0.75	0.57
4	8.3x3.83	618	0.79	0.60
5	8.04x3.94	617.8	0.79	0.60
6	8.23x3.84	496.6	0.63	0.48
Mean		574.85	0.73	0.56
Std.Dev		56.74	0.07	0.05
Asbonded +PBHT [CMSX-4 - IN 738]				
CMSX-4/IN 738				
1	7.93x3.85	727.1	0.93	0.70
2	8.13x3.95	628	0.80	0.61
3	7.93x3.97	819.7	1.04	0.79
4	7.93x3.95	728.4	0.93	0.70
5	7.79x4.03	649.1	0.83	0.63
Mean		710.5	**0.90**	0.69
Std.Dev		76	0.10	0.07
Asbonded + PBTE [CMSX-4 - IN 738]				
CMSX-4/IN 738				
1	7.82x4.00	492.8	0.63	0.48
2	8.040x4.00	501.8	0.64	0.48
3	8.06x3.88	511.5	0.65	0.49
4	8.06x3.88	571.5	0.73	0.55
5	8.02x4.000	483.9	0.62	0.47
6	7.93x3.94	544.5	0.69	0.53
Mean		517.7	**0.66**	0.50
Std.Dev		33.7	0.04	0.03

Table 7: Shear testing data of CMSX-4 – IN 738 bonds using Niflex-110 interlayer at different conditions. PBHT- Post bond heat treatments as mentioned in section 4.1.3 and PBTE- post bond thermal exposure as explained in section 4.1.4.
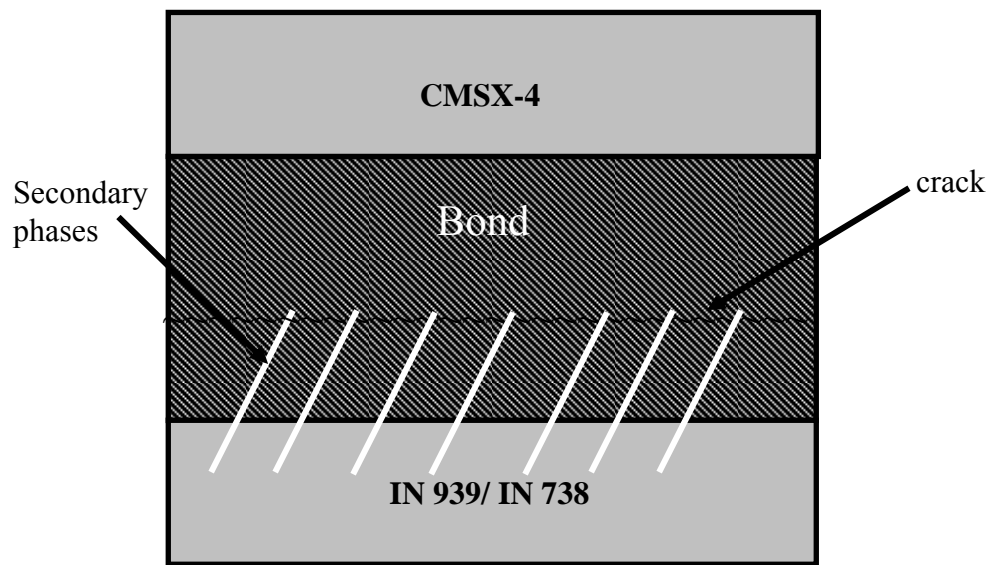
Figure 30 : Schematic showing crack path upon application of shear force on the bonded samples
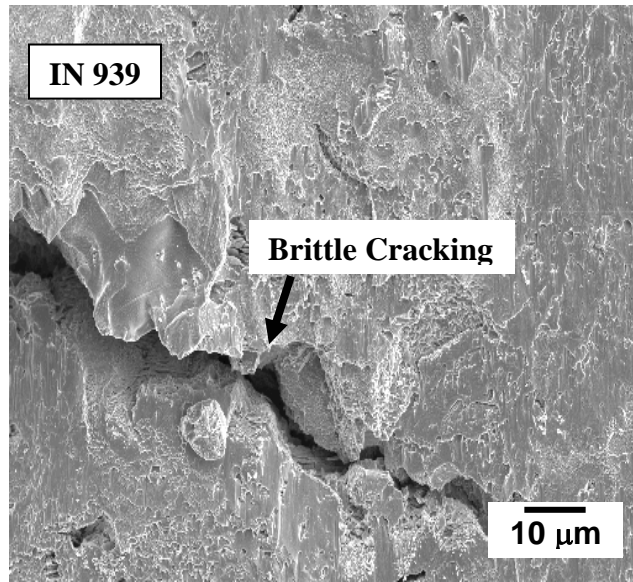
(a)
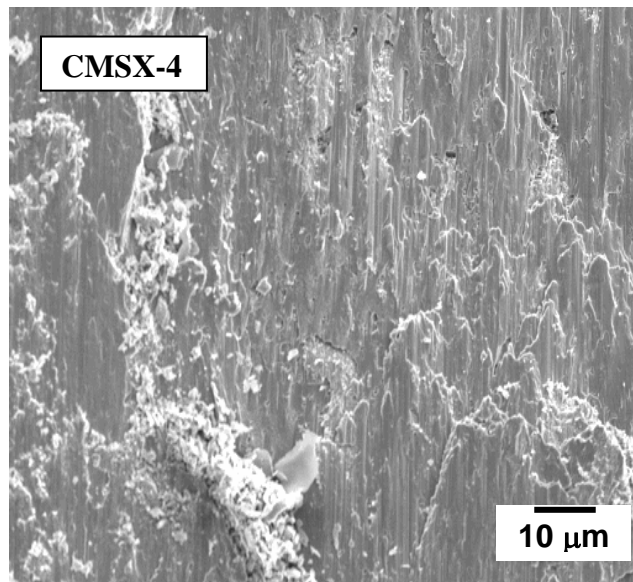
(b)

Figure 31: SEM micrograph in SEI mode, of shear tested CMSX-4 – Niflex-110 – IN 939 bond fracture surface of (a) IN 939 polycrystalline substrate (b) CMSX-4 single crystal substrate. Notice the secondary cracking on IN 939 substrate due to the secondary phases precipitated in the diffusion zone of the polycrystalline substrate.
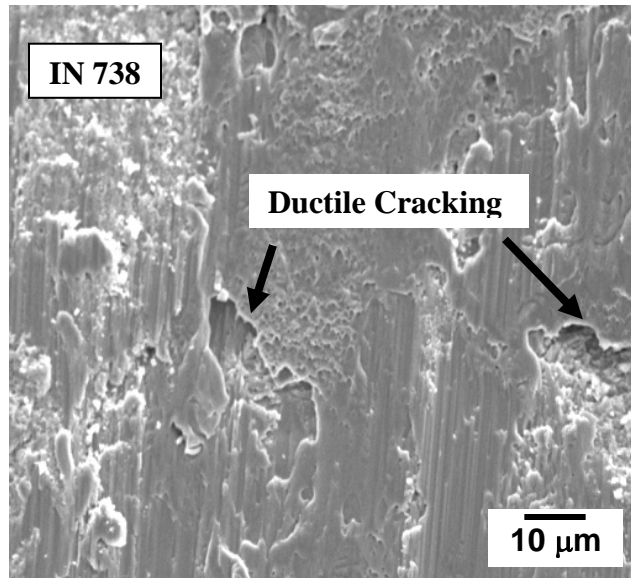
(a)
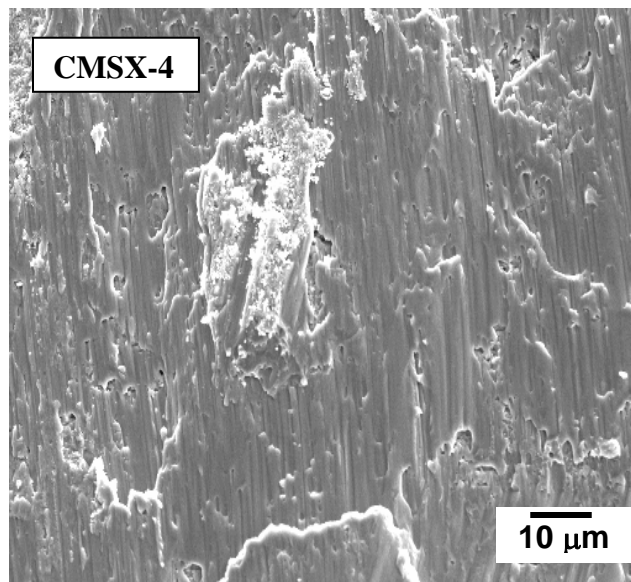
(b)

Figure 32: SEM micrograph in SEI mode, of shear tested CMSX-4 – Niflex-110 – IN 738 bond fracture surface of (a) IN 738 polycrystalline substrate (b) CMSX-4 single crystal substrate. Notice the ductile shear fracture on both of the substrates and dimpling on IN 738.
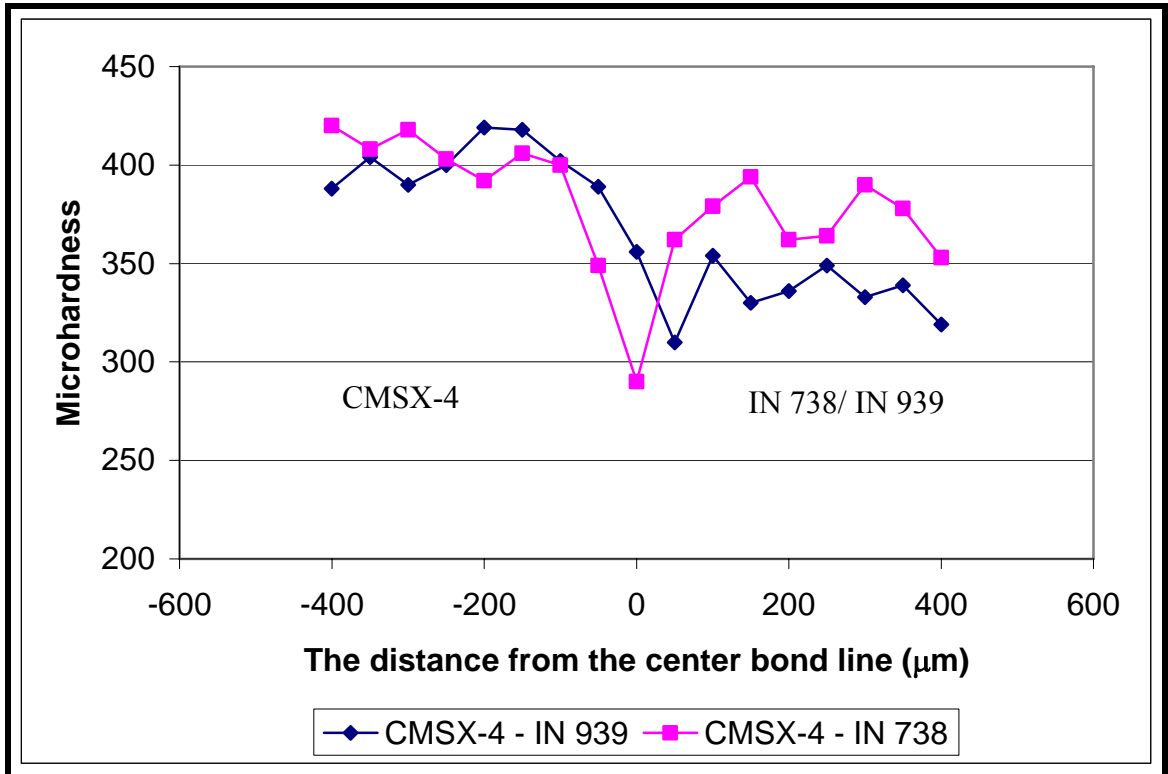
Figure 33: Vickers microhardness across bondline of CMSX-4 – IN 738 and CMSX-4 – IN 939 bonds after 240 minutes at 1160 ^{0}C using Niflex-110 interlayer. Notice that the bondline is of lower microhardness than that of the substrates.

5.1.5   Characterization of Post-Bond Heat Treated TLP bonds

5.1.5.1   Microstructure after PBHT

Post-bond heat-treatment (PBHT), described in Section 4.1.3, was conducted to

diffuse aluminum from the substrates, resulting in more γ' at the bondline and to reform

the substrate γ' distribution which was dissolved during bonding. CMSX-4 – IN 738

bonds using a Niflex-110 interlayer, after being subjected to a two stage PBHT, resulted

in an increase of volume fraction of γ' and also reformation of γ', which was already

dissolved during the bonding process. This is clearly visible in Figure 34 and Figure 35.

In addition, coarsening of the γ' phase and modification of the shape of the γ' into

circular particles was observed. This might have been caused due to the reduction in total

interfacial energy, as explained by Sharghi-Moshatghin et al. [29]

On the other hand, in CMSX-4 – IN 939 bonds, the PBHT process did not change

the volume fraction of γ' to any great extent, although it was already greater than in the

CMSX-4 – IN 738 bonds. The increase in size of the γ' phase and a shape change of γ'

from rectangular to circular were also observed [Figure 36 and Figure 37]. Also, the

secondary phases seen in the diffusion zone of the polycrystalline substrate [See Section

5.1.1.4] in the as bonded samples, were still observed and remained stable even after

PBHT, unlike for the CMSX-4 – IN 738 combination.

5.1.5.2   Microstructure after PBTE

Post-bond thermal exposure (PBTE), as described in Section 4.1.4, was conducted

to investigate the microstructural stability of the bonds. Coarsening of γ' was seen on the

bonds subjected to PBTE. Also, a significant region of deleterious phases, such as sigma,

and Laves, was observed in the polycrystalline substrate of the joint after the high

temperature exposure [Figure 38]. In addition, in bonds involving CMSX-4 – IN 939, the

secondary phases in the diffusion zone of the polycrystalline substrate remained stable for

all times examined for all interlayers, even after post-bond thermal exposure of up to 1

week at 1,000 $^{\circ}$C.
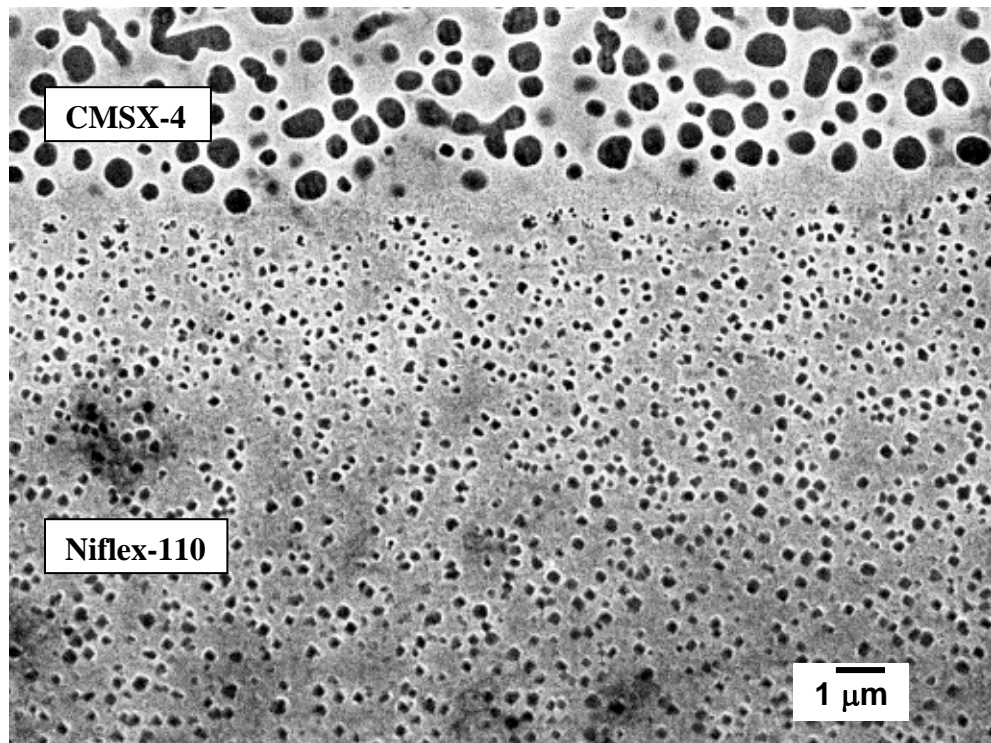
Figure 34: SEM micrograph in SEI mode, of As bonded CMSX-4 – Niflex-110 – IN 738 showing gamma-prime (γ') at the bondline.
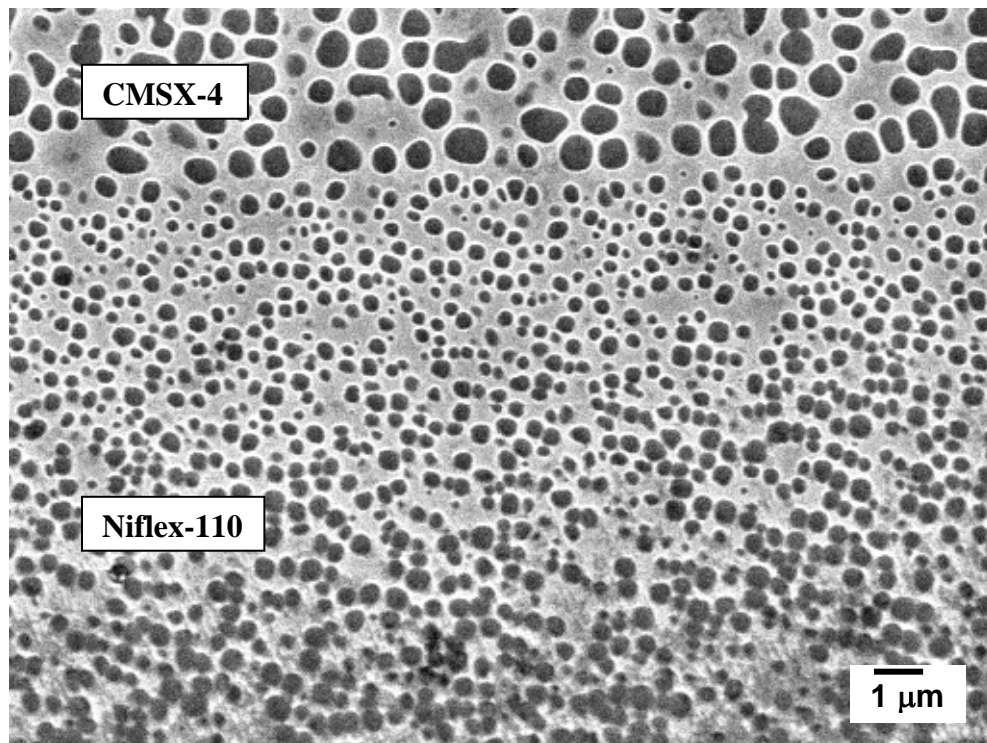
Figure 35: SEM micrograph in SEI mode, of As bonded + PBHT CMSX-4 – Niflex-110 – IN 738 showing gamma-prime (γ') at the bondline. Notice the increase of volume fraction of γ' after PBHT (compare it to previous Figure)
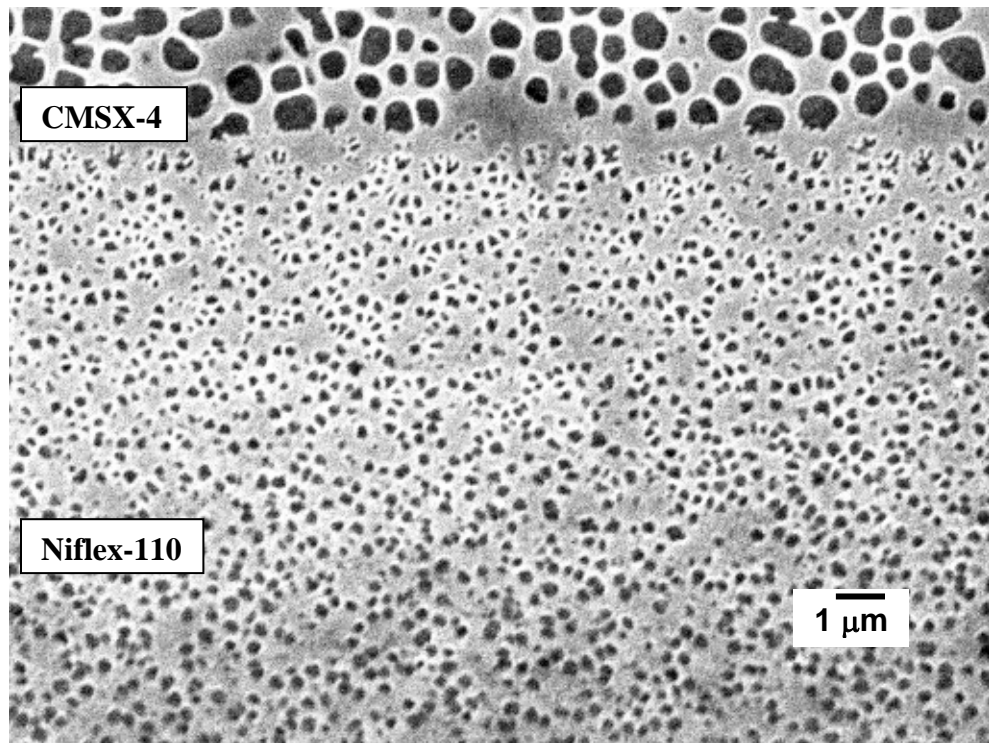
Figure 36: SEM micrograph in SEI mode, of As bonded CMSX-4 – Niflex-110 – IN 939 bond showing gamma-prime (γ') at the bondline.

Compare this with Figure 34 and note the high amount of γ' at the bondline and in the bulk, which was dissolved during bonding.
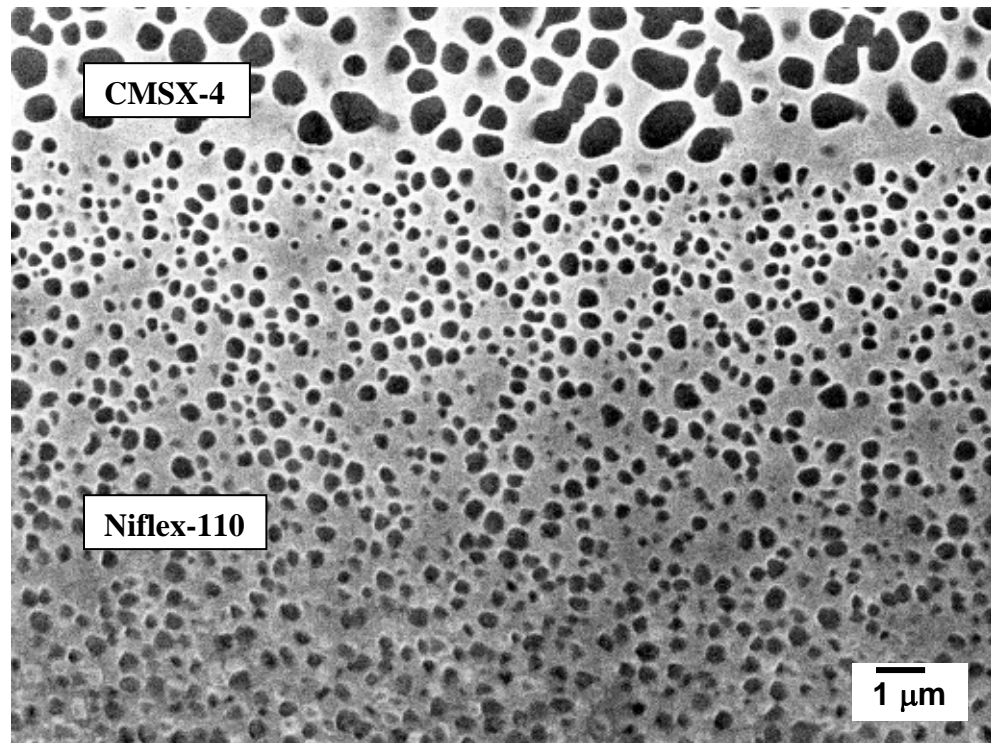
Figure 37: SEM micrograph in SEI mode, of as bonded + PBHT CMSX-4 – Niflex-110 – IN 939 showing gamma-prime (γ') at the bondline. Notice the modification of shape of γ' into circular, and the reformed γ' distribution, which was dissolved during bonding (compare to previous Figure).
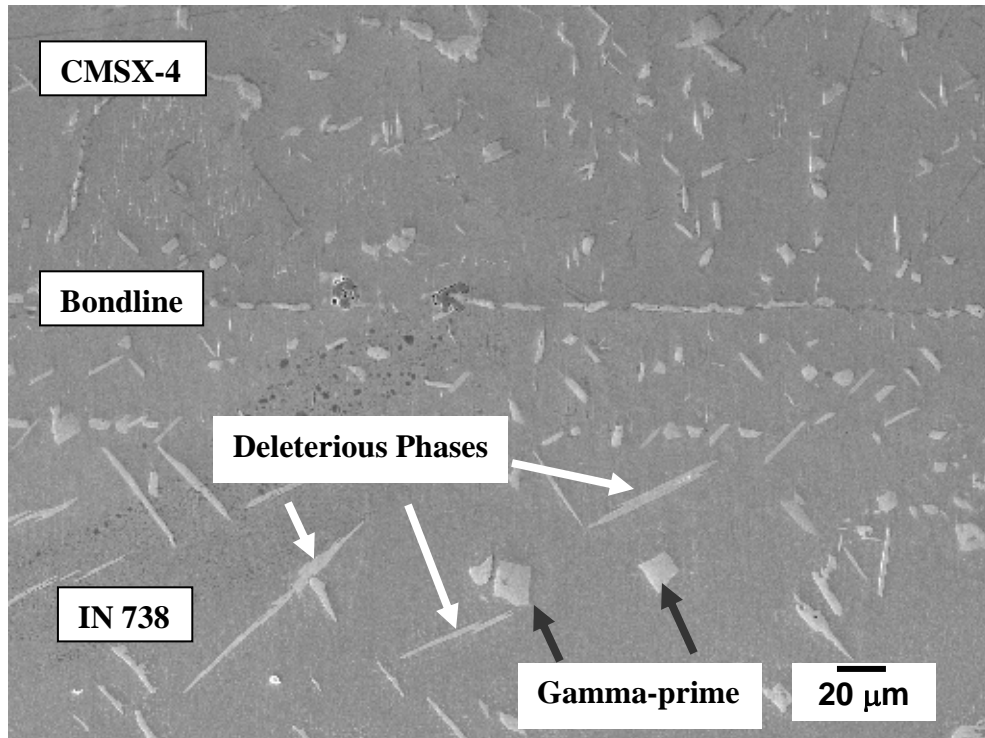
Figure 38: SEM micrograph in SEI mode, of asbonded+PBTE CMSX-4 – Niflex-110 - IN 738 bond showing coarsened as-bonded gamma-prime (γ') and deleterious phases.

5.1.6 Structure-Property Relationships of TLP Bonds following a PBHT and PBTE

5.1.6.1 Shear tests

Shear testing was done on CMSX-4 – Niflex-110- IN 738 and CMSX-4 –Niflex-110 - IN 939 bonds after PBHT. Shear testing conducted on as-bonded +PBHT CMSX-4 – IN 738 joint resulted, on average, in 90% of the bulk shear strength of the weakest bulk material in the bond (IN 738), an increase of about 15% when compared to the strength of an as bonded joint [Table 7]. This increase in shear strength of CMSX-4 – IN 738 bonds can be attributed to the increase of volume fraction of γ' at the bondline and the reformed γ' distribution, after PBHT [Figure 35]. PBHT might have caused diffusion of aluminum from the substrates, resulting in more γ' at the bondline, and also helped in reforming the γ' distribution dissolved during bonding.

In contrast, shear testing of CMSX-4 – IN 939 resulted, on average, in 92 % of the bulk shear strength, which showed no increase in shear strength, unlike the comparable IN 738 combination [Table 6]. This might be due to the lack of change in the volume fraction of γ'. However, fractography of bonds subjected to PBHT, showed secondary cracking in the polycrystalline substrate corresponding to those observed in microstructure.

Also, bonds that were thermally exposed to 1,000 °C for 1 week showed a decrease in shear strength which can be attributed to the coarsening of γ' and the formation of secondary phases in the polycrystalline substrate. Bonds prepared using IN 939 as a polycrystalline substrate showed similar results, with decrease in the shear strength after PBHT.
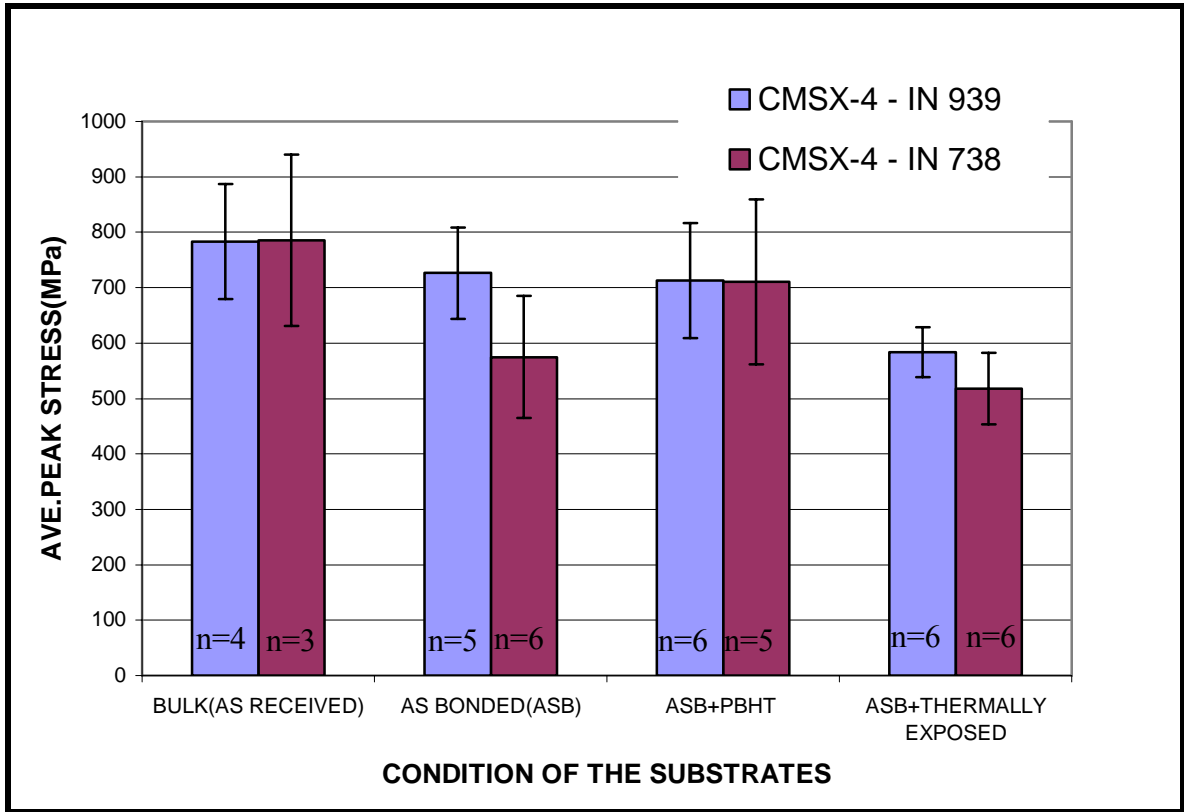
Figure 39: Average shear stress versus condition of substrates. ASB refers to Asbonded, PBHT-post bond heat treatment, PBTE- post bond thermal exposure. Note that the increase in shear strength in CMSX-4 – IN 738 after PBHT and the decrease after PBTE. (Error bars denote the 1.96 times standard deviation Error bars denote 1.96 times standard deviation to represent a 95% confidence limit)

5.2   Oxide dispersion strengthened iron based superalloys

5.2.1   Microstructural Characterization

As mentioned earlier, MA956 and PM2000 are the two substrates studied. The microstructure of diffusion bonds made with the substrates cut in the working direction will be discussed in this section.

5.2.1.1   Diffusion bonding of MA 956

Diffusion bonding of MA 956 was conducted in both the fine grain and coarse grain conditions. In the fine grain condition, satisfactory bonds were achieved in the Longitudinal-Longitudinal (L-L) bond orientation, where the bondline was parallel to the direction of extrusion of the ODS bulk material, under low stresses, $1 - 5$ MPa at 1250 °C, for bonding times up to 6-8 minutes. The bonding process was followed by PBHT to induce recrystallization across the bondline. The microstructure of the bond can be seen in Figure 40. Grain growth across the bond-line was achieved in the fine grain to fine grain bonds, as can be seen in Figure 41. However, occasional voids were visible at the bond-line even after the PBHT. In addition, satisfactory bonds were obtained when a fine grain condition substrate was joined to a coarse grain condition substrate in the L-L orientation as shown in Figure 42. However, when two MA956 substrates in the coarse grain condition were joined, bonds with large unbonded regions were observed, as shown in Figure 43.

Based on the above observations, acceptable bonds were obtained only when a fine grain condition material was involved. This can be attributed to the huge amounts of stored energy possessed by unrecrystallized (fine grained) ODS alloys [129]. In their studies on diffusion bonding, Bokstein et al. and Orhan et al. [131] explained that a

submicron grain size can lead to higher grain boundary diffusion, and during the bonding process the grain boundaries intersect these voids. Also, these grain boundaries may act as favorable paths for the atoms to diffuse to the voids during the diffusion bonding process, thereby resulting in closing of the voids and, hence an increase in the bonding rate. Similar results showing that coarse grained substrates result in poor bonds have been reported in diffusion bonding of MA6000 [102], a Ni-base ODS alloy, and MA956 [118,119] in Transverse-Transverse (T-T) orientation, where the bondline was perpendicular to the direction of extrusion of the ODS bulk material.

5.2.1.2 Diffusion bonding of PM2000

Diffusion bonding of PM2000 was conducted for the fine grain samples only. In ODS alloys, yttria stringers are aligned in the direction of extrusion, resulting in elongated grains and the number of yttria stringers cut by the bondline is governed by the orientation of the substrate. To study the effect of substrate orientation on microstructural bond development at the bondline, bonding was performed in both the T-T orientation and L-L orientations. Satisfactory bonds were obtained for both orientations, under low pressures 1 - 5 MPa, and for bonding times up to 6-8 minutes. The microstructures of the bonds are shown in Figure 44 and Figure 45. However, a few unbonded regions were observed at the bondline in the transverse orientation.

Bonding was followed by PBHT at 1385 °C for 2 hours to induce recrystallization across the bondline. Recrystallization occurred in the substrate, but no grain growth across the bondline was found. An increase in porosity was also observed after PBHT [128]. This can be attributed to the release of the hydrogen gas that was entrapped in the bulk material during alloying, which resulted in pore formation in the bonds during

PBHT. A detailed survey of as-received PM2000 bulk material is presented elsewhere 128]. Substrate preparation techniques such as electropolishing and post bond moving zone recrystallization heat treatment might lead to minimization of unbonded regions and to attain recrystallization across the bondline [119].

5.2.2 Structure-property relationships of ODS alloys

Room temperature shear tests were performed to evaluate the mechanical properties of the bonds and to derive the structure-property relationships of the bonds. Shear tests were initially conducted on as-received bulk material in both the as-received unrecrystallized fine grain samples and the recrystallized coarse grain samples and these served as a baseline for the comparison with the bonded materials. Tests were conducted on PM2000 diffusion bonds of unrecrystallized fine grain substrates bonded to similar material followed by PBHT, in both the T-T and L-L orientations. However, it should be noted that the final bonded area did not exceed 90% of the total substrate faying surface area. The peak shear stresses of the bonds in the transverse and longitudinal orientations, along with the peak shear stress of as-received bulk material for comparison, are shown in Figure 46.

The peak shear stress of the recrystallized bulk material is lower than that of the as-received unrecrystallized bulk material, which is expected due to the reduction in grain boundaries and the resulting decrease in grain boundary strengthening in the recrystallized material. Some of the variation in the peak shear stress with orientation of the substrate was also observed. The transverse orientation showed higher peak shear stresses than for the longitudinal orientation in the bulk material. Shear strengths of the

post bond heat treated bonds in both the T-T and L-L orientations were on the order of 70% of those in the bulk recrystallized material.

Shear tested specimens were examined using SEM, and fracture was observed to occur at the bondline. Shear testing on coarse grained MA956 revealed that cleavage cracking was associated with a planar shear fracture, as shown in Figure 47 and Figure 48. In contrast, shear testing on PM2000 bulk material resulted in a planar shear with no secondary cracking, which can be attributed to the increase in grain boundaries and thus the grain boundary strengthening that is found in a fine grained material, as shown in Figure 49. Fractography on as bonded plus post bond heat treated PM2000 bonds revealed some secondary cracking, which can be attributed to the recrystallization in the substrate due to PBHT. This can be seen in Figure 50.
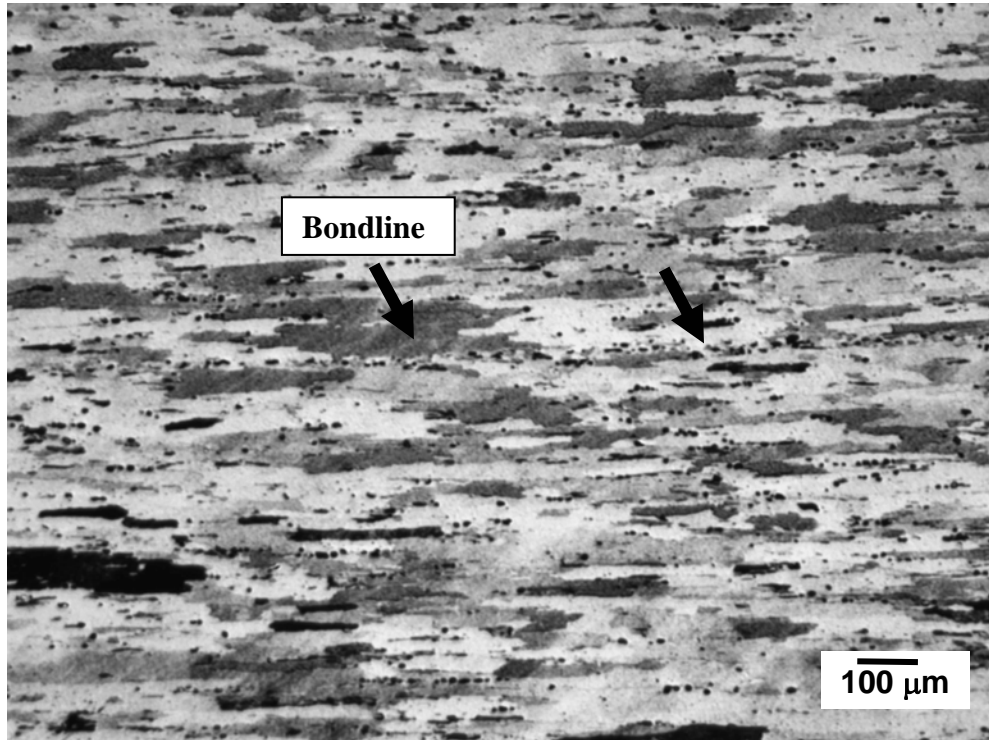
Figure 40 : LM micrograph, showing diffusion bond of MA956 fine grain - fine grain (longitudinal orientation) at 1250 °C for 121 s, followed by PBHT [1 h at 1300 °C]. Notice the invisible bondline free of unbonded regions at the bondline [127,128].
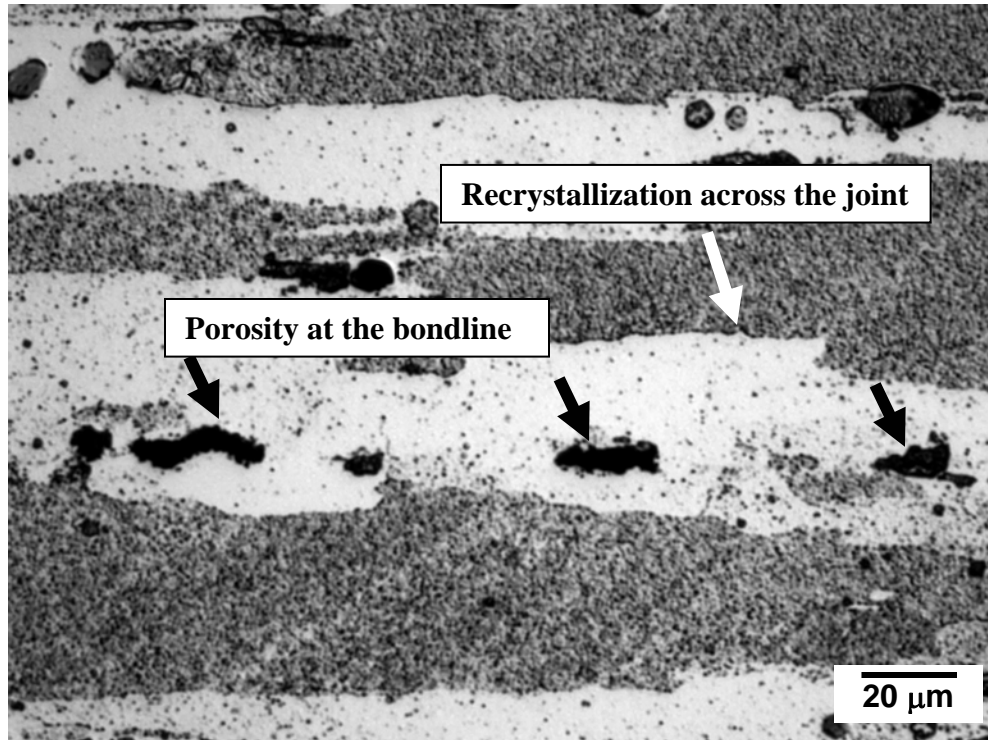
Figure 41: LM micrograph showing diffusion bond of MA956 fine grain - fine grain (longitudinal direction) at 1250 °C for 121 s, followed by PBHT [1 h at 1300 °C]. Note the grain growth across the bondline and also the voids present at the bondline [127,128].
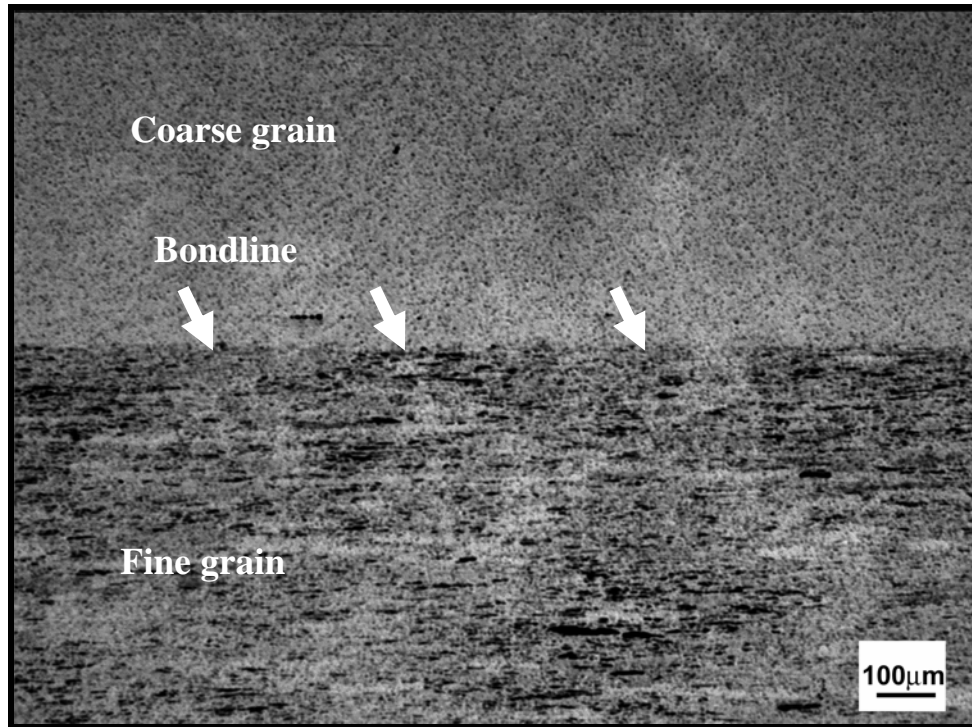
Figure 42: LM micrograph showing diffusion bond of MA956 coarse grain - fine grain (longitudinal direction) at 1250 °C for 170 s. Note the bondline with no voids present at the bondline [127,128].
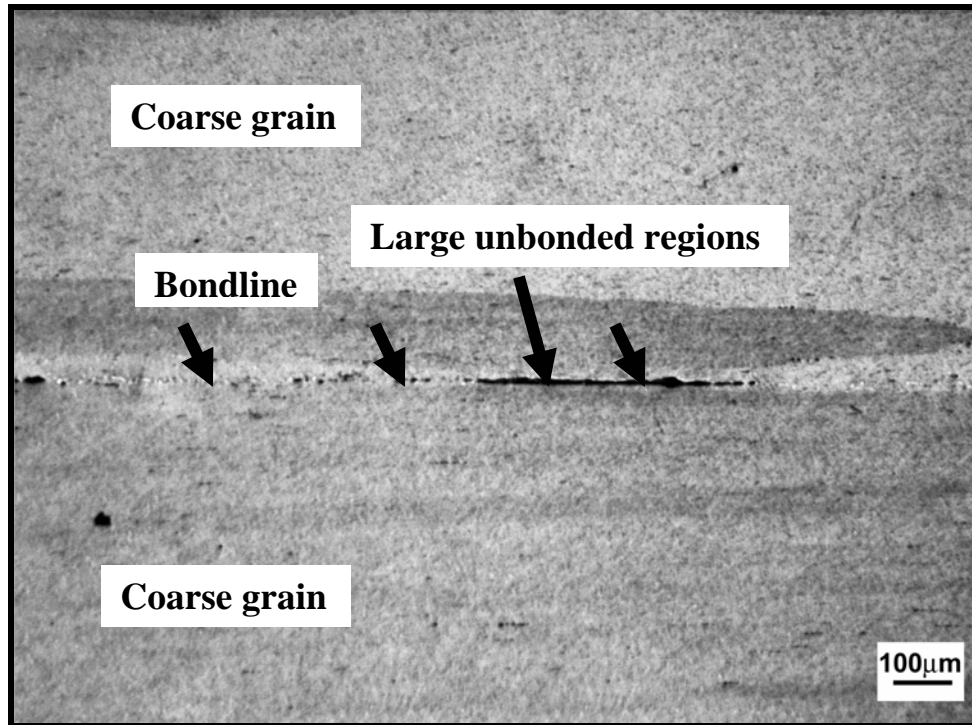
Figure 43: LM micrograph showing diffusion bond of MA956 coarse grain - coarse grain (longitudinal direction) at 1250 °C for 174 s. Note the bondline with large unbonded regions present at the bondline127,128].
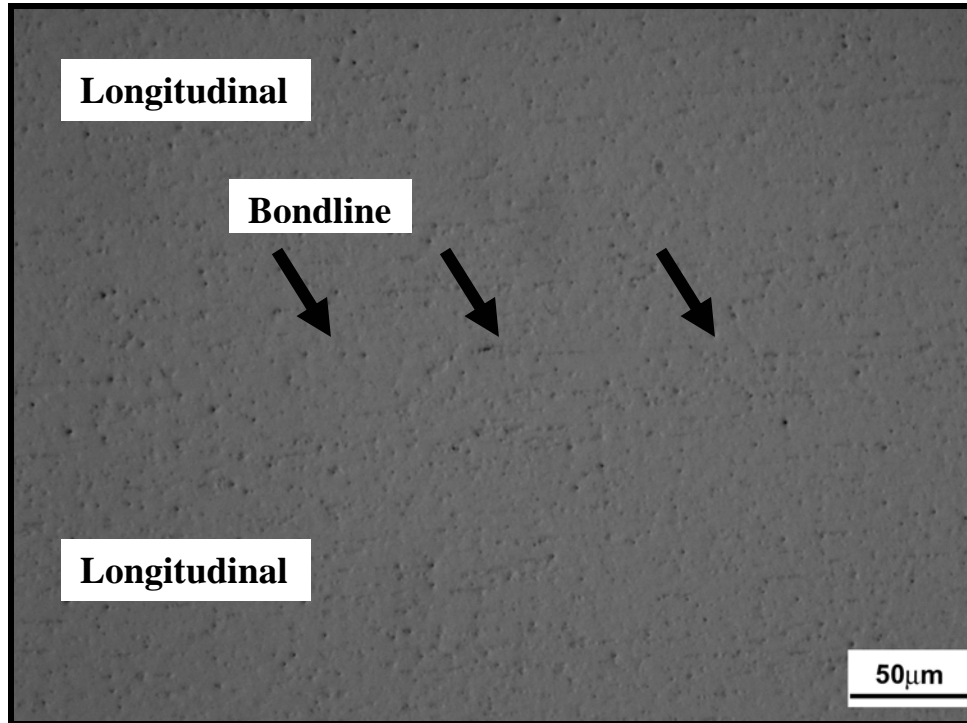
Figure 44: LM micrograph showing diffusion bond of PM2000 in L-L orientation at 1250 °C for 310 s, in as-bonded (unetched) condition. Note the bondline free of unbonded regions [127,128].
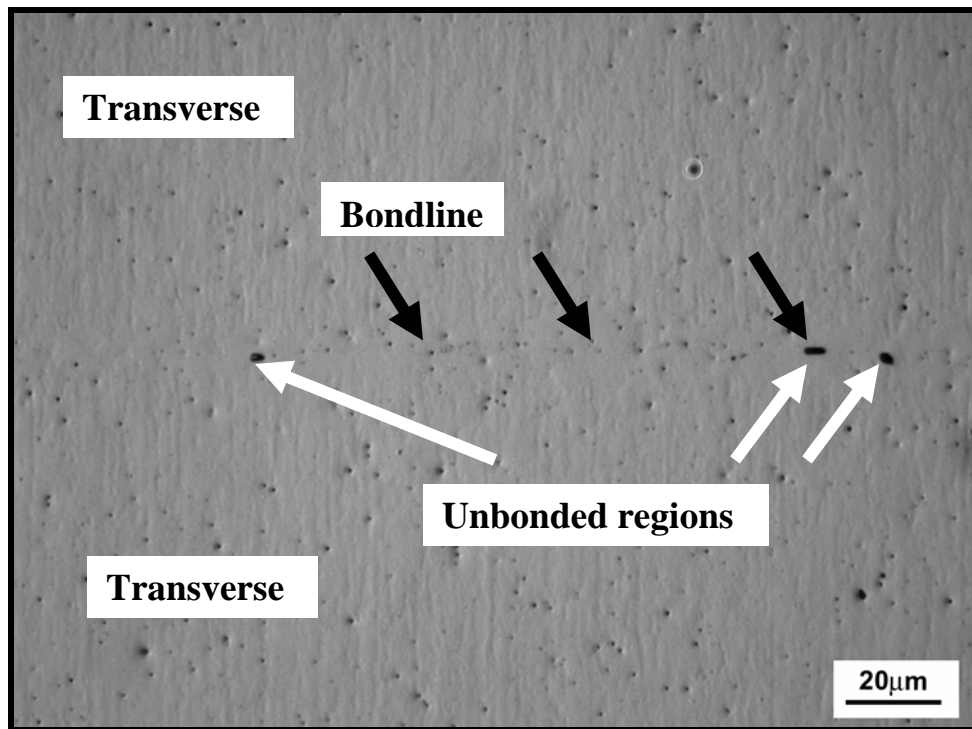
Figure 45: LM micrograph showing diffusion bond of PM2000 in Transverse orientation at 1250 °C for 300 s, in as-bonded (unetched) condition. Note the bondline free of unbonded regions occasionally seen at the bondline 127,128].
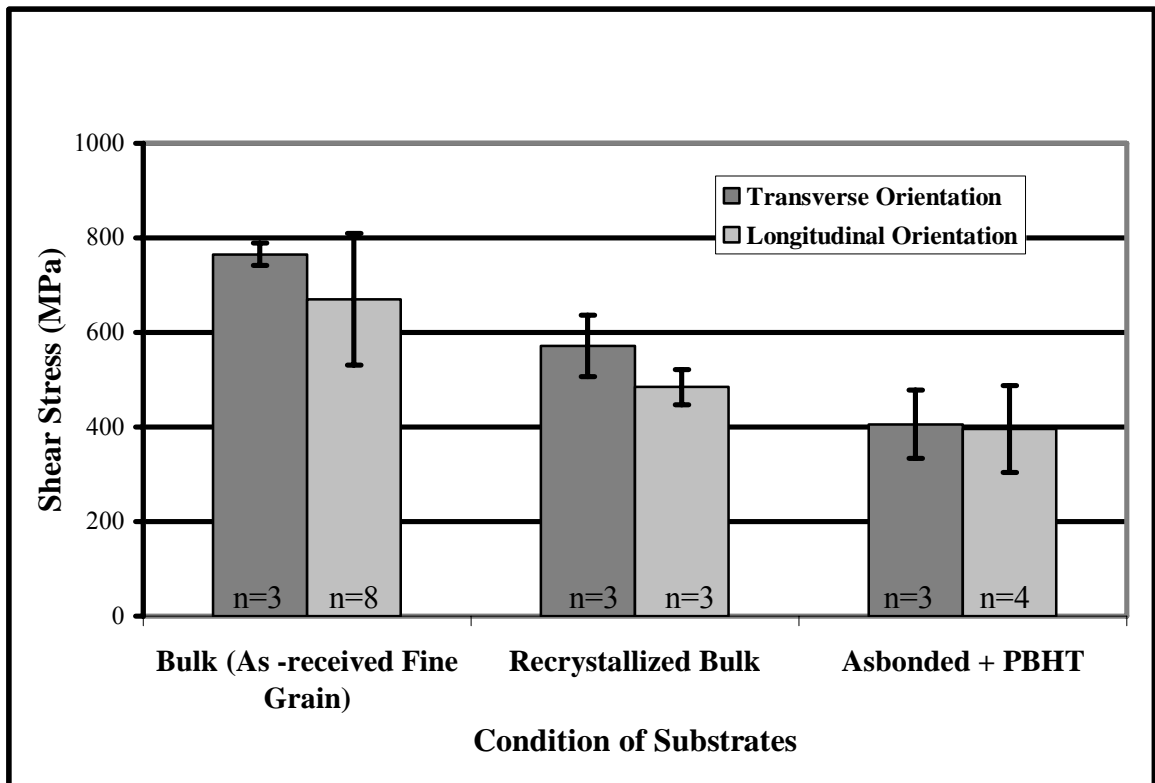
Figure 46: Average shear stress versus condition of substrates. PBHT-post bond heat treatment. Note that the shear strength of the bulk material decreased after recrystallization treatments and that of as bonded followed by PBHT is of the order of 70% of the strength of the bulk material. (Error bars denote 1.96 times standard deviation to represent a 95% confidence limit)
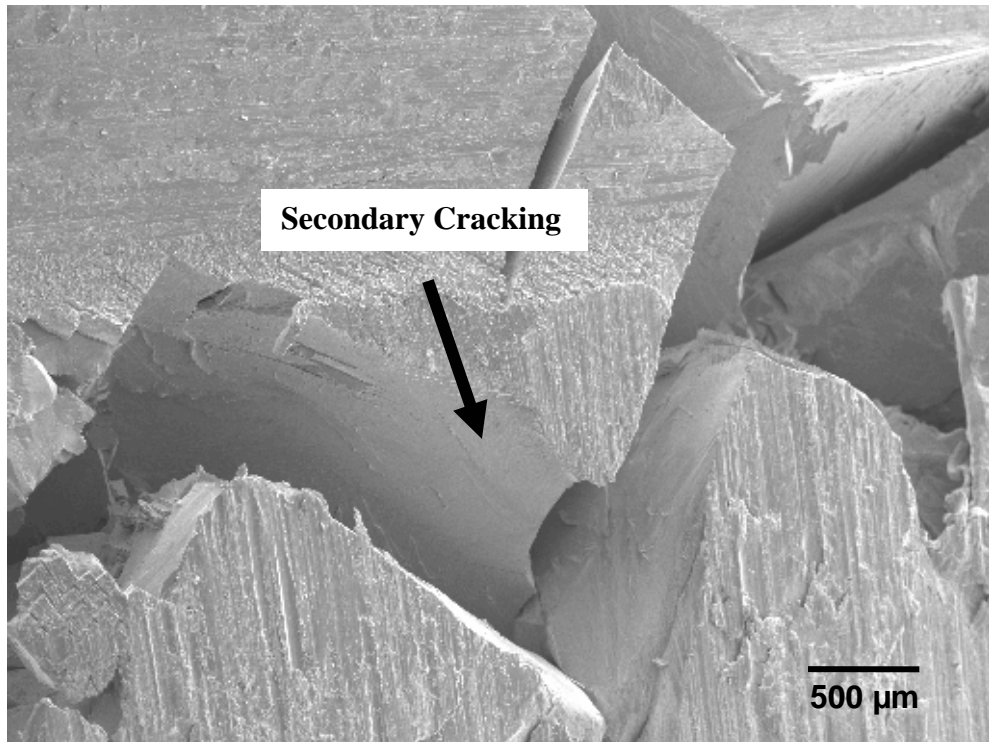
Figure 47: SEM micrograph in SEI mode, of MA 956 coarse grained bulk material room-temperature shear fracture surface. Notice the main shear fracture surface is planar, but there is extensive secondary cracking labeled.
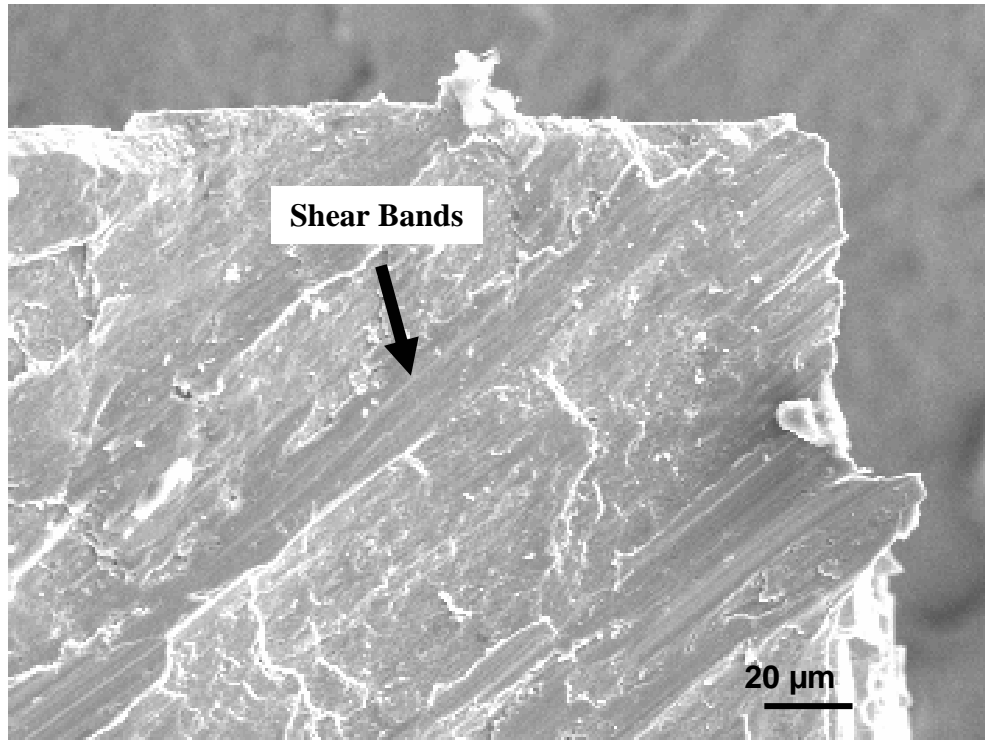
Figure 48: SEM micrograph in SEI mode, of coarse grained MA 956 bulk material, showing detail of fracture surface of room-temperature shear test. Notice the cleavage cracking and shear bands on fracture surface labeled.
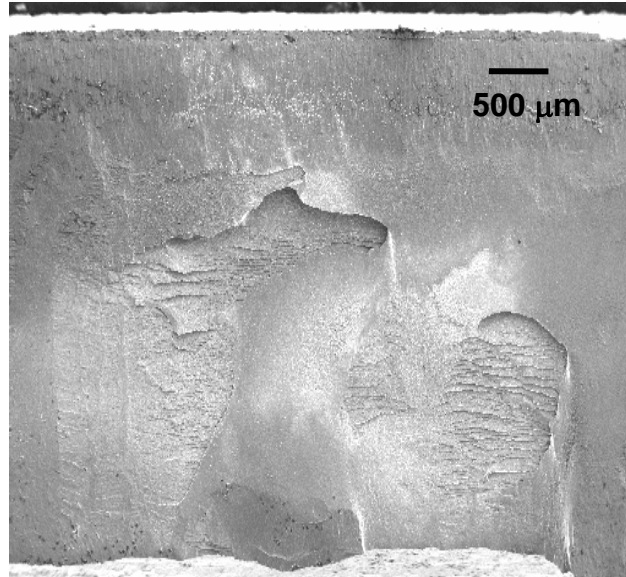
(a)
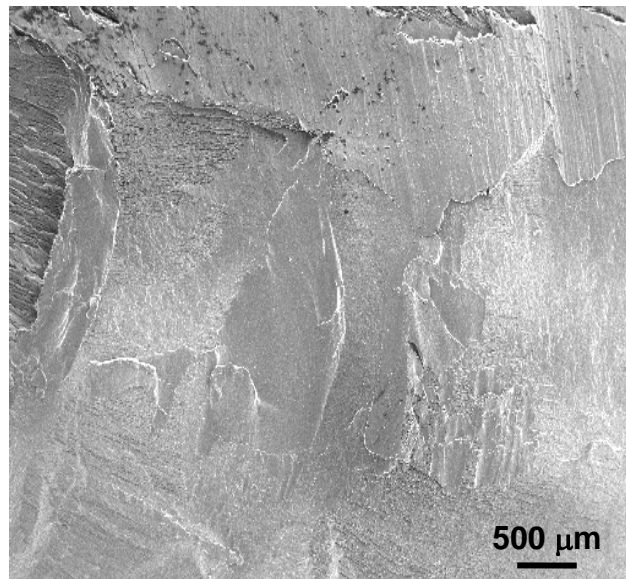
(b)

Figure 49 : SEM micrograph in SEI mode, of fine grained bulk PM 2000, showing fracture surface of (a) longitudinal sample and (b) transverse sample. Notice that the main fracture surface is slightly less planar, but there is no secondary cracking.
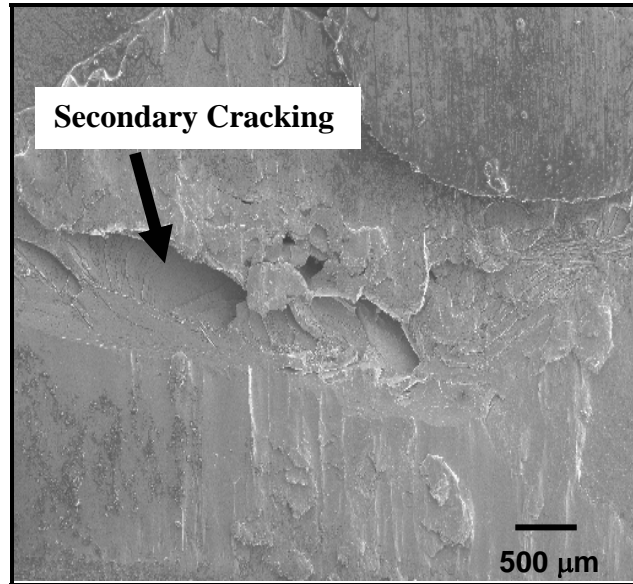
(a)
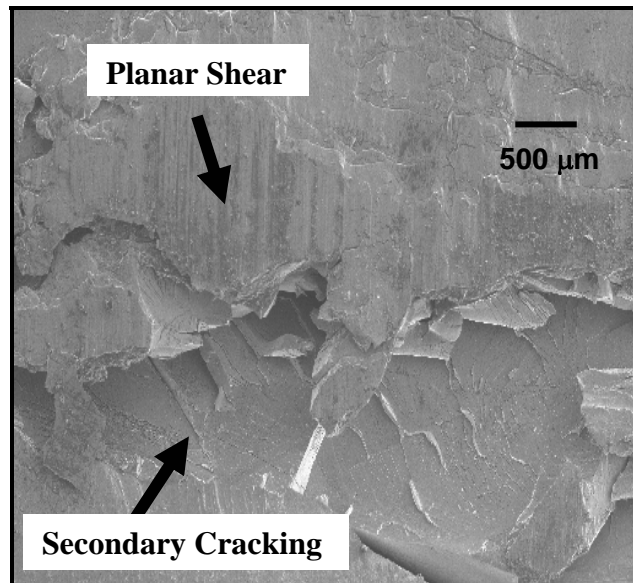
(b)

Figure 50: SEM micrograph in SEI mode, showing fracture surface of PM2000 transverse-transverse bonds at 1250 °C for 309 s, followed by PBHT 2 h, 1385 °C. Notice the secondary cracking associated with planar shear.

6 CONCLUSIONS

- Competition between wetting of the faying surfaces and formation of the eutectic along the grain boundaries of the composite interlayer was observed. This led to non-bonded regions at the faying surfaces, unless a boron-rich interlayer was employed.

- Adequate wetting occurred in the case of conventional BNi-3 foil interlayers, but composite interlayers exhibited premature isothermal solidification and sometimes led to porosity at the faying surfaces due to inadequate amount of melting point depressant (MPD) present.

- The single crystal CMSX-4 substrate showed a greater extent of wetting compared to the recrystallized CMSX-4, due to the absence of grain boundaries. The results from the wettability studies on recrystallized CMSX-4 were comparable to those for IN 738 and IN 939.

- Suppression of bondline boride formation was achieved using both the Niflex-115 and Niflex-110 interlayers. However, wettability studies confirmed the formation of borides in the early stages of bond development using the Niflex-110 interlayer, which were not seen with Niflex-115 interlayer.

- In all the bonds examined, there was relatively little gamma-prime at the bondline when compared with the bulk substrates. For a given wide-gap interlayer, more

gamma-prime was formed at the bondline of CMSX-4 – IN939 compared to CMSX-4 – IN738.

- A variety of second phases, which appeared to consist primarily of borides/carbides and/or topologically close-packed (TCP) phases, were observed to form in the substrate diffusion zone on the polycrystalline side of both the CMSX-4 – IN738 and CMSX-4 – IN939 bonds, as shown in the early stages of bond development. However, in the case of bonds involving IN738, the formation of these second phases could be suppressed after the completion of solid-state homogenization, by using either of the two composite interlayers, but could not be avoided in the bonds using BNi-3 foil as an interlayer. In contrast, when bonding IN939, the second phases remained stable for all times examined for all interlayers, including post-bond thermal exposures of up to 1 week at 1,000 $^{\circ}$C.

- Two factors dominated the room temperature mechanical properties of the wide-gap bonds. The first was the extent of gamma-prime formation at the bondline. Results from shear testing and fractography of the bonds indicated ductile shear failure at the bondline, which might have been caused due to the formation of insufficient gamma-prime within the joint, leaving a relatively soft bondline region. The second factor was the presence of second phases in the diffusion zone of the polycrystalline substrate, which led to the formation of brittle secondary cracks. Overall, it is evident that the room temperature shear strength of the bonds was more dependent on the extent of formation of γ' on the bondline than on the secondary phases in the diffusion zone of the polycrystalline substrate.

- In view of the microstructure-wettability-mechanical property relationships, Niflex-115 interlayer might be best suited for joining of single crystal superalloy CMSX-4 with the polycrystalline superalloys IN 738 and IN 939, followed by post bond heat treatments.

- In oxide dispersion strengthened alloys, diffusion bonding produced successful results for MA956 and PM2000 material in the unrecrystallized fine grain condition under low stresses in the range of $1 - 5$ MPa. Shear strengths of the bonds attained 70% of those of the bulk material. Diffusion bonding of ODS alloys with substrate orientation aligned in the direction of extrusion might be a promising technique to achieve bond strengths comparable to that of the bulk material.

- In view of the structure-property relationships revealed in this study, longitudinal-longitudinal orientation in a fine grain condition followed by PBHT is likely to produce the desired results in joining of ODS alloys. However, it should be noted that the batch to batch inconsistency still has a great impact on the microstructure and the mechanical properties of bonds, and this needs to be improved for the process to become commercially viable.

7   Future Work

- *TEM investigations*: The extent of γ' formation was found to have a greater influence on bond mechanical properties than the formation of brittle second phases in the diffusion zone of the polycrystalline superalloy substrates. Hence, extensive TEM studies need to be conducted including an examination of the microstructural bond development of TLP bonded nickel-based superalloys using composite interlayers.

- *Oxidation and hot corrosion studies of TLP bonded nickel-based superalloys*: In use, superalloys will be subjected to aggressive environments including oxidation and hot corrosion. Hence, it is vital to study the effects of the TLP bonding process on the oxidation and hot corrosion properties of TLP bonds using composite interlayers.

- *High temperature mechanical testing of nickel-based superalloys:* Since superalloys will inevitably be subjected to high temperature environments in their real world applications, it is vital that high temperature mechanical testing, including high temperature tensile testing and creep testing of as bonded and PBHT TLP bonded superalloys, be conducted.

- *Porosity in ODS alloys:* Inconsistencies in the batch to batch properties of mechanically alloyed ODS alloys, for example porosity, had a significant impact

on the microstructure-mechanical property relationships of the bonds. Hence, comprehensive investigation of the porosity variations, along with a study of ways to improve the consistency is urgently needed. Hipping the as-cast components, which successfully eliminated non-surface connected porosity considerably in the precipitation hardened superalloy castings [132, 133], seems to be promising and needs further study.

- *Dislocation interactions of ODS alloys:* Iron based ODS alloys were intended for use in temperatures higher than the solution temperature of γ'. However, the interaction of dislocations with the dispersoids at high temperatures is still a subject for debate. At low temperatures (below 400 ^{0}C), mutual dislocation interactions and Orowan looping [134] is the major mechanism. In this mechanism, as the dislocation advances, dislocation loops are left around the dispersoids. On the other hand, at 400-600 ^{0}C, dislocations were seen attaching at the departing side of the dispersoids and as the dislocation advances, no dislocation debris was left behind [135, 136]. At this temperature, it is believed that transition of mechanism from Orowan looping to bypassing is occurring and the normalized yield stress drops at that temperature, which is much less than the yield stresses below that temperature [137-139]. Thus, extensive TEM studies associated with high temperature mechanical testing of bulk and TLP bonded ODS alloys with agglomerated dispersoids would yield valuable information.

- *Finite element analysis of shear testing:* Shear testing is an easy and effective method of eliminating poor bonds. However, the application of shear forces on different types of alloys [nickel-based superalloys, ODS alloys, titanium alloys]

revealed a difference in their behavior, and consequently an extensive computational analysis of shear testing using the finite element method is recommended.

- *High temperature testing of TLP bonded ODS alloys:* ODS alloys were designed to withstand temperatures higher than those at which nickel-based superalloys can operate, and since TLP bonding results in a reasonable dispersoid continuity and elongated grain structure, high temperature testing, including creep, cyclic oxidation tests, and high temperature tensile testing of TLP bond should be performed and the results compared with those for substrates joined using other techniques.

8   BIBLIOGRAPHY

1.   E.F. Bradley: "SOURCE BOOK ON MATERIALS FOR ELEVATED-TEMPERATURE APPLICATIONS", American Society for Metals, Metals Park, Ohio, 1969, pp. 275-298

2.   G.P.Sabol, R.Stickler: "MICROSTRUCTURE OF NICKEL-BASED SUPERALLOYS: REVIEW ARTICLE" Phys. Stat. Sol. 35(11),1969, Westinghouse Research Laboratories, Pittsburgh, Pennsylvania.

3.   C.T.Sims: J. Met., 1966, October, pp.1119-1130.

4.   A.K.Jena, M.C. Chaturvedi: J. Matl. Sci, 1984, (19), pp.3121-3139.

5.   E.F. Bradley: "SUPERALLOYS: A TECHNICAL GUIDE", Metals Park,OH; ASM International, 1988.

6.   P.S. Kotval: Metallography, 1, 1969, pp.1119-1130.

7.   C.T. Sims: "SUPERALLOYS: GENESIS AND CHARACTER" in "Superalloys II",   edited by C.T. Sims, N.S. Stoloff, W.C. Hagel, 1987, John Wiley & Sons, pp. 3-21.

8.   M.Ott, H. Mughrabi: Mater. Sci. & Eng. A, 1999, 272, pp.24-30.

9.   Michael F. Ashby and David R.H. Jones: ENGINEERING MATERIALS I: AN INTRODUCTION TO THEIR PROPERTIES AND APPLICATIONS, Oxford; Butterworth-Heinemann, 1996.

10.   J.W. Lee, J.H. Mc Murray and J.A. Miller: Weld. J., 64(10), 1985, pp.18-21.

11.   G.M. Slaughter: Weld. J., 58(10), 1979, pp.17-28

12.   W.A. Owczarski: "PHYSICAL METALLURGY OF METAL JOINING", edited by R. Kossowsky and M.E. Glicksman, Metallurgical Society of AIME, Warrendale, PA, 1980, pp.166-190

13.   C.Y. Su, W.C. Lih, C.P. Chou and H.C. Tsai: J. Mater. Proc. Technol., 115, 2001, pp.326-33

14. K. Schneider, B.Jahnke and R. Burgel: Mater. Sci. Technol, 1(8), 1985, pp.613-619

15. R. Creal: Heat Treatment, 19(10), 1987, pp.30 – 32

16. T.J. Kelley: Weld. J., 62(10), 1983, pp.57-58

17. J.R. Kelley: Weld. Des. Fabricat., 57(7), 1985, pp.43 – 45.

18. D. Mckeon: Weld. J., 3, 1971, pp.201s-206s

19. K.C. Wu, R.E. Herfert: Weld. J., 46, 1967, pp.32s-38s

20. W.P. Hughes, T.F. Berry: Weld. J., 46, 1967, pp.361s-367s

21. J.R.Thamburaj, W.Wallace, and J.A.Goldak: Int. Metall. Rev., 28(1), 1983, pp.1-22.

22. A.E.Dray: Ph.D.Thesis. 1985, University of Cambridge, Cambridge, UK.

23. X. Wu, R. S. Chandel, and H. Li: J.Matl. Sci., 36(6), 2001, pp. 1539-1546.

24. S.J. Lee, S.K. Wu, and R.Y. Lin: Acta. Mater., 46, 1998, pp.1283-1286.

25. I. Tuah-poku, M. Dollar, and T.B. Massalski: Metall. Trans. A, 19A(3), 1988, pp. 675-686.

26. D.S. Duvall, W.A. Owczarski, D.F. Paulonis: Weld. J., 53(4), 1974, pp. 203-214

27. W.F. Gale, D.A. Butts: Sci. Technol. Weld. Join., 2004, 9(4), pp. 283-300.

28. Y. Zhou, W.F. Gale, and T.H. North: Int. Mater. Rev., 40(5), 1995, pp.181-196

29. R. Sharghi-Moshatghin, S. Asgari: J. Alloy. Compd. 368, 2004, pp.144-151.

30. R.A. Stevens, P.E.J. Flewitt: Mater. Sci. Eng., 37, 1979, pp.234–247.

31. P.K. Footner, B.P. Richards: J. Mater. Sci., 17, 1982, pp.2141–2153.

32. G.J. Karen: Ph.D Thesis. 1983, Stanford University, USA.

33. J.S. Benjamin: Met. Trans. A., 1(10), 1970, pp.2943-2951.

34. L. Habraken: "MATERIALS AND GAS TURBINES", in "High Temperature Alloys for Gas Turbines", edited by D. Coutsouradia, P. Felix, H. Fichmeister, L. Habraken, and M.O. Speidel, 1978, Applied Science Publishers Ltd., pp.xiii-xiv.

35. W. Boesch: " INTRODUCTION-SUPERALLOYS", in "Superalloys, Super composites and Superceramics", edited by J.K. Tien and T. Caulfield, 1989, Academic Press Inc. Ltd., pp.1-7

36. S. Ahmed: JOM, 42(8), 1990, pp. 24-26

37. M.H. Van de Voorde: "ADVANCED HIGH TEMPERATURE MATERIALS" in "Research and Development of High Temperature Materials for Industry", edited by E. Bullock, R. Brunetaud, J.F. Conde, S.R. Keown, and S.F. Pugh, 1989, Elsevier Applied Science, pp.1-12

38. J.H. Wood and E.H. Goldman: "PROTECTIVE COATINGS" in "Superalloys II", edited by C.T.Sims, N.H. Stoloff, and W.C. Hagel, 1987, John Wiley & Sons, pp.359-384

39. O.D. Sherby and P.M. Burke: "MECHANICAL BEHAVIOR OF CRYSTALLINE SOLIDS AT ELEVATED TEMPERATURE" in "Progress in Materials Science", edited by B. Chalmers and W. Hume-Rothery, 1968, Vol.13, Pergamon Press, pp.325-390

40. C.T. Sims: "HIGH TEMPERATURE ALLOYS IN HIGH-TECHNOLOGY SYSTEMS" in "High Temperature Alloys for Gas Turbines", edited by D.Coutsouradia, P. Felix, H. Fichmeister, L. Habraken, and M.O. Speidel, 1978, Applied Science Publishers Ltd., pp.13-79.

41. J.R. Stephens: "RESOURCES-SUPPLY AND AVAILABILITY", in "Superalloys, Super Composites and Superceramics", edited by J.K. Tien and T. Caulfield, 1989, Academic Press Inc. ltd., pp.9-48.

42. J.R. Davis: "NICKEL, COBALT AND THEIR ALLOYS", in "ASM Specialty Handbook", ASM International. 2000.

43. C.R.Brooks: "HEAT TREATMENT, STRUCTURE AND PROPERTIES OF NON-FERROUS ALLOYS". 1982.

44. M. J. Donachie and S. J. Donachie: in "SUPERALLOYS A TECHNICAL GUIDE", 2nd edition, ASM, 2002. pp.26.

45. E.W. Ross, and C.T. Sims: "NICKEL-BASE ALLOYS" in "Superalloys II", edited by C.T. Sims, N.S. Stoloff, W.C. Hagel, 1987, John Wiley & Sons, pp.101.

46. N.S. Stoloff: "FUNDAMENTALS OF STRENGTHENING" in "Superalloys II", edited by C.T. Sims, N.S. Stoloff, W.C. Hagel, 1987, John Wiley & Sons, pp.61-96.

47. T.L. Lin: Matl. Sci. Eng. A, 128, 1990, pp. 23-31.

48. M.Yamaguchi: Philos. Mag. A, 45, 1982, pp. 867-871.

49. V. Paidar: Philos. Mag. A, 45, 1982, pp.883-895.

50. C.E. Campbell and W.J. Boettinger: Metall. Mater. Trans. A, 31A, 2000, pp.2835-2847.

51. P.R. Mobley, G.S. Hoppin III: Weld. J., 40, 1961, p.610s.

52. B.L. Gruzdev: Weld. J., 53, 1974, p.543.

53. W.A. Owczarski, D.S. Duvall, C.P. Sullivan: Weld. J., 45, 1966, 145-s.

54. M. Prager, C.S. Shira: Welding Research Council Bulletin, 128 (1968).

55. M.H. Haafkens, G.H. Matthey: Weld. J., 61 (1982) pp.25-32.

56. T.J. Kelly, in: R.A. Patterson, K.W. Mahin (Eds.), Proceedings of the Conference on Weldability of Materials, ASM International, USA, 1990, pp.151–157.

57. W.B. Busch, H.D. Kunze, Proceedings of the Conference on Materials Development in Turbo-Machinery Design, The Institute of Metals, UK, 1988, pp. 81–87.

58. G. Cam, M. Kocak: Int. Mater. Rev. 43 (1998) 1.

59. M.B. Henderson, D. Arrell, M. Larsson, G. Marchant: Sci. Technol. Weld. Join., 9, 2004, pp.13-18.

60. O. Hunziker, D. Dye, S.M. Roberts and R.C. Reed: Proc. Conf. on Numerical Analysis of Weldability, Graz-Seggau, Austria, 1999.

61. M.B. Henderson, D. Arrellb, M. Heobel, R. Larsson and G. Marchant: Conf. in the Microstructure & Performance of Joints in High-Temperature Alloys, London, UK,Nov. 2002.

62. A. Dhooge and A. Vinckier: Int. J. Pressure Vessels and Piping, 27, (1987), pp. 239-269.

63. G. Cam and M. Kocak: Int. Mater.Rev., 43, No. 1, (1998), pp. 1-44.

64. M. Prager, M. Shira: "WELDING OF PRECIPITATION-HARDENING NICKEL-BASE ALLOYS" in "Welding Research Council", Bull. No.128, New York, 1968

65. R.P. Newman, T.R. Gurney: Brit. Weld. J., 11, 341, 1964.

66. R.R. Gatts, G.J. Sokol: "EFFECTS OF CLOSURE WELD CONFIGURATION ON THE FATIGUE STRENGTH OF OMEGA SEALS" , KAPL-2000-21, Reactor Metallurgy Report No.24, Metallurgy, 1.1-1.11, 1964

67. W. Choi, S. Kim, C. Lee, J. Jang: "EFFECT OF HEATING RATE ON TRANSIENT LIQUID PHASE DIFFUSION BONDING OF NI-BASED SUPERALLOY GTD-111" in "Designing, Processing and Properties of Advanced Engineering Materials: Proceedings on the 3rd International Symposium on Designing, Processing and Properties of Advanced Engineering Materials", Nov 5-8 2003. Jeju Island, South Korea, Trans Tech Publications Ltd,, Zurich-Ueticon, Switzerland.

68. Y.Zhou, W.F. Gale, T.H. North: Int. Mater. Rev., 40(5), 1995, pp.181-196.

69. Y. Nakao and K. Shinozaki: Matl. Sci. and Technol., 11, 1995, p.304.

70. Y. S. Kwon, J. S. Kim, J. S. Moon, and M. J. Suk: J. Mater. Sci., 35, 2000, pp. 1917-1924

71. W. F. Gale, X. Wen, T. Zhou, and Y. Shen: Mater. Sci. Tech., 17, 2001, pp. 1423-1433

72. Y. S. Kwon, J. S. Kim, J. S. Moon, and M. J. Suk: J. Mater. Sci., 35, 2000, pp. 1917-1924.

73. E.Lugscheider, T. Schittny and E. Halmony, Weld. J.(Res. Suppl.), 68(1), 1989, 9s-13s.

74. W.D. Zhuang and T.W. Eagar: Weld. J.(Res. Suppl.), 76, 1997, pp. 157s-162s.

75. W.F. Gale, Y. Xu, X. Wen, and Z.A.M. Abdo: Metall. Mater. Trans. A, 30A, 1999, pp.2723-2726.

76. Y.Guan and W.F. Gale: Mater. Sci. Technol., 15, 1999, 207-212

77. W.F.Gale, D.A. Butts, M. Di Ruscio and T.Zhou: Metall. Mater. Trans. A, 33A(10), 2002, 3205-3214.

78. W.F. Gale and Y.Guan: Mater. Sci. Technol., 15, 1999, 464-467.

79. M. K. Kitchings, Y. Guan, and W. F. Gale: "MICROSTRUCTURAL DEVELOPMENT DURING TRANSIENT LIQUID PHASE BONDING OF STRUCTURAL INTERMETALLIC COMPOUNDS," in "Analysis of in-Service Failures and Advances in Microstructrual Characterization",edited by E. Abramovici, D. O. Northwood, M. T. Shehata, and J. Wylie, ASM International, Materials Park, OH, 1999, pp. 425-430.

80. J.S.Benjamin: Met. Trans. A, 1970, 1(10), pp.2943-2951.

81. C. Suryanarayana, E. Ivanov, and V.V. Boldyrev: Matl. Sci. and Eng. A, 304-306, 2001, pp. 151-58.

82. M.Ruhle: in Proc. 1st Intl. Conf. Heat Resistant Matls. Sep 23-26, 1991. Fontana, Wisconsin: ASM.

83. G.H.Gessinger: "POWDER METALLURGY OF SUPERALLOYS", 1984, Elsevier, pp.213.

84. A.Czyrska-Filemonowicz, B.Dubiel: J. Matl. Proc. Technol, 64, 1997, pp.53-64.

85. C. White: "ADVANCED HIGH TEMPERATURE MATERIALS" in "Research and Development of High Temperature Materials for Industry", edited by E. Bullock, R. Brunetaud, J.F. Conde, S.R. Keown, and S.F. Pugh, 1989, Elsevier Applied Science, pp.71-78.

86. P. Krautwasser, A. Czyrska-Filemonowicz, M. Widera, F. Carsughi: Matl. Sci. and Eng. A, 177, 1994, pp.198-208.

87. H.R.Seth: Ph.D Thesis, 1991, Northwestern University, USA.

88. R.C.Benn: Frontiers of High Temperature Materials, Inco Alloy International. 1983.

89. A.Czyrska-Filemonowicz: J. Matl. Proc. Technol., 53, 1995, pp.93-100.

90. T.J. Kelly: "WELDING OF MECHANICALLY ALLOYED ODS MATERIALS", in "Proceedings of Trends in Welding Research", edited by S.A. David, ASM, Metals Park, OH, 1982, pp. 471-478.

91. L.E. Shoemaker: "JOINING TECHNIQUES FOR A FERRITIC OXIDE DISPERSION STRENGHTENED ALLOY", in "Proceedings of the International

Conference on Trends in Welding Research", edited by S. A. David, ASM, Metals Park, OH, 1986, pp. 371-77.

92. P.A. Molian, Y.M. Yang, P.C. Patnaik: J. Mater. Sci., 27, 1992, pp.2687-2694.

93. C.Y. Kang, T.H. North, D.D. Perovic: Metall. Mater. Trans. A, 27A, 1996, pp. 4019-4029.

94. T.I. Khan, E.R. Wallach: J. Matl. Sci, 30, 1995, pp.5151-5160.

95. T.I. Khan, E.R. Wallach, J. Matl. Sci, 31, 1996, pp.2937-2943.

96. H. Kinoshita, N. Akasaka, H. Takahashi, I. Shibahara, and S. Onose: "Microstructural Change on Electron Irradiated Oxide Dispersion Strengthened Ferritic Steels", J. Nucl. Mater., 1992, Vol. 191-194(2), pp. 874-78.

97. D.A. Butts, T. Zhou, W.F. Gale: Internal Communication on Joining of Superalloys, Aug.2002.

98. E.H. Bradley: Source Book on Materials for Elevated-Temperature Applications.Wiley, 1979.

99. S. V. Orel, L. C. Parous, and W. F. Gale: Weld. J. Suppl., 74, 1995, pp. 319s-324s.

100. D. S. Duvall, W. A. Owczarski, D. F. Paulonis, and W. H. King: Weld. J. Suppl., 1972, 53, pp. 41s-49s.

101. A. Rabinkin: Weld. J., 68(10), 1989, pp. 39-45.

102. T. J. Moore, and T. K. Glasgow: Weld. J. Suppl., 64(8), 1985, pp. 219s-226s.

103. W. Li, T. Jin, X. F. Sun, Y. Guo, H. R. Guan, and Z. Q. Hu: Scripta Mater., 48, 2003, pp. 1283-1288.

104. T. J. Kelly: Weld. J. Suppl., 61(10), 1982, pp. 317s-319s.

105. A. Ekrami and T. I. Khan: Mater. Sci. Tech., 15, 1999, pp. 946-950.

106. Y. Zhai and T. H. North: J. Mater. Sci., 32, 1997, pp. 5571-5575.

107. C. A. Blue, V. K. Sikka, R. A. Blue, and R. Y. Lin: Metall. Mater. Trans. A, 27A, 1996, pp. 4011-4017.

108. Z. Li, Y. Zhou, and T. H. North: J. Mater. Sci., 30, 1995, pp. 1075-1082.

109. W. F. Gale and S. V. Orel: J. Mater. Sci., 31, 1996, pp. 345-349.

110. W. F. Gale, D. A. Butts, M. D. Ruscio, and T. Zhou: Metall. Mater. Trans. A, 33A, 2002, pp. 3205-3214.

111. S. V. Orel, L. C. Parous, and W. F. Gale: Weld. J. Suppl., 74, 1995, pp. 319s-324s.

112. Y. Guan, and W. F. Gale: Mater. Sci. Tech., 15, 1999, pp. 207-212.

113. W. F. Gale and Y. Guan: Metall. Mater. Trans. A, 27A, 1996, pp. 3621-3629.

114. P.Yan and E. R. Wallach: Intermetal., 1(2), 1993, pp. 83-97.

115. A. Hill and E. R. Wallach: Acta Metall., 37(9), 1989, pp. 2425-37.

116. M. G. Nicholas: "JOINING PROCESSES", Kluwer Academic Publishers, The Netherlands, 1988.

117. T. W. Eager: "Processes of Joining Materials".
     http://web.mit.edu/3.37/www/chapter.shtml (06/09/2005).

118. T.J. Moore, and T.K. Glasgow: Weld. J., 64, 1985, pp. 219-226.

119. I.A. Bucklow: "Diffusion Bonding a Creep Resistant Fe-ODS Alloy", conf. proc., Advances in Joining Newer Structural Materials, Proceedings of the International Conference, Montreal, Canada: Elmsford, NY: Pergamon. (1990), pp. 299-304.

120. G. Zhang, R. S. Chandel, H. P. Seow and H. H. Hng: Mater. Manuf. Processes, 18, 2003, pp. 599-608.

121. S.V. Chitti: Masters thesis, Auburn University, 2005

122. J.-M. Veys and R. Mevrel: Mater. Sci. Eng., 88, 1987, pp.253-260.

123. H.W. Grunling, K.Schneider and L. Singhesier: Mater. Sci. Eng., 88, 1987, pp.177-189.

124. T.C. Totemeier, W.F. Gale and J.E. King: Matl. Sci. Eng., A169, 1993, pp.19-26.

125. T. Zhou, Ph.D. thesis, Auburn Uiniversity, 2002.

126. Section 14.95 of the ANSYS Theory Reference

127. V.G. Krishnardula, R.Aluru, N.I. Sofyan and W.F. Gale: Proceedings of 7th International Conference on Trends in Welding Research VI, Pine Mountain, GA, in Press, 2005.

128. V.G. Krishnardula: Ph.D. dissertation, Auburn University, 2005.

129. H.K.D.H. Bhadeshia: Mater. Sci. Eng., A223, 1997, pp.64-77

130. B.S. Bokstein, V.S. Gostomelskii, V.A. Ivanov, A.L. Petelin, and S.A. Petelin: Mater. Lett., 39(1), 1999, pp. 77-79.

131. N. Orhan, M. Aksoy, and M. Eroglu: Mater. Sci. Eng., A271, 1999, pp. 458-68.

132. W.R. Freeman, Jr.:"INVESTMENT CASTINGS" in "Superalloys II", edited by C.T.Sims, N.H. Stoloff, and W.C. Hagel, 1987, John Wiley & Sons, pp.411.

133. S. Reichman and D.S. Chang: "POWDER METALLURGY" in "Superalloys II", edited by C.T.Sims, N.H. Stoloff, and W.C. Hagel, 1987, John Wiley & Sons.

134. E.Orowan: Symp. on Internal Stresses in metals and Alloys., 1948. London

135. P.Guyot: Acta. Metall., 12, 1964, pp. 941-949.

136. R.Lagneborg: Scripta. Metall., 7, 1973, pp. 605-610.

137. J.Rosler and E.Arzt: Acta. Metall., 36, 1988, pp.1043-1049.

138. D.J.Srolovitz, M.J.Luton, and R.A.Petkovic-Luton: Acta Metall., 31, 1988, pp.2151-2158

139. D.J.Srolovitz, et al.: Acta Metall., 32, 1984, pp.1079-1083.